NASA Contractor Report 180900

Sensors for Ceramic Components in Advanced Propulsion Systems

Summary of Literature Survey and Concept Analysis
Task 3 Report

Prepared by
W.H. Bennethum
L.T. Sherwood
GE Aircraft Engines
Advanced Technology Operation
Cincinnati, Ohio 45215

August 1988

Prepared for
National Aeronautics and Space Administration
Lewis Research Center
Contract NAS3-25140

NASA
National Aeronautics and
and Space Administration

NASA Contractor Report 180900

Sensors for Ceramic Components in Advanced Propulsion Systems

Summary of Literature Survey and Concept Analysis
Task 3 Report

Table of Contents

Table of Contents (Continued)

Table of Contents (Concluded)

List of Illustrations

List of Tables

1.0 Introduction

This report describes work performed by GE Aircraft Engines for NASA Lewis Research Center in support of the "Sensors for Ceramic Components in Advanced Propulsion Systems" program (NASA Contract No. NAS3-25140). The work effort of this program is organized under several major categories as follows.

Task 1 - Survey of Sensor Concepts

Task 2 - Analysis of Sensor Concepts

Task 3 - Review and Report

Task 4 - Sensor System Design and Test Plan Formulation

Task 5 - Fabrication of Sensor System

Task 6 - Performance of Tests and Analysis of Results

These tasks are described in detail in the Statement of Work portion of NASA contract NAS3-25140. Pertinent excerpts from this document are included in Appendix A. This report is a summary of Tasks 1 and 2.

A Literature Survey was conducted to identify journal articles, conference proceedings, books, and vendor information on various methods of surface temperature, strain, and heat flux measurement. We have made extensive use of the Dialog Information Services Inc. data bases. The most useful data base has been the Aerospace Dataspace, which is an on-line version of two publications: International Aerospace Abstracts (IAA), and Scientific and Technical Aerospace Reports (STAR). We have also used Dialog's Searchable Physics Information Notices (SPIN) and the National Technical Information System (NTIS) data bases. Numerous journal articles and other sources of relevant information have been assembled.

We have attempted to focus our attention on concepts which are appropriate for use in the hot section of a gas turbine engine, where nonintrusive or low profile characteristics are often necessary to avoid aerodynamic perturbations and interference with the parameter being measured. In cases where sensor concepts with potential for functioning in a gas turbine hot section could not be found or were limited in quantity, we have selected alternate concepts and have attempted to describe the nature of the limitations regarding use in operating test engines. In addition, we have attempted to rate concepts on the basis of chemical, metallurgical, and thermal compatibility with typical ceramic materials capable of operating in a combustion gas (oxidizing) environment. Since specific ceramic materials have not been identified, we have used typical characteristics for the types of ceramic materials which may be used in future engine components.

In addition to reviewing the literature, we have discussed concept details with authorities in the field to gain an understanding of capabilities and limitations with regard to gas turbine hot section application on ceramic components. In some cases,

where data were not available or were contradictory, we have conducted laboratory tests to evaluate feasibility.

The process of looking for sensing concepts adaptable to high temperature ceramic materials operating in a hot gas stream has resulted in elimination of numerous concepts which appeared inappropriate for practical application in such an environment, and has influenced our perspective regarding specific sensor configuration. For example, in the area of thermoelectric surface temperature measurements, considerable attention is given to thin film sensors, but application of bonded wire elements is not discussed because of the temperature and aerodynamic perturbations caused by typical bonded wire sensors. Also, concepts have been limited to those capable of functioning in an oxidizing environment. Refractory metal alloys of tungsten, rhenium, and molybdenum are not suitable for use at elevated temperatures in an oxidizing atmosphere without having an impervious protection coating capable of surviving thermal soaking and cycling. Such a coating could not be found in the literature and is not considered feasible in the near future. Hence, these materials have not been reviewed or considered for future development.

For purposes of comparing the relative merits, it is useful to group sensor concepts into two broad categories: (1) nonintrusive, where no physical sensing element is attached to the surface at the point of measurement; (2) applied sensors, which do require application of the sensor at the point of measurement.

Nonintrusive sensors have many advantages, including avoidance of aerodynamic or sensing element perturbations, but are limited in some respects (namely, line of sight), which makes it necessary to include applied sensors as part of a comprehensive review of measurement techniques. Criteria used to select and rank concepts included the following.

1. Environmental survivability in gas turbine hot section flow path characterized by:
   - Turbulent, variable density, high velocity combustion gases
   - Oxidizing atmosphere
   - High vibration and thermal shock environment
2. Compatibility with component material
3. Minimum sensor interference with component functionality or sensed parameter
4. Component modifications required to accept sensing element must not significantly reduce functionality or life of the component
5. Accuracy, resolution
6. Fabricability
7. Measurement system cost
8. Operating temperature range
9. Life expectancy.

Two reports which cover a range of sensing techniques with slightly different perspectives (from this document) are References 1-1 and 1-2.

2.0 Surface Temperature Measurement

2.1 Summary Listing of Candidate Techniques

For purposes of quick reference, a listing of the characteristics of the surface temperature techniques with some potential for use on high temperature ceramic materials is included in Table 1. Some of the information in these tables is strongly dependent on the specific measurement problem and should not be generalized. The rationale for doing so here is to aid in comparing the various techniques. It is strongly recommended that a thorough understanding of the advantages and problems associated with any specific measurement system be achieved by reviewing the discussion in the following sections of this document and the references associated therewith.

2.2 Concept Description and Analysis - Thin Film Thermocouples

2.2.1 Thermoelectric Elements

2.2.1.1 Candidate Material Characteristics

Table 2 contains a detailed tabulation of high temperature conducting materials for sensor elements. The data were collected from References 2-1 through 2-34. These materials can be broadly grouped into two categories: (1) intermetallics and (2) metals. The intermetallics, except for SiC and $ReSi_2$, have high resistivities and positive temperature coefficients of resistance (TCR). The metals generally have lower resistivities (~10X) as well as positive temperature coefficients of resistance. Both groups of materials have low thermoelectric potentials except for the intermetallics - SiC, $CrSi_2$, $ReSi_2$, and B_4C. All of the materials have melting points over 3000° F (except $TiSi_2$) and range from very good to poor resistance to oxidation at 3000° F. Several of the intermetallic materials have excellent oxidation resistance (SiC formed by Chemical Vapor Deposition and $MoSi_2$). The noble metals are less oxidation resistant. Oxidation or recession rate data reported in the literature for noble metals ranges over several orders of magnitude at the same temperature (discussed in a later section of this report).

The resistance of intermetallic materials to oxidation depends on a number of factors associated with a particular test specimen (purity, density, composition, microstructure, type of native oxide formed, and test conditions). As a group, these materials are more resistant to oxidation at elevated temperatures than metals. Many intermetallics grow a stable native oxide on the surface when oxygen is present at high temperatures. This oxide layer protects the underlying material and greatly slows the rate of weight gain with time (parabolic rate kinetics). Some examples include:

1.	$MoSi_2$ and SiC	-SiO_2	Protective Oxide
2.	$TaAl_3$	-Al_2O_3	Protective Oxide
3.	$ZrBe_{13}$	-BeO	Protective Oxide

Table 1. *Surface Temperature Measurement Concept Characteristics.*

	Sensor Description														
	Upper Temperature Limit, °C	Probability of Success, %	Life, hr	Environmental Restrictions	Time Response, seconds	Accuracy, %	Resolution, %	Aerodynamic Interference	Surface Mod	Line of Sight	Full Field or Point	Spatial Resolution, mm	Relative Cost	Deficiencies	Comments
Radiation Pyrometers															
Single Wavelength, 0.4 - 1.2 μm	None	50	N/A	None	10-6	±10	±0.3	None	No	Yes	Point	1	Inter-mediate	• Seriously Affected by Reflected Radiation • Surface Emittance Must be Known	• Rework Required to Obtain Sight Path
Single Wavelength, 8 μm	None	75	N/A	None	10-6 10-1	±5	±1.0	None	No	Yes	Point	5	Inter-mediate	• Some Detectors Must be Cooled or Chopped • Special Optical Materials Required to Transmit at 8 μm	• Rework Required to Obtain Sight Path • Response Time Depends on Detector
Dual Wavelength, 0.4 - 1.2 μm	None	75	N/A	None	10-6	±10	±0.3	None	No	Yes	Point	1	Inter-mediate	• Some Require Knowledge of Combustion Gas Temperature • Emittance Must be Same at Both Wavelengths	• Rework Required to Obtain Sight Path • Calculation Intensive Data Reduction
Multiple Wavelength (6), 0.4 - 1.2 μm	None	25	N/A	None	10-6	?	±0.3	None	No	Yes	Point	0.160	Inter-mediate	• Not Able to Compensate for Reflected Radiation	• Rework Required to Obtain Sight Path • Calculation Intensive Data Reduction • Emittance Not Required
Multiple Wavelength (200), 0.4 - 1.2 μm	None	25	N/A	None	?	?	±0.3	None	No	Yes	Point	0.100	Inter-mediate	• Not Able to Compensate for Reflected Radiation	• Rework Required to Obtain Sight Path • Calculation Intensive Data Reduction • Assumes Emittance to be a Linear Function of Wavelength
Rejection of Reflected Radiation by Polarization	None	25	N/A	None	?	?	±0.3	None	No	Yes	Point		Inter-mediate	• Ability to Differentiate Between Emitted and Reflected Radiation by Polarization for Ceramics is Uncertain	• Rework Required to Obtain Sight Path
Thermographic Phosphors	1200 1950	80 10	30 10	None Unknown	0.01	3	1.0	Slight	Yes	Yes	Point	2	High	• Requires Coating Sensing Area • Coatings for Use Above 1200°C Not Well Identified • Complex Excitation/ Detection	• Not Sensitive to Emittance or Reflected Radiation • New Technology
Temperature Sensitive Coatings, Paints, Kryptonates	1100 1700	75 75	<1 <1		N/A N/A	5 1	10.0 0.5	Slight No	Yes Yes	No No	Field Field	5 5	Low High	• Measures Maximum Exposure Temperature • Requires Access to Part for Examination • Paints Have Poor Resolution	• Useful for Limited Applications Where Area Thermal Profiles Are Required

Table 1. *Surface Temperature Measurement Concept Characteristics (Concluded).*

	Sensor Description														
	Upper Temperature Limit, °C	Probability of Success, %	Life, hr	Environmental Restrictions	Time Response, seconds	Accuracy, %	Resolution, %	Aerodynamic Interference	Surface Mod	Line of Sight	Full Field or Point	Spatial Resolution, mm	Relative Cost	Deficiencies	Comments
Thin Film Thermocouples Platinum Rhodium Alloys (Nonsilicon Substrates or Insulating Films)	1300 1500	75 25	25 10	None None	>0.1	2	0.2	No	No	No	Point	1	Low	• Requires Careful Match of Substrate Properties • Volatile Oxide Limits Temperature	• Should Work on Alumina Substrate • Development of Coatings May Extend Temperature Range
Ceramic and Intermetallic Alloys SiC, $MoSi_2$, WSi_2	1300 1600	75 25	50 20	None None	>0.1	3	0.1	No	No	No	Point	1	High	• Calibration Stability Not Known • Oxidation Effects May Limit Temperature	• New Technology • Should Work on Silicon Alloy Substrates • Coatings May Improve Life
Iridium-Rhodium	1300 1600	75 10	10 1	None None	>0.1	2	0.2	No	No	No	Point	1	Low	• Iridium Oxide Highly Volatile • Calibration Stability Not Known	• Coating May Improve Performance
Tungsten Rhenium Alloys	2000	2	1	Oxidation Protection	>0.1	2	0.2	No	No	No	Point	1	High	• Oxygen Impervious Top Coat Required	• Development of Top Coat is Major Challenge
Acoustic Thermometer Attached Sensor	1900 1500	25 50	50 50	None	0.5	±2	±1	Yes	Yes	No	Point	5	Intermediate	• Attachment of Sensor Presents Problems • Senses Average Temperature Over Sensor Length	• Not Useful for Many Applications
Acoustic Thermometer Intrinsic Type (Noncontact)	None	10	N/A	None	?	?	?	No	No	Yes	Bulk	?	High	• Technology Not Well Developed	• Laser Generated Acoustic Pulse
Noise Thermometer	1600	25	50	None	>1			No	No	No	Point	5	Intermediate	• EMI Sensitive • Isolation From Substrate Difficult at High Temperatures	• Thin Film Configuration Suitable Only for Low EMI Environments. (No Reference to Thin Film Configuration in Literature)
Fiber Optic Sensor (Polarimetric Type)	1700	10	10	None	0.001			Yes	Yes	No	Line		Intermediate	• Sensitive to Leadpath Temperature Variations • Very Difficult to Install and Lead Out Sensor	• Applied Sapphire Sensor
Resistance Thermometer - (Pt) (Pt) (Ceramic)	1100 1300 1600	75 25 10	50 50 50	None Isolated from Si None	0.01	0.1 1 5	0.3 0.1 0.5	No	No	No	Point	5	Intermediate	• Must be Isolated from Strain • Must be Isolated from Incompatible Substrate Materials • Oxidation Will Cause Drift	• Thin Film Sensor Configuration
Raman Scattering	?	?	N/A	None	10^{-6}	3	1	No	No	Yes	Point	1.0	High	• Limited Range of Materials • Signal Amplitude Decreases at Higher Temperatures	• Feasibility Not Well Defined • For Nonresponsive Substrates, Coatings May Work

Table 2. *Candidate Conducting Materials for Temperature Sensors Applied to Ceramic Substrates.*

Material	Method of Preparation	Density, %	X-ray Density	Melting Point, °F	Thermal Expansion Coefficient, 10^{-6}/°F	Thermo-electrical Potential (μV/degree)	Resistivity, R.T., μ ohm-cm	Temperature Coefficient of Resistivity (3), ppm/°F	Oxidation Resistance-Air	
									Wt. Change mg/cm^2/hr	Temperature, °F
$MoSi_2$	Vac. Hot Press	99.0	6.24	3720	4.9	-3.0	90 to 100	+6380	+0.3	3000
S. Kanthal ($MoSi_2$)	Extruded		6.24	3992			56.6	+4083	+0.004	3092
WSi_2	Hot Press	92-100	9.86	3840	4.6	-0.2	70	+2910	<+0.2	3000
Cr_3Si	Hot Press	92	6.43	3218	7.13				+0.015	2500
$CrSi_2$						+200	600	+2930		
$TaSi_2$	Hot Press		9.08	4300	4.9	+14	35-45	+3320	+0.24	3000
$TiSi_2$	Thin Film	96	4.04	2750	6.9	+5.2	13-16	+4630	+0.075	2190
$ReSi_2$	CVD			3596		+174	~7000	Reported to be Oxidation Resistant at 3272°F(6)		
SiC	CVD(7)	99+	3.22	4712	2-2.4	-106(4)	10^5-10^7		+0.025	2912
SiC		100			2.6	-351	16 x 10^5		2500Å SiO_2-10 hr at 3000°F(7)	
B_4C			2.52	4442	1.73	+80	0.3 - 0.8		±10	2000
$TaAl_3$			6.33						+0.07(1)	2597
Platinum	Wire	100	21.45	3223	4.9	-3.3	10.0	+2166	-4.08 (2)(5)	3000
Rhodium	Wire	100	12.41	3571	4.6	+2.5	4.7	+2572	-6.5 (2)(5)	3000
Iridium	Wire	100	22.65	4429	3.8	+1.2	4.7	+2372	-63.4 (2)(5)	3000
Rhenium	Wire		9.68	5756	3.9				>1000	2552
Tungsten		100	19.3	6098	2.5	+1.5	5.48		300	1790

(1) Oxide flakes on cooling
(2) Formation of a surface oxide which is volatile, porous and nonprotective (linear rate kinetics)
(3) TCR of thin films is typically about 50% of bulk
(4) Beta-SiC crystal, n-type: Proceedings Conference on SiC, 1959
(5) R.B. Kaplan et al., "Oxidation Protection of Rhenium Thrustors for 2480°K Cyclic Operation by Means of CVD Coatings," Ultramet, 7/30/86
(6) R.B. Kaplan, private communication
(7) Raytheon CVD SiC test bar-etched step measured at GE Evendale (SiO_2 surface film after 10 hours at 3000°F in air furnace)

Metals do not form a stable, protective oxide and show a continuous weight loss with time at elevated temperatures (linear rate kinetics).

Figure 1 shows a comparison of weight gain and weight loss at 1650° C in air for platinum group metals (platinum, rhodium, and iridium) and several intermetallic compounds (SiC, $MoSi_2$, WSi_2, and $TaSi_2$).

Noble metals and alloys react with oxygen at high temperatures to form volatile oxides. The recession rate or loss of metal depends on a number of factors such as specimen size and form, test furnace configuration, and flow rate of air past the test specimen. Many investigators report widely different recession rates for the same material. Figure 2 illustrates this variability. The data reported by R.B. Kaplan (Ultramet, Reference 2-2) was measured in a furnace with a cool wall temperature and an air flow rate of 2 feet/minute. The data from the Phillips (Reference 2-3) paper was measured under static air conditions. The Ultramet data was used to derive Figure 1 since the test conditions more closely approximate jet engine environments.

Figure 1 shows that $MoSi_2$ and SiC are the most stable materials at 3000° F in air by several orders of magnitude. This is due to the self passivating or native oxide layer (SiO_2) that grows on the surface and protects the underlying material from further oxidation. The silicide materials cited in Reference 2-4 probably do not represent the best oxidation resistance that might be obtained with purer and denser forms made by CVD techniques. $MoSi_2$ represents about 80% of the material in Super Kanthal heating elements manufactured by Kanthal Furnace Products. Kanthal Super 33 has a maximum element temperature rating of 1800° C (3270° F) for air operation. The material is reported to be ductile at temperatures above 1200° C. Oxidation resistance of Kanthal heating elements is "due to a thin adhesive protective layer of SiO_2 on the surface. The thin protective layer does not flake off when the element is cooled down in spite of the great differences in coefficient of expansion" (Reference 2-5).

Figure 1 shows the effect of a CVD HfO_2 top coat applied to iridium by Ultramet. The recession rate of iridium with a top coat was reduced to less than 3% of the metal loss of a bare wire (Reference 2-2). If a similar coating could be developed for platinum and rhodium alloy films (which have lower recession rates than iridium), then the recession rates might be reduced to .01 mg/cm^2/hour at 3000° F.

2.2.1.2 Materials Compatibility

Thermal Expansion Match

Matching the thermal expansion coefficients (TEC) between film and substrate becomes more important as the ratio of film thickness to substrate thickness increases. Differences in TEC's can produce high shear stresses at the interface between film and substrate when the structure undergoes a temperature change. Separation can occur if the shear stress exceeds the strength of the bond.

The choice of substrate and film combinations narrows as the TEC match required becomes closer. This is illustrated in Table 3 which lists some selected candidate insulators and conductors for high temperature sensors (candidate materials were selected from a more extensive listing of TEC's in Table 4). The column on the right in Table 3

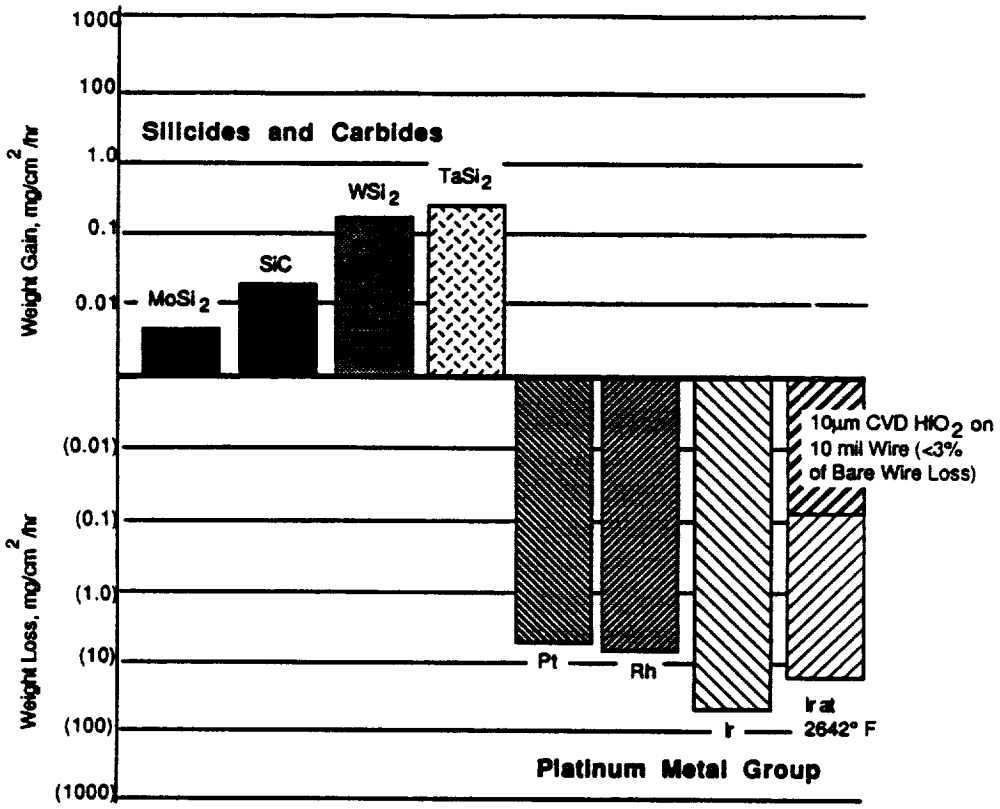

Figure 1. *Weight Gain (Loss) Due to Oxidation for Candidate Conducting Materials at 3000 °F in Air.*

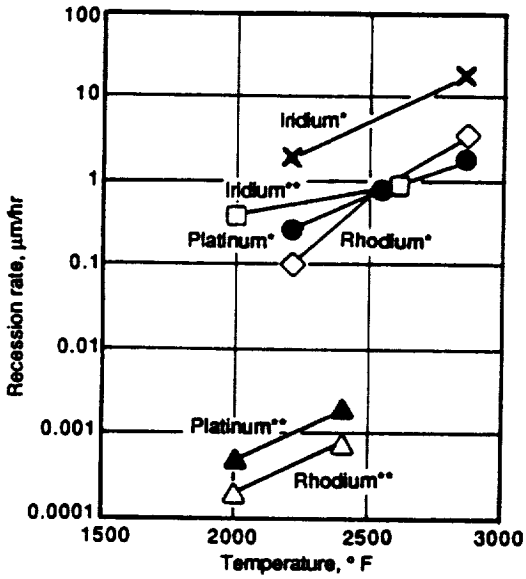

*R.B. Kaplan et al., Ultramet, NAS3-24868, July 30, 1986
**W.L. Phillips, Trans. ASM, 1964, Vol. 57

Figure 2. *Recession Rate for Platinum, Rhodium, and Iridium.*

Table 3. *Candidate Sensor Materials - Thermal Expansion Match to ±30%.*

Material	Thermal Expansion Coefficient, °F x 10^{-6}	Thermal Expansion Coefficient Match, ±30%
Non–Metallic		
SiC (CVD)	4.6	$MoSi_2$, $TaSi_2$, Rhodium, Platinum, Al_2O_3, HfO_2, BeO
$MoSi_2$	4.9	$TaSi_2$, WSi_2, Rhodium, Platinum, Al_2O_3, HFO_2, BeO
$TaSi_2$	4.9	$MoSi_2$, WSi_2, Rhodium, Platinum, Al_2O_3, HFO_2, BeO
Metallic		
Iridium	3.8	SiC, $MoSi_2$, $TaSi_2$, WSi_2, Rhodium, Platinum AlN, Si_3N_4, Al_2O_3, HfO_2
Rhodium	4.6	$MoSi_2$, WSi_2, $TaSi_2$, Platinum, Iridium, Al_2O_3, HfO_2, BeO
Platinum	4.9	$MoSi_2$, WSi_2, $TaSi_2$, Rhodium, Iridium, Al_2O_3, HfO_2, BeO
Insulators		
SiO_2	0.28	None
AlN	2.3–3.0	SiC (CVD), Iridium, Si_3N_4
Si_3N_4	3.3	SiC (CVD), Iridium, AlN, Al_2O_3
Al_2O_3	4.3	$MoSi_2$, $TaSi_2$, WSi_2, Rhodium, Platinum, HfO_2, BeO
HfO_2	5.0–5.5	$MoSi_2$, $TaSi_2$, WSi_2, Rhodium, Platinum, Al_2O_3, BeO
BeO	5.0	$MoSi_2$, $TaSi_2$, WSi_2, Rhodium, Platinum, Al_2O_3, HfO_2
MgO	7.8	None

Table 4. *Thermal Expansion Coefficients of Some Insulators and Conductors.*

Material	Temperature Range, °F	Thermal Expansion Coefficient ($°F \times 10^{-6}$)
SiO_2	68 to 2280	0.28
Pyrolytic Graphite		0.55
Si_3N_4 – Reaction Bonded	0 to 2550	1.4–1.8
Silicon	392	1.73
Boron Carbide	0 to 2550	1.73
Carbon–Carbon		1.9
Si_3N_4 – Hot Pressed	0 to 2550	2.0
SiC – Fine Grain, Reaction Sintered	0 to 2550	2.04
Isotropic Boron Nitride	0 to 2550	2.24
Zircon (67% ZrO_2, 33% SiO_2)		2.3
SiC – Bonded with Si_3N_4	0 to 2550	2.4
SiC – CVD		2.6
Tungsten		2.5
Molybdenum		2.7
ZrO_2	68 to 2190	3.06
AlN	68 to 3000	3.0
Zirconium		3.1
Si_3N_4 – CVD		3.28
Tantalum		3.6
Mullite (76%Al_2O_3, 23% SiO_2)		3.7
Iridium		3.8
Chromium		3.8
Al_2O_3–99+%, Sintered	77 to 1830	4.3
Al_2O_3–99+%, Sintered	77 to 1470	4.5
Al_2O_3 – CVD		4.4 to 4.9
Rhodium		4.6
Platinum		4.9
THO_2	68 to 2550	5.28
BeO	68 to 2550	5.3
Titanium		5.3
MgO	68 to 2550	7.8
Gold		7.9
Al_2O_3 – Sputtered	68 to 1112 – Deposit at 250°F (Changes with Temperature History)	8.1
Nickel		8.4
Inconel 700	700 to 1400	8.8
René 41	1800	9.3
304 Stainless Steel		9.6
Copper		9.8
Aluminum		13.2

shows the TEC match to within 30% of the materials in the left-hand column.

Film Adherence-Design Considerations

The adherence of films deposited on a particular substrate depends on a number of interrelated factors, some of which are listed below.

- Type of Substrate - Oxide films generally bond chemically to oxide surfaces and exhibit strong adhesion. Metal films may not form chemical bonds to an oxide surface unless the metals are oxygen-active. Oxygen-active metals such as Cr, Ti, Al, Ta, and Si form strong bonds to oxide surfaces.

- Substrate Surface Roughness - Thin films deposited on polished surfaces may not form strong bonds. Good adhesion will depend on the film and substrate material, deposition method, and interfacial stresses produced. If the substrate surface is texturized or roughened by physical, chemical, or mechanical methods, a wider combination of film materials will bond fairly well to the substrate.

- Film Thickness - Generally, the thinner the film, the better it will adhere to a substrate.

- Surface Contamination - Clean surfaces are a prerequisite for the development of strong bonds between film and substrate.

- Film Stress - Films under high tensile stress will crack and craze, and films under high compressive stress will buckle if the stresses exceed the bond strength or elastic limit of the material. Control of film stresses depends on many variables (type of material, deposition methods and conditions during deposition, substrate temperature, TEC, etc.).

Thermodynamic Considerations

At elevated temperatures, materials in intimate contact with each other may interact to form new compounds or lower melting eutectics. Early failure of a sensor system could result from an incompatible combination of materials.

Selection of material combinations for sensor systems should take into account possible reactions at elevated temperatures.

2.2.1.3 Noble Metal Sensing Elements

Published data for high temperature, air environment thin film thermocouples (T/C's) have primarily used Pt-10%Rh versus Pt (ANSI, type S). These metal films are usually greater than 2 μm thick. This work has generally been limited to applications on metallic engine hardware where the temperatures have been less than 1100° C. This thermoelectric combination is well suited for this range, but does not seem adequate for the higher temperature requirements of this program. The maximum working temperatures, as suggested by Samsonov and Kislyi (Reference 2-1), for some thermocouples of interest are listed in Table 5, column 2. Another source (Reference 2-6) suggests that Pt-30%Rh versus Pt-6%Rh and Pt-40%Rh versus Pt-20%Rh are acceptable in air intermittently to 1800° and 1850° C, respectively. This implies that the survivability of thin film thermocouples would be slightly higher with higher percentages of rhodium. The references cited were based on

Table 5. *Thermocouples Based on Noble Metals.*

Thermocouple	Max. Working Temp, ° C	Maximum Working Temp. for Thin Film TC's, ° C
Pt/Pt10%Rh	1600	400
Pt/Pt8%Re	1800	
Pt6%Rh/Pt30%Rh	1800	1500
Pt20%Rh/Pt40%Rh	1800	1550
Rh/Rh8%Re	1900	
Ir/Pt40%Ir	2000	
Ir40%Rh/Pt40%Rh	1900	

wire thermocouples and need to be derated for use as thin film sensors. Estimated maximum working temperatures, assuming compatible substrates and topcoats to retard oxidation, are listed in Table 5, column 3. Based on our experience with thin-film (type B) thermocouples, the maximum working temperature for the noble metal thermocouples would probably be less than 1600° C.

2.2.1.4 Silicon Carbide Sensing Elements

Fabrication Considerations

- *Doping Methods (SiC)*

CVD SiC Films - CVD SiC can be doped during formation by introducing controlled amounts of the appropriate gases. According to R.B. Campbell (private communication), SiC can be doped to achieve a resistivity of about 0.1 ohm-cm and possibly as low as 0.01 ohm-cm with nitrogen (n-type) and aluminium (p-type). The films are grown in an ambient atmosphere of nitrogen or aluminum trichloride. The doping level can be controlled by the amount of these gases added in the vapor phase. Campbell noted that doping after the material has been formed is very difficult because of the low diffusion rates of dopants. For example, aluminum will diffuse to a depth of only 0.1 to 0.2 mm after 3 hours at 2000° C.

Polycrystalline beta-SiC films (Reference 2-7) were prepared by CVD methods and doping was accomplished by adding trimethyl-aluminium and diborane during film formation.

A beneficial effect of low diffusion rates should manifest itself during high temperature operation of a thin film SiC T/C under severe environmental conditions. More stable thermoelectric outputs should be obtained compared to thin film metal T/Cs, which typically have high diffusion rates for metallic impurities that could alter calibration.

The Raytheon CVD SiC test specimen that was used to measure emf characteristics on this program was undoped. It has a room temperature resistivity of about 160 ohm-cm. If this material were deposited as a 5 μm thick film, the resistance of the T/C leg might be too high for the measurement instrumenta-

tion to record accurate data. However, doping the material to 0.1 ohm-cm will result in a resistance value of 4000 ohms/inch (of leadpath) at room temperature (5 μm thick film x 0.05 inch wide). The resistance of SiC decreases by about an order of magnitude for each 100° F increase in temperature. Therefore, at 1500° C, the portion of the T/C leg in the hot zone will have a resistance about 27 ohms/inch. This value is comparable to thin film metal T/C's.

Sputtered SiC Films - SiC films with widely varying properties have been made by sputtering techniques. Beta-SiC (Reference 2-8) was sputter deposited from silicon and carbon targets onto a substrate maintained about 700° C. The films were deposited on sapphire substrates and had p-type conductivity with a resistivity of ~1 ohm-cm.

Sublimation grown SiC (Reference 2-9) was post-deposition doped with nitrogen by ion implantation to $1x10^{19}$ molecules/cm^3 to produce n-type material. Ion implantation could also be used to dope sputtered SiC films after deposition.

Ion implantation (Reference 2-10) was used to dope SiC crystals. Nitrogen implantation and annealing produced n-type conductivity in the implanted areas that were originally p-type crystals.

It should be feasible to dope sputtered SiC films by adding nitrogen or diborane to the sputtering gas (argon) to produce "as deposited" n- or p-type films. Sputtering from a predoped target material should also produce the desired conductivity type. Deposition on a heated substrate (700° C) and postdeposition annealing appear to be necessary to achieve high quality, polycrystalline films.

- *Potential Problem Areas*

Areas that will require investigation to establish a viable high temperature intermetallic sensor technology include the following.

- Although SiC and $MoSi_2$ as well as other silicide films have been made by sputtering and CVD methods, no literature reports have been found on the application or development of these materials as thermoelectric elements. A report of the use of sputtered SiC films as RTD sensors (Reference 2-11) claims an operating temperature limit of 400° C.

- The properties of CVD SiC (oxidation resistance, thermoelectric output, etc.) discussed previously in this report are based on bulk or "free standing" specimens. Deposition of this material as thin films (1 to 10 mm thick) on the candidate ceramic engine parts to fabricate a sensor system on the surface of these parts may result in different properties.

- Methods for lead attachment to the SiC films must be developed.

- Feasibility of a high output SiC p-type versus SiC n-type (thermocouple) has been demonstrated. These results must be translated into a thin film structure using CVD and/or sputtering techniques. Doping and patterning processes must be developed.

- The stability and maximum temperature limits of thin film SiC thermoelectric T/Cs must be established in high velocity combustion gas environments.

- Methods of fabricating insulating films (base coats and interlevel insulation)

compatible with SiC and silicide thermocouple elements must be identified and tested to determine operating temperature limits on conducting substrates.

Oxidation Characteristics of SiC

Silicon carbide is available in a number of forms, including materials fabricated by sintering, hot pressing and CVD, or pyrolytic deposition. These different forms of the same basic material compound vary widely in their density, microstructure, and purity. As a result, the oxidation resistance and maximum service temperature in air can range from 1300° to over 1600° C. The following is an analysis of the expected maximum operating temperature of SiC thin film T/C's under oxidizing conditions.

- Some forms of SiC are highly resistant to oxidation up to about 1650° C. No quantitative data have been found for CVD SiC. This material can be made with high purity and density and should be a good candidate for thin film thermocouples deposited on ceramic engine parts.

- Assuming CVD SiC oxidizes at a rate comparable to that reported for $MoSi_2$ (Reference 2-12) at ~1650° C (0.004 mg/cm^2/hour), then an SiO_2 film would form on the surface at a rate of only 250Å/hour. By comparison, an iridium (Reference 2-3) film would be reduced in thickness at a rate of 8000Å/hour at 1650° C without an effective passivating cover coat.

- Minamoto (Reference 2-13) reports that a carbon/SiC T/C showed essentially linear and stable output to 1800° C in flowing argon. A total of 14 cycles from room temperature to 1800° C were made following a stabilization heat treatment at 2100° C.

- SiC/SiC thermocouples (Reference 2-14) are reported to have a life of 50 hours at 1700° C under oxidizing conditions.

- Samsonov et al. (Reference 2-1) report that SiC/SiC thermocouples may be used for lengthy work in oxidizing gaseous media at temperatures up to 1500° to 1750° C; stable readings are obtained up to 50 hours.

- Lauenko et al. (Reference 2-15) studied the oxidation of SiC to 1500° C in air. They self bonded SiC (99.5% purity) and recrystallized SiC (99.9% purity/19% porosity). The self bonded material oxidized at a rate of 0.33 mg/cm^2/hour, and a bubbled aluminosilicate glass layer formed on the surface. It was concluded that the resistance to oxidation of SiC-based materials is not governed by porosity but by the content of calcium, magnesium, and aluminum in the materials.

- Schiroky (Reference 2-16) reports that a smooth, bubble free oxide film forms on CVD SiC at temperatures below 1700° C. At 1735° C he reports a dramatic increase in bubbles in the oxide film and the formation of tunnel-like pits in SiC. (SiO_2 "melts" at 1728° C).

- *Oxidation of Raytheon CVD SiC Test Bar*

Figure 3(a) shows a plot of the expected oxidation rate or increase in the thickness of a surface layer of SiO_2 with time at 1650° C for a Raytheon CVD SiC test bar. The SiO_2 film thicknesses were estimated to be 2500Å after 10 hours and 25,000Å (±1000Å) after 60 hours. This estimate was obtained by

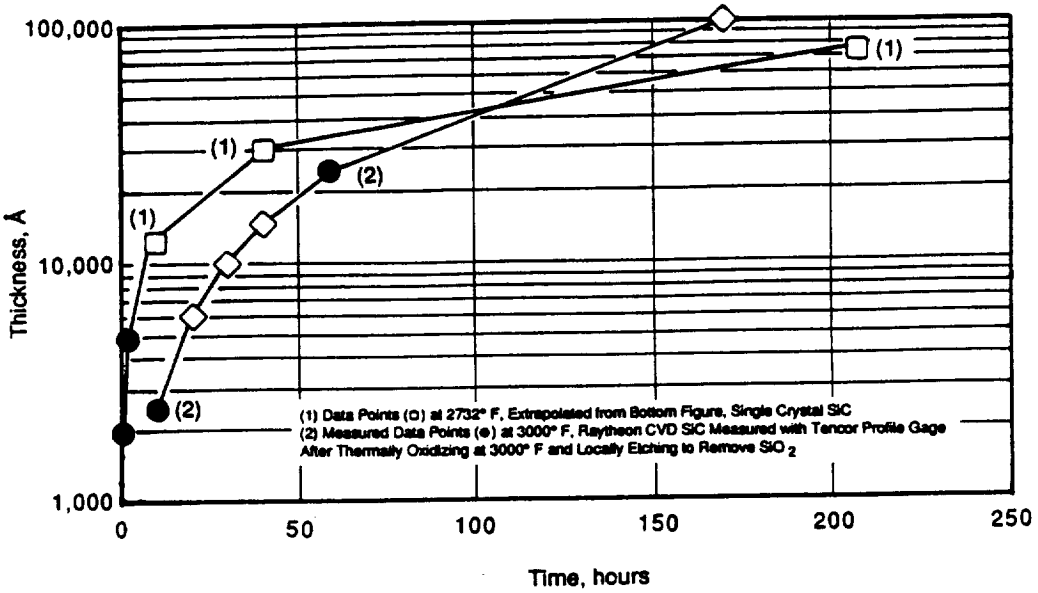

(a)Oxidation Rates at 2732 and 3000° F

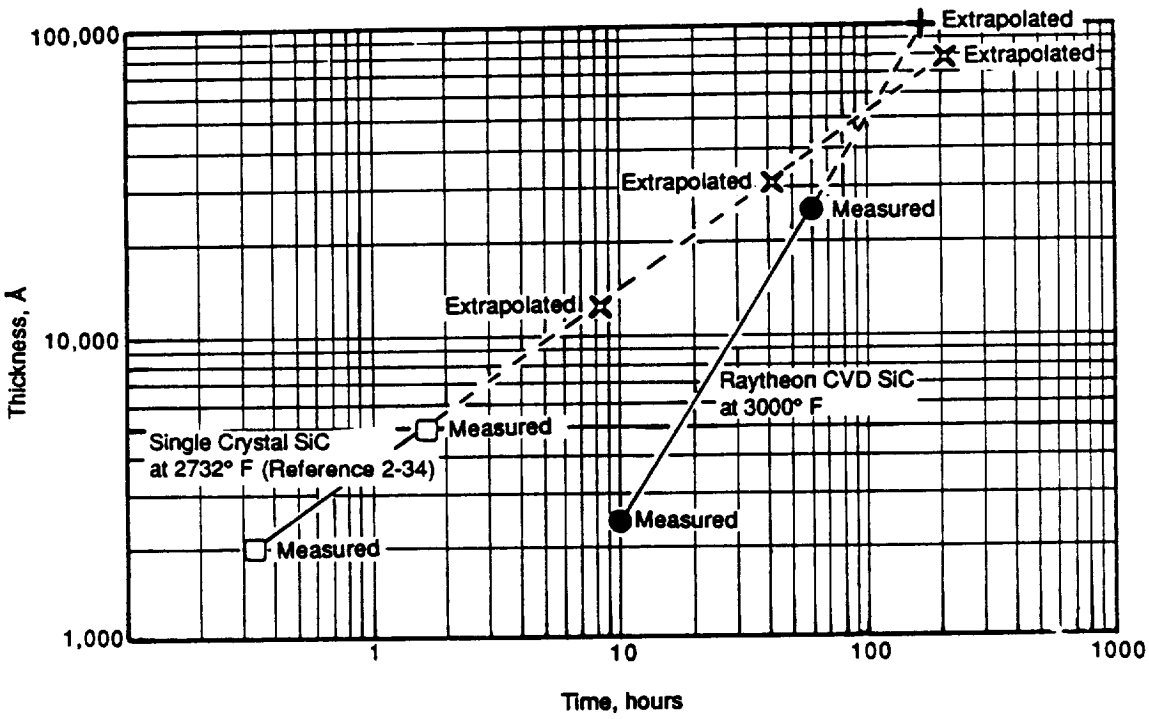

(b) Extrapolation Method

Figure 3. *Comparison of Oxidation Rates for Two High-Purity Forms of SiC.*

measuring an etched step using a Tencor profilometer stylus instrument. Although the surface of the SiC bar was polished with diamond abrasive prior to the furnace test, considerable surface roughness was recorded by the Tencor instrument. This accounts for the uncertainty in the film thickness. Figure 3(a) illustrates how the data in Figure 3(b) were extrapolated beyond 60 hours. These measurements were made by GE during Task 2 of this program.

The furnace test included a bar made from sintered SiC (Norton). After 10 hours at 1650° C, this bar showed severe corrosion (formation of a bubbly glassy layer on the surface). The Raytheon CVD SiC bar appeared to be unchanged except for some spotty glassy patches. This material apparently was deposited from previous contamination in the furnace or else it came from within the Norton SiC test bar.

Comparison of Noble Metal and Silicon Carbide Characteristics

A great deal of information is available in the literature on SiC. This material is used extensively in industrial applications as a structural ceramic and as furnace heating elements. Over the past 25 years, a growing interest has developed in SiC semiconductor films for integrated circuit applications. Research is underway to produce single crystal films for high temperature electronics and other applications (References 2-17 through 2-21). This extensive body of information will benefit the development of SiC films for high temperature thermoelectric thermometers on this program.

A somewhat analogous situation exists for $MoSi_2$ because of its industrial use for above 1650° C furnace heating elements (Super Kanthal). However, this material does not have the mechanical or semiconducting properties of SiC.

In addition, silicon carbide is considered to be primary candidate for high temperature sensors because of the following characteristics:

- Operation in Air - SiC forms a self-passivating, nonvolatile surface oxide (SiO_2) that limits further oxidation by restricting diffusion of oxygen. We believe the potential exists for T/C operation in air to above 1650° C for extended periods of time (50 hours or more).

  Oxidation of platinum metals is not a self-limiting process. The metals form a volatile surface oxide in air and lose weight continuously as a function of time and temperature. An effective top coat will be needed for higher temperature operation of thin film T/Cs.

- Thermodynamic Stability - SiC films should be compatible with all of the candidate ceramic engine parts (substrates) at high temperatures due to free energy of formation considerations. Since many of these materials contain silicon or silicon additives and/or impurities, the formation of platinum silicides with low melting points is a potential failure mode for thin film platinum based T/Cs deposited on silicon-bearing substrates.

- Adherence - SiC can develop an SiO_2 interface oxide during film growth that will produce a stable and strong bond to the substrate. Sputtered platinum alloys do not adhere well to nonmetallic substrates because the alloys do not form a strong and stable interfacial oxide.

- The thermoelectric output of SiC is about 15 times greater than a Type K T/C and about 70 times greater than a Pt-6%Rh T/C. A high output SiC T/C will accurately detect very small temperature changes. For example, such a device will produce a signal of about 60 microvolts to detect a temperature change of 0.1° C compared to only 2 microvolts for a Type K T/C.

  The following is from Reference 2-22:

  "The thermoelectric power of a material depends on the sum of the potential energy and the kinetic transport energy (for one kind of carrier, i.e. electrons in the conductor). In semiconductors, the absolute value of both these energies are additive and the thermoelectric power is large. In metals, the potential energy is less than zero, and differs little from the kinetic transport energy. Therefore, their sum is small and the thermoelectric power by comparison is small. The absolute thermoelectric power of semiconductors usually exceeds that of metals by at least an order of magnitude."

- Catalytic Effects - Platinum thermocouple elements exposed to incompletely burned gases that exist in engine environments can produce catalytic burning on the T/C surface leading to a local increase in temperature. Therefore, the temperature measured does not represent the actual engine temperature. A SiC T/C with a surface oxide layer of SiO_2 is not expected to induce catalytic burning.

- Thin Film T/C Instabilities - Structural and thermoelectric instabilities caused by contamination, loss of material, and catalytic effects are expected to be less of a factor for SiC T/C's due to the SiO_2 native oxide and the low diffusion rates of dopant elements at high temperatures.

2.2.2 Insulating Materials

2.2.2.1 Candidate Insulating Material Characteristics

Table 6 shows high-temperature insulating materials that may be suitable as base coats, diffusion barriers, or top coats in a thermoelectric sensor system. The data was obtained from many different sources. These materials can be grouped into two categories: (1) oxides and (2) nitrides.

All of the materials have melting points over 1650° C (3000° F) and resistivities at 538° C (1000° F) in the 10^{10} ohm-cm range (except SiO_2 and HfO_2). As Table 6 shows, the resistivity of all materials decreases rapidly with increasing temperature. Between 1371° C (2500° F) and 1650° C (3000° F), both oxides and nitrides have resistivities in the range from 10^6 to 10^4 ohm cm. SiO_2 has a lower resistivity (7×10^3 at 2500° F).

Figure 4 shows a plot of resistivity versus temperature for most of the insulators listed in Table 6. Figure 5 shows a similar chart from a different reference source (Reference 2-23). Figures 4 and 5 and Table 6 show that the resistivities of all of the insulator compounds are essentially the same at about 3000° F. As pointed out by Bauer and Bates (Reference 2-23), enhanced emission and gas conduction effects are very significant at high temperatures and can introduce considerable measurement error (shunt conducting paths). It appears, therefore, that no definitive insulator material

Table 6. *Candidate Insulating Materials for Temperature Sensors Applied to Ceramic Substrates. From References 2-23 through 2-32.*

Material	Method of Preparation	Test Sample			X-ray Density	Melting Point, °F	Thermal Expansion Coefficient, 10^{-6}/°F	Resistivity, ohm-cm, °F				
		Thickness	Purity	Density				1000	1500	2000	2500	3000
Al_2O_3	Sinter	-	99.7	-	3.965	3659	4.3	8×10^{10}	2×10^{8}	5×10^{6}	3×10^{5}	5×10^{4}
Al_2O_3	Sputter	12 µm	99.9	-	3.965	-	8.1	1×10^{10}	2×10^{7}			
MgO	-	-	-	-	3.56	5072	7.8	4×10^{12}	8×10^{9}	4×10^{7}	2×10^{6}	8×10^{4}
BeO	-	-	99.5	-	3.03	4622	5.3	1×10^{13}	2×10^{10}	7×10^{7}	4×10^{5}	2×10^{4}
SiO_2	-			-	2.32	3142	0.28	2×10^{7}	4×10^{5}	5×10^{4}	7×10^{3}	
HfO_2	-			-	9.68	5031	-5.5	2×10^{8}	1×10^{6}	3×10^{4}		
Si_3N_4	CVD				3.18	3452	3.3	8×10^{10}	2×10^{8}	8×10^{6}	6×10^{5}	6×10^{4}
Silicon Nitride (Oxidation Resistance: Weight Gain = 0.000167 mg/cm^2 /hour at 2822 °F)												
BN	CVD	1 Mil	>99.9	100	2.25	4946		1×10^{14}	2×10^{10}	1×10^{7}		
BN	CVD	Mfg. Data							1×10^{11}	5×10^{8}	3×10^{6}	5×10^{4}
Boron Nitride (Oxidation Resistance: Weight Gain = 3.0 mg/cm^2 /hour at 2200 °F)												
AlN							2.3-3.0					

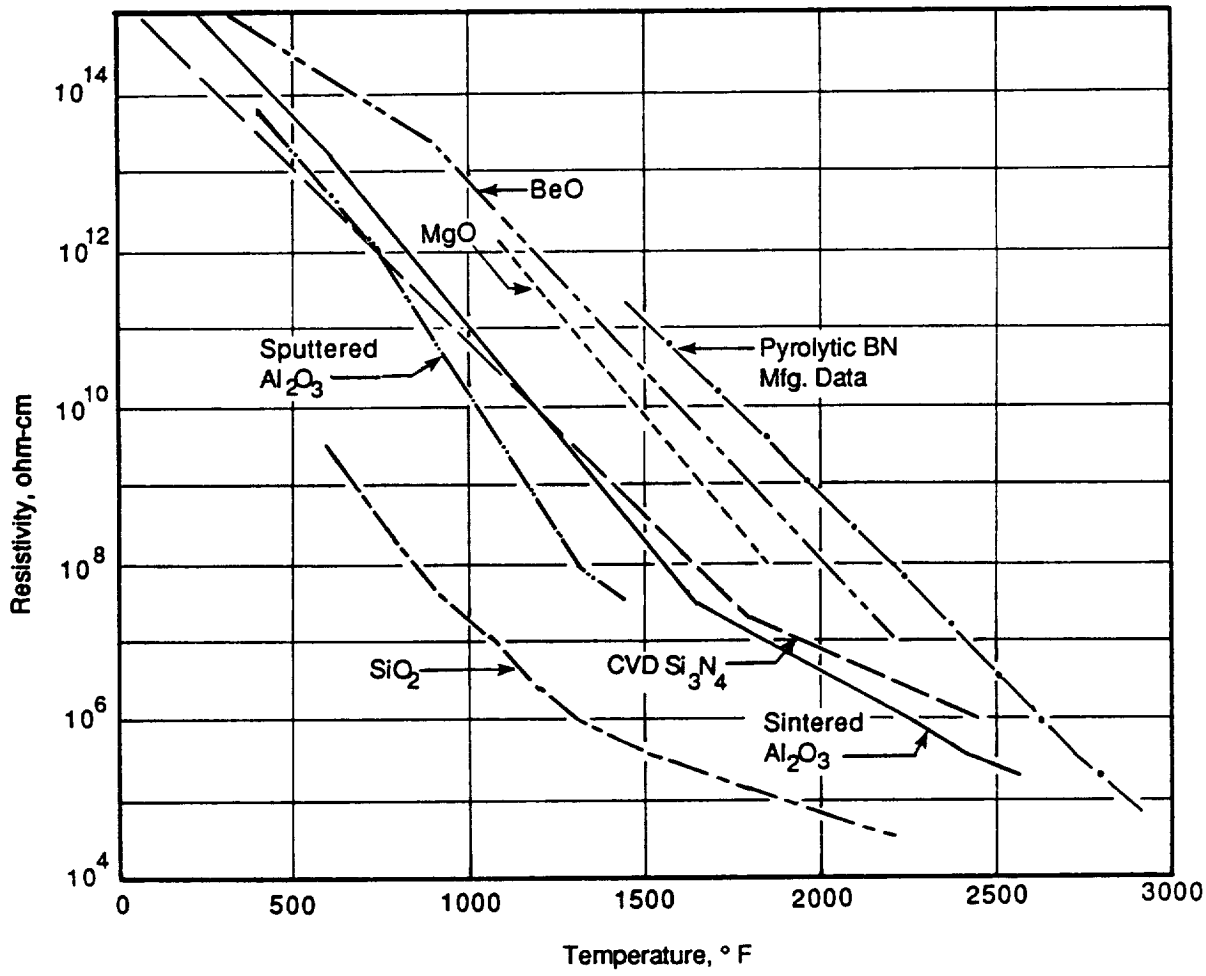

Figure 4. *Resistivity Versus Temperature - High Temperature Insulators. Data is from References 2-23 through 2-32.*

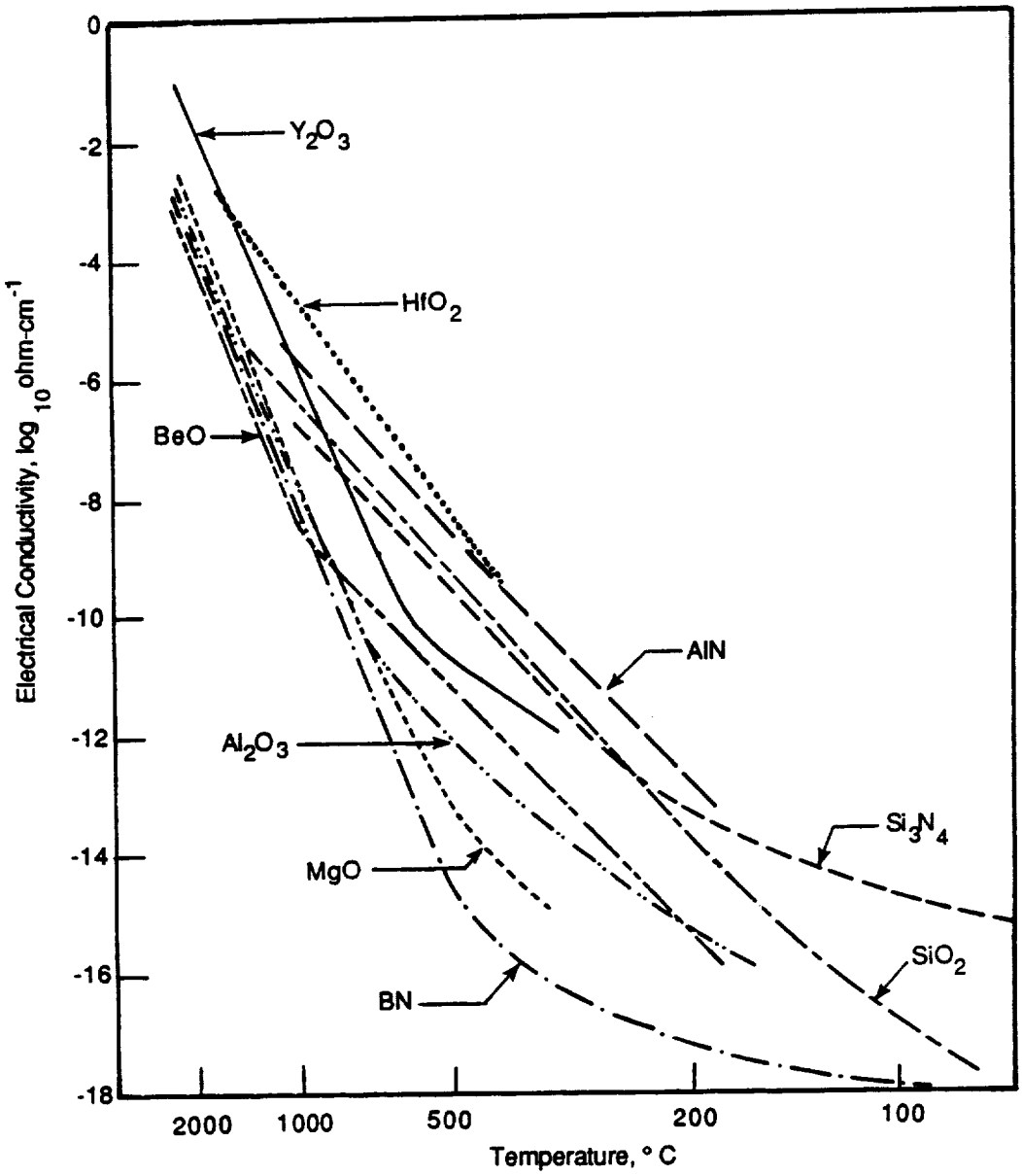

Figure 5. *Electrical Conductivity Versus Temperature - High Temperature Insulators. From Reference 2-23.*

selection can be made for 3000° F sensor structures based on materials with the highest resistivity at 3000° F.

The oxidation resistance of all of the materials in Table 6 is very high, with the notable exception of boron nitride (BN). Figure 6 shows a plot of pyrolytic boron nitride (PBN) (Union Carbide, Boralloy) and CVD Si_3N_4 resistivity versus temperature. Comments are also made regarding oxidation rates. The PBN rate increases from a negligible value at 1382° F to 0.05 mg/cm^2/minute at 2200° F. The oxidation rate of CVD Si_3N_4 is reported to be 0.000167 mg/cm^2/hour at 2822° F (Reference 2-24). At these temperatures, a protective surface film of SiO_2 probably forms in a manner similar to $MoSi_2$ or SiC. The surface of PBN, by comparison, is converted to B_2O_3, which is a low melting glass. Eventually, all of the BN changes to B_2O_3.

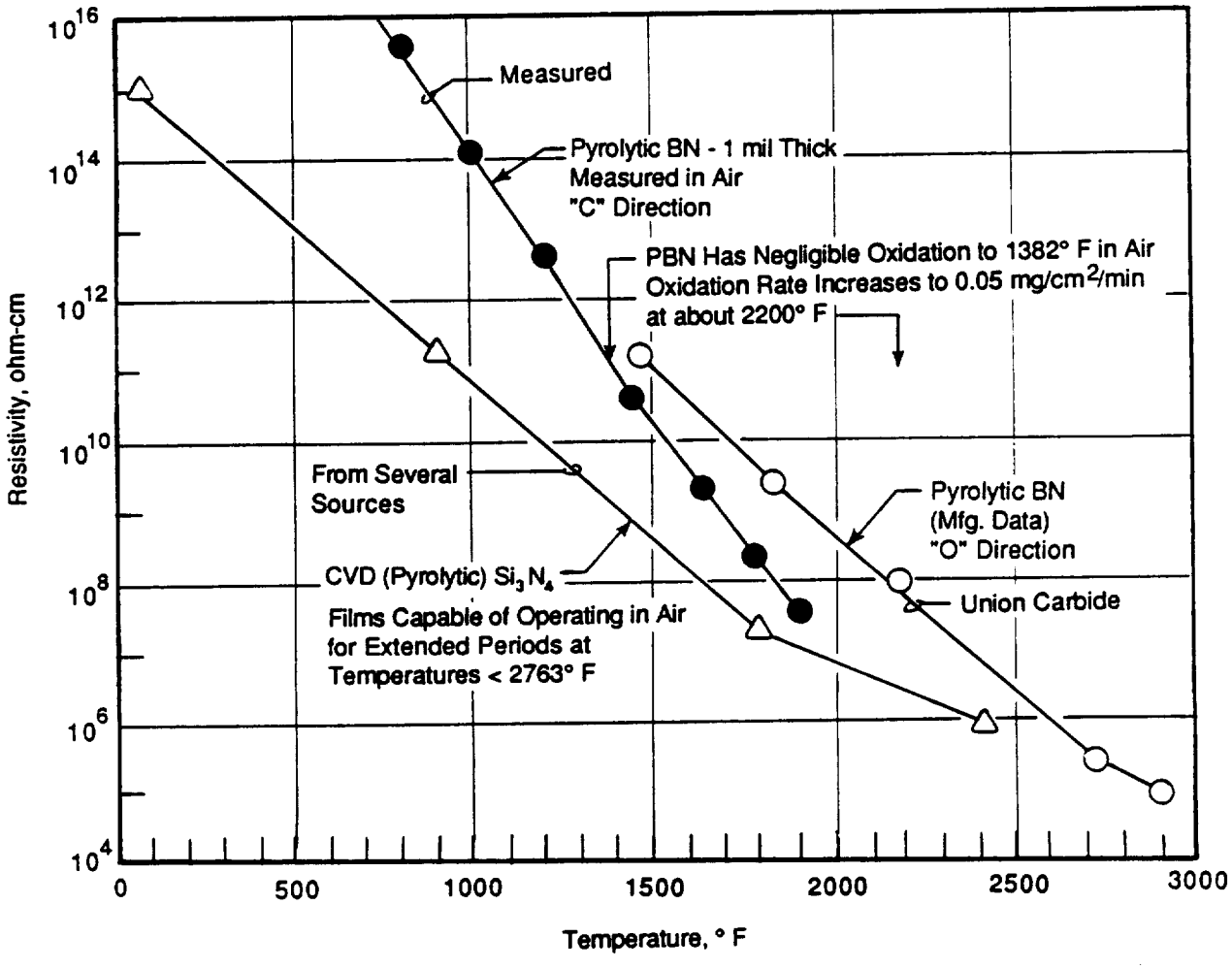

Figure 6. *Resistivity Versus Temperature - Pyrolytic Boron Nitride and Silicon Nitride.*

2.3 Concept Description and Analysis - Radiation Pyrometry

2.3.1 Concept Description

During the past 20 years, optical pyrometry has gained widespread acceptance as an invaluable technique for surface temperature measurement in hostile environments in general and for turbine blade measurements in particular. A radiation pyrometer measures the radiance of the surface it views. In general, this radiation consists of both radiation emitted by the target surface and radiation reflected off of it.

Most pyrometers used in turbine engine applications are spectral devices; that is, they measure one or more narrow radiation bands. The spectral radiance of real bodies may be calculated by multiplying the spectral radiance of a blackbody (derived from Planck's equation) by the emittance of the target surface. Emittance is a function of various factors including the chemical composition of the material, the surface condition, the angle of emission, the wavelength, and the temperature.

2.3.2 Types and Characteristics

Spectral band pyrometers measure radiation only in a narrow wavelength band (practically at one specific wavelength) so that the "effective wavelength" (Reference 2-35) is essentially independent of temperature. If the spectral emittance of the specimen surface is known at the effective wavelength, then the difference between the true temperature and the temperature determined by the pyrometer can be calculated.

Wide band or total-radiation pyrometers measure what is often termed the brightness temperature, which is defined as that temperature at which a blackbody would emit the same radiant flux as the specimen surface at the effective wavelength of the pyrometer. They measure a much broader spectral range than that measured by narrow band pyrometers. The effective wavelength of these pyrometers is temperature dependent, so that numerical methods are required to accurately determine surface temperature from radiation measurements made with these instruments. Before the silicon cell became widely used in the 1960's, total radiation pyrometers using thermopile detectors were the predominant industrial pyrometer. These devices are sensitive to more than 90% of the radiation emitted from the target, so that the curve of measured radiation versus temperature follows the Stephan-Boltzman curve. Actual temperature can be calculated if the total emittance of the specimen surface is known.

Numerous pyrometers measure radiation from more than one spectral band. The most widely used of these pyrometers is the two-color, or ratio, pyrometer (Reference 2-36) in which the temperature is determined from the ratio of the radiation measured at two different wavelengths. In principle, these instruments are insensitive to emittance as long as the emittance of the specimen is the same for both wavelengths. The assumption of nonvarying emittance at the individual wavelengths is reasonable for many materials, and for special cases, problems can be minimized by making the two bands close to each other.

Instruments based on intensity ratio at two wavelengths are usually more sensitive to the effect of radiation reflected from the

specimen surface. This has been demonstrated experimentally in our laboratory and verified by discussions with manufacturers of commercial instruments.

Considerable effort has gone into using multiple wavelength pyrometers to reduce the effect of emittance on temperature measurements using radiation pyrometry. Svet (Reference 2-37) and Quinn and Compton (Reference 2-38) suggested that it is possible to calculate temperature from spectral radiance measurements made at multiple wavelengths without prior knowledge of emittance value. These techniques involve assuming a functional dependence between spectral emittance and wavelength and then using the radiance data to determine adjustable parameters and temperature by solving simultaneous equations. Babelot et al. (Reference 2-39) described a multiwavelength pyrometer that was designed to achieve a spatial resolution of 100 μm and a time resolution of 10 ns. Using the data from six spectral bands, they claimed they could determine the functional dependence of emittance on wavelength. Hunter et al. (Reference 2-40) presented a method of determining temperature by using a multichannel analyzer to measure 200 spectral bands simultaneously. Assuming only that emittance was a smooth function of wavelength, they were able to calculate temperature without prior knowledge of emittance. They demonstrated that their technique was accurate to within 1% when measuring the temperature of platinum up to 1724 K. Neither of these instruments was capable of compensating for the effect of reflected radiation.

Other investigators have expressed doubt that multi-wavelength pyrometry is a practical method of eliminating errors caused by varying emittance. Coates (Reference 2-41) showed that in the absence of precise knowledge of the relationship between emittance and wavelength, it is impossible to estimate the uncertainty associated with temperature measured with an n-wavelength pyrometer, where $n > 3$. He showed that even if the spectral dependence of emittance is accurately known, calculated temperatures are increasingly sensitive to errors in the radiance measurement as the number of channels, n, increases. Since accurate knowledge of emittance of solids as a function of wavelength is generally unavailable, Coates believes that multichannel pyrometry has little to recommend it. Nordine (Reference 2-42) concurred with Coates and concluded that measuring three or more spectral radiances had little practical value without unprecedented increases in the precision and accuracy of spectral radiance measurements.

2.3.3 Effect of Reflected Radiation

Most multiwavelength pyrometers are designed to enable surface temperature measurements to be made without prior knowledge of emittance. Knowledge of emittance is not in general sufficient to permit calculation of true surface temperature from the radiance measurement. Radiation reflected from other hot surfaces into the entrance aperture of the pyrometer can cause significant errors in temperature measurements. Atkinson and Strange (Reference 2-43) reported errors in pyrometer temperature measurements of turbine blades of 75 K at an actual surface temperature of about 1300 K. Because ceramics generally have lower spectral emittance at a wavelength of 1 μm than oxidized metal surfaces, the problems associated with

reflected radiation can be expected to be more pronounced for ceramic turbine parts.

A method for dealing with reflected radiation using a dual wavelength band pyrometer is based on the fact that radiation from a high temperature source will affect the two bands differently (Reference 2-43). It is assumed that the primary source of reflected radiation is the combustion gas and that the target is surrounded by parts operating at temperatures not much different from itself. In addition, the amount of energy from the hot gas reflected from the target surface is a function of complex geometry factors which are difficult to calculate but which may affect the wavelength bands equally. Equations were derived for these assumptions and used to calculate reflected radiation errors based on estimated combustion gas temperature. Two bands within the operating range of a silicon detector were used to evaluate the concept on a laboratory test strip (using a tungsten filament lamp as the reflector source) and a rotating turbine blade row in an operating gas turbine engine.

Results of these tests were promising. However, Atkinson and Strange's assumptions may not be applicable to ceramic materials, especially those which show large changes in emittance as a function of wavelength in the wavelength range of the detector.

The concept of identifying reflected radiation by examining the polarization characteristics of total (emitted and reflected) radiation from a target surface is described by T.P. Murray (Reference 2-44). The instrument was developed to measure the surface temperature of metals with large variations in emittance without specific prior knowledge of the actual target surface emittance. It involved examining the combined radiance from a target surface which included emitted energy due to its own temperature plus energy reflected from a blackbody source at known temperature by means of a rotating polarizing analyzer. The polarization of the normally unpolarized blackbody radiation caused by reflection from the target was 90° to the emitted radiation from the target surface. Relationships were derived showing that the temperature of the blackbody source was equal to the target surface whose emittance was unknown when the a.c. component of the signal from the rotating analyzer was zero.

The polarization characteristics on which Murray relied are not generally found in diffuse radiators typical of most ceramic materials. We believe, therefore, that the probability of successful isolation of reflected from emitted radiation using polarization techniques appears to be low.

The problems associated with reflected radiation can be minimized by limiting the radiance measurements to wavelengths in which the specimen has a high emittance. A suitable spectral range in which most ceramics have high values of emittance and in which the combustor gas stream has low absorption is found between 8 and 10 μm.

2.3.4 Adaptability to Ceramic Materials

Noncontact sensing, unlimited temperature range, and maturity of the technology make radiation pyrometry a strong candidate for use in measurement of ceramic surface temperatures. Effects of unknown or variable surface emittance and transmittance and reflected radiation from surrounding components and combustion gases are major obstacles in obtaining accurate

measurement in a gas turbine hot section environment.

Most historical applications of radiation pyrometers in gas turbine engines have been related to measurement of surface temperature of metallic turbine blades. Typical blade materials have relatively high (0.85 to 0.9) emittance values after a short time at operating temperature and do not change significantly over time. The effect of radiation reflected from nearby surfaces and combustion gases, which flucuates widely, is minimized by the high emittance of metallic superalloys in the wavelength band of silicon detectors (0.4 to 1.2 μm).

Ceramic materials are difficult to categorize with respect to emissivity. Typical emittance values for some ceramic materials are listed in the following table at two wavelengths.

Table 7 illustrates that some ceramics closely approximate metallic superalloys in emittance characteristics, but others do not. For those materials with very low emittances, errors due to reflected radiation will be unacceptably large unless a method for accounting for it is incorporated in the measuring system.

Table 7. *Average Normal Spectral Emittance at Two Wavelengths (From Reference 2-45).*

Material	λ = 1 μm	λ = 8 μm
Alumina	0.10	0.85
Zirconia (coating)	0.10	0.85
Silicon Nitride	0.82	0.98
Silicon Carbide	0.90	0.95

2.3.5 Long Wavelength Pyrometer

One method of reducing the effect of reflected radiation is to select a wavelength band where emittance values are as high as possible. For example, it is possible to reduce the observed reflected energy on a zirconia coated surface from 90% to 15% by shifting the detector wavelength from 1 to 8 μm.

Although long wavelength pyrometry does not solve the problem of reflected radiation entirely, it leaves us in approximately the same position with respect to ceramics as we are in now with the metallic superalloys and silicon detectors. In addition to the higher emittance of ceramics at 8 to 10 μm, long wavelength pyrometry may reduce the effect of reflected radiation in a second way. The relatively steeper slope of the Planck radiation curve at short wavelengths means that, if the reflected component is a given fraction of the total radiation emitted from the specimen surface, then it will have a correspondingly greater effect at short wavelengths than at long wavelengths.

A comparison of error caused by reflected radiation on a target surface is shown in Figure 7 for two combinations of wavelength and emittance (1 μm and 0.3; 8 μm and 0.8). A target surface temperature of 1366 K (2000° F) is assumed for this calculation. A sketch of the target and reflector arrangement and definition of terms is included in Figure 8.

Use of a long wavelength detector does not solve the problem of determining emittance of the target surface. Knowledge of emittance is still necessary to permit calculation of temperature from measured radiant energy. Emittance measurements can be made on the target surface over a range of temperature and spectral bands prior to installation

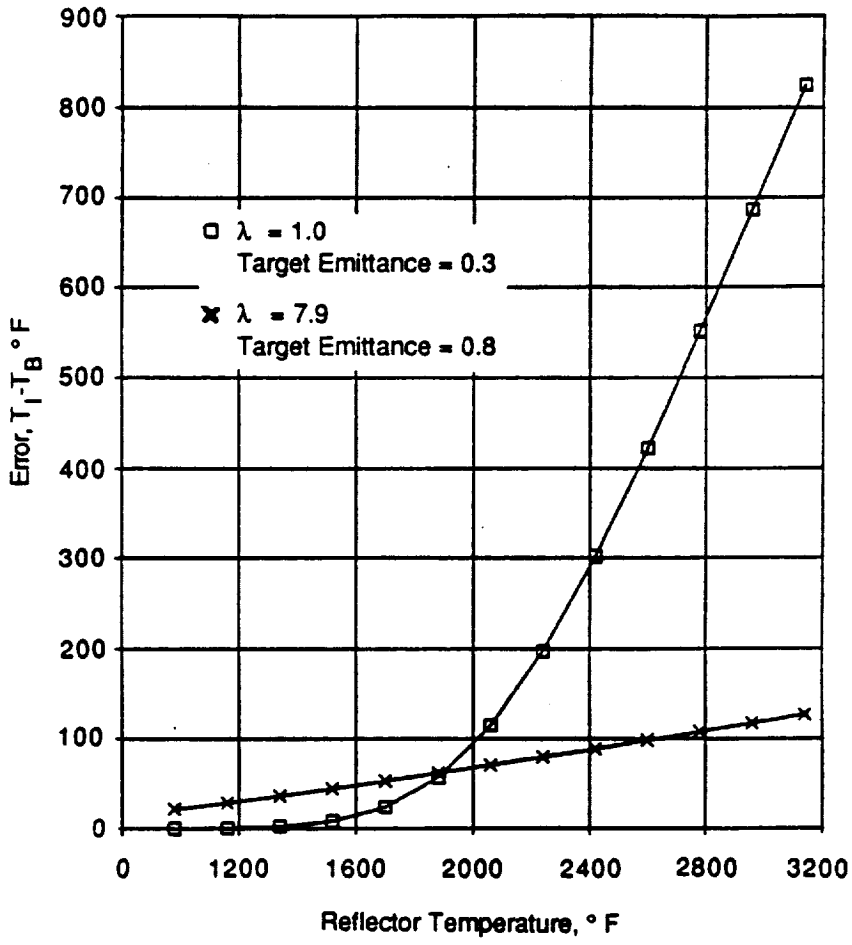

Figure 7. *Error Due to Reflected Radiation for Fixed Target Temperature of 2000° F as a Function of Reflector Surface Temperature. See Figure 8 for calculation procedure.*

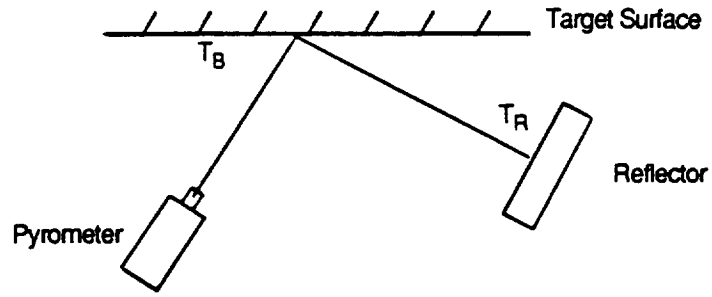

$$W_T = E_B W_B + (1 - E_B)(F_{R-B})(E_R W_R)$$

$$W_T = E_B W_I$$

$$W_I = \frac{C_1 \lambda^{-5}}{e^{(C_2/T_I \lambda)} - 1}$$

$$T_I = \frac{C_2}{\lambda \ln\left(\frac{C_1 \lambda^{-5}}{W_I} + 1\right)}$$

Error = $T_I - T_B$

T_I = Indicated Target Temperature

T_B = Target Surface Temperature = Constant 1366 K (2000° F)

T_R = Reflector Surface Temperature

E_B = Target Emittance = 0.3 at1μm; 0.8 at 8μm

E_R = Reflector Emittance = 1.0

F_{R-B} = View Factor

W_T = Total Spectral Radiance

W_B = Spectral Radiance Emitted from Target

W_R = Spectral Radiance Emitted from Reflector

W_I = Indicated Spectral Radiance from Target

C_1 = Planck's First Radiation Constant

C_2 = Planck's Second Radiation Constant

λ = Wavelength

Figure 8. *Calculation Procedure for Plot of Error Versus Reflector Temperature (Figure 7).*

of the component into the test vehicle. Where this is not practical, it is possible to make emittance measurements on the installed component by measuring the reflected energy from an excitation pulse at the specific wavelength for which the detector has been calibrated. This technique has been demonstrated in our laboratory using a prototype instrument described in Reference 2-46.

The error caused by target surface emittance uncertainty at two wavelengths is plotted as a function of temperature in Figure 9. At 1 and 7.9 μm, errors of 0.1 and 0.05 respectively are assumed. Justification for the higher uncertainty at the lower emissivity is based on larger variability in emittance data at lower emittance levels (Reference 2-45) This is believed to be realistic for situations where emittance for a typical target surface is measured in a laboratory environment and then used to calculate temperature from target surfaces exposed to effects of time at temperature in a gas turbine flowpath. If this assumption is not valid, and emittance uncertainties are the same at all wavelengths, then larger errors in temperature will be caused at the longer wavelengths.

There are some special problems created by the use of long wavelength detectors which should be considered.

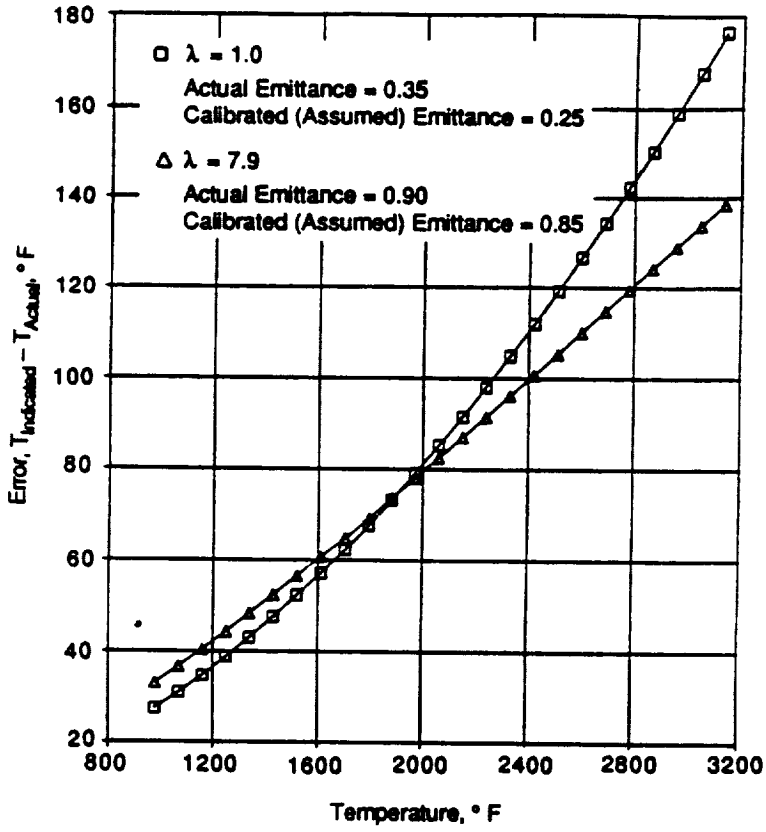

Figure 9. *Error Due to Emittance Uncertainty at Two Levels of Emittance as a Function of Temperature.*

- Sensitivity: The relationship between radiant energy and temperature in the 8 μm region reduces the sensitivity compared with that near 1 μm. This will result in reduced resolution and a lower signal-to-noise ratio, or may increase the minimum target area.

- Detector Performance: Many detectors suitable for use at 8 μm are less convenient than silicon. Cryogenic cooling of the detector or chopping of the optical signal may be required.

- Optical view path materials are much more limited for 8 μm systems. Quartz and sapphire are not suitable. Special optical materials will be required. Fiber optic coupling may not be practical.

2.4 Concept Description and Analysis - Resistance Thermometry

2.4.1 Platinum Resistance Thermometer

Numerous thermometers are based on the temperature variation of resistance of pure metals or metal oxides. Since the 1920's, the platinum resistance thermometer (PRT) has been used as a standard from cryogenic temperatures to over 900 K. Crovini (Reference 2-47) and Quinn and Compton (Reference 2-48) reviewed platinum resistance thermometry, primarily in regard to its use as a temperature standard. The latter paper also evaluates measuring circuits used in platinum resistance thermometry.

Evans and Burns (Reference 2-49) reported data on the stability of platinum resistance thermometers at temperatures as high as 1400 K. They used disks of synthetic sapphire, silica, and other materials, spaced along a central Pt rod. Lengths of Pt wire about 40 mm long were threaded through holes in the disks and welded in series at their ends, forming a "bird cage" resistor. In some cases, their thermometers showed resistance drifts corresponding to temperature changes no larger than a few hundredths of a degree after several hundred hours at 1400 K. Although valuable as a calibration instrument, the high-precision platinum resistance thermometer is a fragile and delicate instrument which does not have direct applicability to measurement of component surface temperature in turbine hot sections.

2.4.2 Resistance Temperature Detectors

There is a class of resistance thermometers known as resistance temperature detectors (RTD's) that are intended for industrial use. In these devices, a platinum or platinum alloy resistance element is embedded in ceramic or glass. This gives the resistance sensor robustness, but at the same time reduces its stability compared to that of the PRT. There are two main reasons for temperature instability of RTD's. First, differences in thermal expansion between the resistor and the matrix in which it is embedded can introduce strains in the element which may cause the resistance to change. Second, the matrix material or impurities therein can react with the sensor, causing calibration shift. The contamination problem limits available industrial RTD's to temperatures less than about 1200 K (Reference 2-50). Thin film configurations of RTD's can be expected to increase problems associated with contamination of the sensor as well as making the sensor more susceptible to stress. For these reasons, GE does not believe that platinum alloy RTD's are good candidates

for high temperature measurements in the hostile combustor environment.

Metal oxide semiconductors, or thermistors, are widely used as industrial resistance temperature elements. They typically consist of mixed oxides of nickel, manganese, and cobalt which have a negative temperature coefficient of resistance. For temperatures above about 600 K, more refractory oxides are required. The oxides of rare-earth elements have been used up to about 1000 K, while devices based on yttria-doped zirconia are available for temperatures up to about 1300 K. Anderson and Stickney (Reference 2-52) tested high purity alumina and mullite sensing elements made from solid rods to 1833 K, with good success. They suggest that an upper temperature limit of 1944 to 2500 K may be possible using MgO or BeO sensing elements. However, we could find no additional references to successful use of ceramic element RTD's at high temperatures.

Sensing elements fabricated from ceramic materials have potential for operating at temperatures well above 1400 K. The lack of information in the literature concerning stability of these sensors is not encouraging. The problems of lead integrity and sensor stability can be expected to become more severe in the hostile combustor environment. These factors lead to the conclusion that ceramic element low profile RTD's for surface temperature measurement in turbine engine hot sections have some potential, but will require considerable effort and have a relatively low probability of success.

2.5 Concept Description and Analysis - Laser-Induced Fluorescence

2.5.1 Concept Description

Remote temperature measurement by laser-induced fluorescence (LIF) has been well established for gas and surface temperature measurements (References 2-52 through 2-55). In many applications, LIF techniques offer a relatively simple analytical technique that is well suited for a variety of laboratory and industrial applications.

Certain fluorescent materials, known as thermographic phosphors, can be used as temperature indicators in either of two modes (Reference 2-56). Both the ratio of selected emission line intensities and the lifetime of a particular line have been used to determine temperature. The ratio approach is a rather more complex experimental procedure and consequently has been used less for surface temperature measurements. More commonly, temperature is determined by measuring the fluorescent decay time of the phosphor. In many instances, luminescent decay follows the Arrhenius relation: Decay Time Constant is proportional to $e^{-(E/kT)}$, where T is the temperature, E the activation energy, and k is Boltzmann's constant. The lifetime of such an excited state can be measured by exciting the luminescent material with pulsed radiation of an appropriate energy, thereby causing it to fluoresce as it decays back to the ground state. By monitoring the decrease of the fluorescent intensity with time after the excitation has ceased, the lifetime of the excited state can be deduced. The decay time of the fluorescent material is observed to decrease with increasing temperature. Hence, an empirical correlation of the decay

time with temperature can provide the basis for a temperature measurement system.

When using LIF of thermographic phosphors to make surface temperature measurements, it is highly desirable, although not strictly necessary, that the decay of at least certain spectral lines originate from a single component process so that the decay follows the Arrhenius relation. In such cases, the decay time can be determined by measuring the fluorescent intensity at two instants after the phosophor has been excited. It is even more important, however, that the decay at a given temperature be highly reproducible, that it not be a function of excitation intensity, and that there be no hysteresis with respect to either prior excitation or prior thermal exposure.

2.5.2 Current Capabilities

An active development program, funded by the Air Force and the Department of Energy, is underway at Los Alamos National Laboratory to explore using LIF of rare earth phosphors to measure surface temperatures in hostile environments (Reference 2-57). This group has determined that the 612 nm spectral line of Eu-doped yttria is a good candidate for the temperature range in which they are interested (up to 1500 K). At 1500 K, the lifetime of this line is approximately 10 ns, or at the limit of the resolution of the signal precessing equipment used by the Los Alamos group. By 1700 K, the decay time is expected to be less than 1 ns, a reasonable lower limit for a practical fluorescent decay measurements (Reference 2-58), although significantly shorter lifetimes can be measured using single photon counting methods (References 2-59 and 2-60). Even if suitable instrumentation were available to measure 1 ns decay times, Eu-doped yttria may not provide sufficient signal intensity for measurements at temperatures significantly higher than 1500 K.

Developmental work with LIF of high temperature thermographic phosphors has proceeded beyond the stage of questions concerning feasibility: it is feasible. Significant questions remain regarding the extent to which LIF methods can be applied in combustor environments. An outstanding question concerns the maximum surface temperature at which fluorescent measurements of thermographic phosphors can be made. As discussed above, LIF measurements cannot currently be expected to measure surface temperatures above 1700 K, and 1500 K may in fact be a practical limit for Eu-doped yttria.

2.5.3 Candidate Phosphors and Upper Temperature Limits

A significant increase in the measurable temperature using thermographic phosphors can only be expected from other phosphors (or other spectral lines of Eu-doped yttria). Little research has been done to determine whether or not candidates for higher temperature measurements exist. It is known, however, that Eu-doped yttria fluoresces up to its melting point near 2700 K (Reference 2-61); whether or not it exhibits a useful thermographic effect at such temperatures is not known. There are other thermographic phosphors whose properties warrant investigation at temperatures exceeding 1500 K. For example, Gd-doped yttria has spectral emission lines that are not quenched at 1300 K and may be a candidate phosphor for temperature measurements over 1500 K. For theoretical reasons, Eu-doped scandium oxide appears to be an attractive high temperature phosphor, although no references to its use could be

found. There is room, therefore, for optimism that suitable phosphors exist to measure temperatures higher than 1500 K. More experimental evidence is needed to answer this question definitively.

2.5.4 Phosphor Application to Test Part

An area of concern related to use of LIF of thermographic phosphors in hostile environments concerns adherence of the phosphor to the test surface. Although LIF surface temperature measurements may be considered noncontacting, they require that the phosphor be applied to the test surface. Several methods have been explored for applying the phosphor, including sputtering, E-beam vaporization, plasma spray, and flame spray (Reference 2-62). Other methods such as chemical vapor deposition may also have application. Satisfactory bonding for high temperature metallic turbine parts has been only partially successful, and this problem may limit the application of LIF temperature methods in hostile environments.

2.5.5 Recommendations

LIF of thermographic phosphors is a promising method of surface temperature measurements for selected applications. It is probably too complex for routine measurements, however. We believe that it may find important use as a calibration tool for other surface temperature methods.

2.6 Concept Analysis and Description - Noise Thermometry

2.6.1 History

Noise thermometry was introduced by Garrison and Lawson in 1949 (Reference 2-63). It is based on measuring the noise voltage, current, or power generated across a resistor to infer the temperature of the resistor. It has the significant advantage of being independent of environmental conditions and of the properties of the material of the resistor. In addition, Johnson noise thermometers are linear devices that measure absolute temperature. Although the principles of noise thermometry have been established for decades, only in the past fifteen years has practical use been made of the technique.

2.6.2 Theory

The mean square noise voltage Vn of a passive device is given by:

$$Vn^2 = \frac{4kTR\,(hf/kt)}{e^{(hf/kt)} - 1} \qquad (1)$$

where h and k are Planck's and Boltzman's constants, respectively, T the absolute temperature, f the frequency, and R is the resistance. For ratios of f/T of less than about 10^7 Hz/K, equation (1) may be approximated by:

$$Vn^2 = 4kTR \qquad (2)$$

For a given frequency bandwidth Δf, the rms voltage Vn, and noise current In are given by

$$\langle Vn \rangle = [4kTR(\Delta f)]^{1/2} \qquad (3a)$$

$$<In> = [4kT(\Delta f)/R]^{1/2} \quad (3b)$$

By multiplying equations (3a) and (3b), the noise power is obtained:

$$<Pn> = 4kT(\Delta f) \quad (3c)$$

which demonstrates that, in principle, noise power is independent of the value of the resistance and is linear with respect to temperature. In fact, noise thermometers can measure either noise voltage, current, or power.

It should be noted that these equations apply only to the sensor: they do not take into consideration interfering signals from such sources as the noise pickup by the cables, internal noise generated by the signal processing, or Johnson noise from connecting leads.

Another important expression for noise thermometry, the Rice equation, describes the statistical error associated with noise measurements. Because noise is a randomly fluctuating quantity, it must be time averaged in order to measure it. The rms fractional uncertainty in the measured temperature, $(\Delta T)/T$, averaged over a time interval t is given by:

$$\Delta T/T = (4\Delta ft)^{-1/2} \quad (4)$$

Obviously, longer integration times and wider bandwidths will reduce the unavoidable statistical error.

2.6.3 Discussion

An attractive feature of noise thermometry is its ability to measure absolute temperature without reference to a calibration table: the calibration of the sensor is inherently linear and the noise is effectively zero at absolute zero. Compared with thermocouples, noise thermometers are reportedly less sensitive to shunting through the insulator and diffusion from the sheath into the sensor. A general analysis of the effect of insulator losses on a noise thermometer was reported by Crovini and Actis (Reference 2-64). They reported that the shunting conductance from BeO insulation around a 100 ohm sensor caused less than 2° C error in a 1800 K temperature measurement; alumina insulation caused about four times as much error. Because Johnson noise is a property common to all materials, noise thermometers are able to use a much wider selection of sensor materials than are thermocouples. Brixy (References 2-65 and 2-66) has investigated doped lanthanum oxide sensors for noise thermometry up to 1800 K and concluded that they offer advantages over traditional metallic resistors at high temperatures and in harsh environments. First, Brixy noted that ceramic resistors were more durable than metallic resistors at high temperatures. Second, their low temperature coefficient of resistance facilitated matching the impedence of the sensor with the transmission cable over a wide temperature range. Noise thermometers should also be subject to considerably less drift than thermocouples. As such, if a suitable thermocouple is not available for a particular application, noise thermometry is an attractive alternative.

One of the main reasons for the growth of noise thermometry has been improvements in signal processing that permit accurate measurement of noise signals which are typically less than a microvolt at a few nanoamperes. Because of the low signal levels, more than one measurement is generally required for accurate temperature

measurement. A variety of signal processing methods have been used in noise thermometry (Reference 2-67). The cross correlation technique, introduced 20 years ago by Brophy (Reference 2-68), simultaneously measures noise voltage with two amplifiers. Signals from the two amplifiers are then correlated so that the uncorrelated noise from the amplifiers and signal cabling is eliminated. Correlation techniques are, however, probably too slow for general use in the gas turbine environment. Brixy (Reference 2-69) developed a four-lead system to eliminate the noise generated by cables, while Klempt analyzed sources of uncertainty in cross correlating noise thermometers (Reference 2-70).

In recent years, Johnson noise power thermometry (JNPT) has received considerable attention. As the name suggests, JNPT involves determining the noise power, from which temperature can be inferred using equation (3c) above. In essence, JNPT involves measuring both the open circuit noise voltage and the closed circuit noise current using separate current and voltage sensitive amplifiers. It is, however, necessary that the gains and signal bandwidths of the amplifiers be known.

One of the earliest noise power thermometers was described by Borkowski and Blalock (Reference 2-71) and was refined by Blalock et al. (Reference 2-72). Their instrument was designed to measure temperatures up to 1000 K and employed a 100 ohm platinum resistor as the noise source. While making two measurements complicates the instrumentation, noise power measurement allows an absolute temperature measurement that is independent of the resistance of the sensor (see above). This is helpful in a hostile environment in which the sensor resistance may vary because of erosion and/or oxidation. Unfortunately, the open circuit voltage and short circuit current cannot be measured simultaneously on the same sensor, so that cross correlation techniques cannot be used to eliminate noise from the amplifiers and transmission cables. The noise power thermometer is, therefore, inherently sensitive to external noise pick-up and noise generated by connecting cables, and probably requires a more "quiet" environment than is generally available in industrial applications.

Despite fundamental virtues, significant practical obstacles must be overcome before noise thermometry can become widely used in industrial applications. The low signal levels produced by sensors make the problem of eliminating noise from non-thermal origins challenging. Spurious noise signals in lead resistances and electronic signal processing components have seriously hampered noise thermometry in practical applications. A quantitative analysis of design considerations of preamplifiers in noise thermometry can be found in Reference 2-71. Tasman (Reference 2-73) noted that other researchers reported virtually eliminating noise generated from the transmission line by using a cross correlation technique. The noise voltage from one sensing resistor was sensed by two identical amplifiers in two branch circuits. Because the noise generated from one branch was not correlated with that in the other branch, the spurious noise output tended toward zero with increasing integration time.

Like thermocouples, noise thermometers are subject to errors caused by leaky insulation. For this reason alone, they probably cannot greatly extend the temperature limits achieved by thermocouples. Because noise

thermometry does not rely on specific material characteristics that can change over time, they retain their calibration better than thermocouples when exposed to long operating times. Further, a much wider range of materials can be considered for noise thermometers than for thermocouples so that it can probably be adapted better to hostile environments.

2.6.4 Adaptability to Gas Turbine Environment

Even if practical obstacles to noise thermometry are overcome, this technique will have limited usefulness in combustor environments. First, the requirement of attaching the sensor to the specimen surface will limit the hostile environments in which noise thermometers can be applied. Second, noise sensors probably do not lend themselves to thin film configurations except in environments free of electromagnetic interference (EMI). The requirement for shielding the sensor from EMI is likely to make noise thermometry a more intrusive technique than thin film thermocouples. Third, noise thermometers are relatively slow devices that require averaging in both space and time. Typically, the noise signal integration periods exceed 10 seconds, although larger signal bandwidths may reduce this appreciably.

With impetus from both the nuclear industry and the space program, noise thermometry is an active phase of development. While experts in the field believe that problems associated with noise thermometry are not insuperable, this technique will probably require more sophistication of the user than do traditional methods such as pyrometry or thermocouple thermometry.

2.7 Concept Description and Analysis - Fiber Optic Temperature Sensors

Fiber optic devices for measurement of temperature can be categorized according to the specific sensed parameter. One type of fiber optic sensor collects energy from a local zone (usually the tip) and converts the measured energy to temperature using techniques similar to those previously discussed with regard to radiation pyrometers. Another type of sensor uses the temperature dependent propagation characteristics of the fibers to sense temperature by means of interferometric techniques. Neither type is ideally suited for surface temperature measurement because both require physical attachment or insertion into a surface cavity at the point of measurement.

2.7.1 Techniques Based on Variability of Fiber Optic Properties

Numerous temperature measuring systems based on interferometers consisting of fiber optic legs have been proposed (References 2-74 through 2-75). In these devices, temperature variations produce phase changes in the optical signal passing through the fibers by varying the propagation constants of the fibers. Although they are not ideally suited for surface temperature measurements because they generally must be attached to the surface, some of them could be adapted for surface measurements.

Fiber optic interferometers can be classified into two categories: single fiber and dual fiber interferometers. Single fiber interferometers consist of one fiber propagating two modes that exhibit different phase delays in response to temperature changes. Dual fiber interferometers (Reference 2-74) use two fibers, each of which carries one mode.

One of the fibers is exposed to the test conditions while the other is kept at constant temperature and acts as the reference. Single fiber interferometers are inherently advantageous for operation in hostile environments for two reasons. First, they are much simpler in construction. Second, since both modes of the interferometer are subject to identical conditions of pressure, stress, and vibration, these devices offer greater common mode rejection for environmental factors (Reference 2-75). In essence, single fiber interferometers respond only to forces that affect the two modes differently.

Corke (Reference 2-76) demonstrated a temperature sensor, the "polarimetric interferometer," based on the temperature induced change in birefringence of a single highly birefringent silica fiber. Temperature changes affect the magnitude of internal lateral stresses and, therefore, the fiber is birefringent. It is expected that neither background blackbody radiation nor spurious internally generated radiation significantly affect the temperature sensor because these sources are incoherent (Reference 2-76). Corke claimed that his polarimetric temperature sensor was suitable for use in hostile environments such as turbine engine hot sections. Since his experiments were restricted to temperatures less than 500 K, this prediction may be optimistic. According to one of Corke's co-researchers, David Jackson, it is questionable whether polarization preserving fibers can be produced to work at combustor temperatures. Until a material is found that exhibits the desired birefringent properties at elevated temperatures, the polarimetric sensor does not warrant serious consideration for use in turbine hot sections. It has been reported that sapphire does exhibit birefringence at high temperatures (Reference 2-77). Yttria-alumina-garnet (YAG) may exhibit desired birefringence up to about 1650 K.

Dunphy and Meltz (Reference 2-78) describe a twin core fiber optic sensor wherein the variability in coupling properties between the cores is temperature (and strain) dependent. By exciting one core and measuring phase shift between the cores at two wavelengths, it was possible to extract temperature and strain data at temperature levels up to 650 K with a sensing length of 6 mm.

It should not be concluded, however, that material limitations are the only constraint on polarimetric temperature sensors. Challenging, although not necessarily insuperable, problems with respect to signal processing, the need for optical components in the vicinity of the sensor to recover phase information may limit the remote use of these sensors. These difficulties, and approaches to their resolution, are discussed in Reference 2-79.

2.7.2 Collected Energy Techniques

This concept is based on measurement of radiant energy transmitted from a sensing zone (usually located near the tip of a fiber optic device) to a detector (typically located at the cold end). If the sensing zone of the fiber is configured as a blackbody cavity, the temperature level can be related to measured energy by Planck's equation. Dils (Reference 2-80) describes a system of this type which uses an opaque coating applied on the outer surface of a sapphire rod to form the blackbody cavity (for measurement of gas temperature). Such a configuration has potential for use up to 2200 K, although problems associated with leakage of radia-

tion through the fiber and coating durability have not yet been fully resolved.

Surface temperature could be sensed by embedding the tip of the fiber optic device in a surface cavity at the point of measurement. We have demonstrated the (mechanical) feasibility of attaching a gold clad quartz fiber optic device on the surface of a metal turbine blade using flame sprayed alumina. This method appears to be satisfactory up to the limit of the gold quartz fiber optic.

2.8 Concept Description and Analysis - Ultrasonic Thermometry

2.8.1 Concept Description

Ultrasonic thermometry makes use of the temperature dependence of the velocity of sound in gases, liquids, or solids (Reference 2-81). The velocity with which sound propagates through a particular material is a function of the physical state of the material, its density, and other physical parameters. For solids, which support both compression and shear, the velocity of sound is directly proportional to the square root of a stiffness modulus M divided by the density. The velocity of sound through the solid depends on the type of wave propagated as well as the state of the material (Reference 2-82).

2.8.2 Resonant Frequency Technique

Several types of ultrasonic thermometers have been developed. In 1972, Benjaminson and Rowland (Reference 2-83) reported a thermometer using changes in the resonant frequency of a quartz crystal to measure temperature. This device, which was developed into a commercial product by the Hewlett Packard Company, offered extremely high temperature resolution and excellent stability. Bell, working in England, developed several practical high temperature sensors based on measuring the resonant peaks of crystalline materials (References 2-84 and 2-85). Using a sapphire tuning-fork sensor, Bell was able to measure temperatures over 2200 K, even in oxidizing atmospheres. Although such techniques can measure high temperatures with excellent resolution and stability, they are limited in their application by the required isolation of the resonator from mechanical contact at all points except nodal points. Therefore, they are not considered candidates for field measurements in hostile environments.

2.8.3 Pulse Echo Technique

Numerous ultrasonic thermometers have been developed based on the measurement of the propagation time of an ultrasonic wave in a refractory wire sensor (References 2-82 and 2-86 through 2-89). Virtually all such systems operate in the pulse-echo mode, the theory of which has been well documented for nearly 20 years (References 2-90 and 2-91). In the pulse echo technique, a magneto-strictive sensor introduces ultrasonic pulses into a transmission line. The sound pulses are partially reflected at discontinuities in the wire and at the end of the wire. Typically, the time delay between echoes measures the ultrasonic propagation time between well-defined points in the sensor. From the measurement of propagation time between points a known distance apart, a line average temperature over the length of the sensor can be determined. Temperature profiles along lengths of wire a meter or longer also can be deduced from ultrasonic measurements. Sensors are typically a few

centimeters long with a total response time comparable to that of thermocouples.

In practical thermometers using the pulse-echo technique, the wire sensor is situated in a protective sheath. Although the pulse-echo method is generally less sensitive to mechanical pertubations than the resonance technique, mechanical contact between the sensor and the sheath has been a problem in ultrasonic thermometry. While light contact pressure can generally be tolerated, high pressures can disturb or even entirely block the echo signal. Particularly at elevated temperatures, the sensor may actually attach to the sheath in a phenomenon known as "sticking." Tasman (Reference 2-92) reviews several methods by which the problems associated with sticking can be addressed and suggests that to a large degree the problem has been successfully addressed in numerous applications. Contact problems could be more severe in the high vibration environments, however.

Although in principle sensors could be fabricated of virtually any material, practical sensors must survive their intended environment and should have a large change in sound velocity over the temperature range of interest. Sensors for measuring high temperatures have been made of rhenium (Reference 2-93), thoriated tungsten (Reference 2-94), and tungsten-rhenium (Reference 2-95), among other materials. This flexibility in terms of sensor materials permits materials capable of withstanding oxidizing environments to be used as sensors. Unfortunately, the speed of sound generally varies less with temperature in ceramics than in metals. Ceramic sensors would, therefore, probably be less sensitive than are metal sensors. Nevertheless, sapphire or ceramics are candidate sensor materials for pulse-echo ultrasonic thermometers operating in hostile oxidizing environments up to 2200 K.

2.8.4 Adaptability to Ceramic Materials

Applying ultrasonic thermometry to ceramic materials would require attaching a sensing element to the component surface so that the sensor is thermally coupled and acoustically isolated from the surface. Metallic materials provide greater variation of acoustic velocity as a function of temperature than typical nonmetals, but may not be practical due to thermal expansion mismatch or chemical incompatibility with ceramic substrates. Small diameter sapphire is a candidate for high temperature applications.

In a review of ultrasonic thermometry, Lynnworth (Reference 2-82) distinguishes two broad categories of sensors. The first category, of which the pulse-echo technique is an example, inserts a sensor whose ultrasonic velocity is to be measured into a thermal enclosure. These methods require attachment of the sensor to the specimen surface. The second of Lynnworth's categories used "the medium itself as the sensor." Successful development of an "intrinsic sensor" could open wide-ranging applications for ultrasonic thermometry. An intrinsic ultrasonic thermometer could, in principle, use a laser to acoustically excite the target surface. It may also be possible to detect the acoustic signal remotely. Promising studies along these lines have been conducted by Rockwell International and indicate potential for contactless measurement of surface temperature in hostile, high temperature environments. We have been unable to obtain specific information about these studies. Remote methods of generating ultrasonic pulses and of measuring the echo

appear to have significant potential for use on high temperature ceramic materials. However, the necessary technology is not well developed at this time.

Ultrasonic thermometry in general, and the pulse-echo technique in particular, should benefit from advances in instrumentation that permit routine measurements of nanosecond time intervals. Improved signal processing instrumentation should allow use of coherent detection schemes to demodulate coded pulse trains. Such methods could reduce the expertise required of operating personnel as well as allowing valid information to be derived from noisy signals. Given the high temperatures (over 2200 K, according to reports summarized in Reference 2-95) that pulse-echo techniques can measure with errors less than 2%, ultrasonic thermometry must be regarded as a candidate for high temperature measurements in hostile environments.

2.9 Concept Description and Analysis - Raman Measurement Techniques

2.9.1 Concept Description

The Raman effect occurs when light illuminates a material containing molecules that can undergo a change in polarization as they vibrate. When Raman scattering is present, light is scattered not only at the frequency of the incident light, but also at frequencies corresponding to the sum and difference of this frequency and the molecular vibrational frequencies. Thus, the Raman spectrum occurs as a series of discrete frequencies, shifted symmetrically above and below the frequency of the exciting radiation. The spectral lines that are most frequently studied are those on the low frequency side, the Stokes lines, which are more intense than the corresponding anti-Stokes lines on the high-frequency side.

Raman scattering techniques have been used extensively to measure temperatures of combustion gases from turbine engines (Reference 2-96). As far as could be determined from a literature survey, however, little work has been done to apply Raman spectroscopy to surface temperature measurements.

2.9.2 Adaptability to Ceramic Materials

It has been shown (Reference 2-97) that for certain ceramic materials, such as silica, the ratio of the intensities of the Stokes and anti-Stokes lines is a function of the temperature of the surface from which the light is scattered. Therefore, the Stokes to anti-Stokes intensity ratio may provide the basis of a surface temperature measurement.

In one important respect, ceramics are good candidate materials for surface Raman spectroscopy: because incident light penetrates ceramic surfaces, signal intensity may be sufficiently high to permit good measurements. Numerous questions surround the use of Raman techniques in combustor environments, however. Whether or not sufficient signal intensity will exist at temperatures exceeding 1200 K is not yet known. The answer may depend on the material; wide bandgap materials such as silicon carbide may have useful signal intensities at combustor temperatures.

Even if laser induced Raman scattering will produce sufficient signal intensity, numerous questions need to be addressed. Pulse-to-pulse laser fluctuations, possible phonon

"hot-spots," and laser induced strain effects may all significantly reduce measurement accuracy (Reference 2-98). Experimental data is needed to establish whether or not Raman spectroscopy can be seriously considered for temperature measurements at combustor temperatures and for which specific materials it is feasible.

2.10 Concept Description and Analysis - Temperature Sensitive Coatings (for Determination of Maximum Temperature)

2.10.1 Description

This type of temperature measurement is accomplished by applying a temperature sensitive material to the surface by coating or molecular diffusion. After exposing the part to temperature, it is examined to detect changes in the coating which can be related to the maximum surface temperature to which the part had been exposed.

Goodman (Reference 2-99) describes a method for applying a surface layer of the radioisotope Kr_{85} to the surface of a part. Subsequent heating of the part causes release of the material. After thermal soaking/cycling is completed, the part is heated under controlled conditions. When the temperature reaches the maximum operating level, additional material will be released in measurable quantities.

A description of the characteristics of more conventional temperature indicating paints is covered in Reference 2-100. These materials are applied as surface coatings and undergo chemical reactions which cause color changes at discrete temperature levels up to 1623 K.

Kasanof and Kimmel (Reference 2-101) describe a series of coatings which melt at specific temperature levels, producing a phase change which can be detected by visual inspection following exposure. These materials are available in smaller temperature increments and are usually easier to interpret than color change coatings.

2.10.2 Recommendations

Temperature sensitive coatings have a limited usefulness because they provide an indication of maximum temperature and usually require removal or partial disassembly for visual access. They are included herein because of usefulness where temperature profiles over surface areas are required.

Accuracy is limited by incremental change levels which vary widely for the paints. Kryptonates require careful processing during application and controlled post test calibration.

2.11 Surface Temperature Sensing Concepts Proposed for Development

2.11.1 Selection Criteria

As outlined in the Introduction section of this document, additional effort associated with NAS3-25140 includes design, fabrication, test, and evaluation of three surface temperature sensing systems suitable for use on high temperature ceramic materials. The process of reviewing the literature and identifying which concepts to pursue has been

complicated somewhat by the general nature of the task. The selection process would have been easier in many respects if the requirements had been more specific.

We have observed that measurement technology tends to become more specialized as temperature levels increase. Substrate material properties and compatibility with sensor interfaces becomes more critical at higher temperatures. A concept which works well for one application may not work at all for another, seemingly similar, one because of a subtle difference.

Therefore, to a large extent, our choice of which sensing concepts to continue into te next phases of this contract are based on our perception of future sensor requirements and the specific ceramic materials which will be used for coatings and components in advanced gas turbine engines. These perceptions are based on historical measurement needs related to hot section component temperature requirements such as: rotating and stationary airfoil cooling effectiveness; hardware life expectancy; thermal transient stress.

We have weighted our selection criteria in favor of concepts which will be applicable to near term measurement needs based on current ceramic coating and structural material capabilities. Although the benefits will be realized sooner, the upper temperature limits will be reduced from the program Work Statement goals.

The concepts we propose to pursue include the following:

- Long Wavelength Radiation Pyrometer: The use of this device is based on the fact that alumina and zirconia ceramics have much higher emittances at wavelengths greater than 8 μm than they do in the visible region of the spectrum. This allows a significant reduction in corrections for reflected radiation errors.

- Ceramic or Intermetallic Thin Film Thermocouples (SiC, $MoSi_2$, WSi_2): These have high potential for operation up to 1600° C, are compatible with silicon based substrates and have high thermoelectric output.

- Platinum-Rhodium Alloy Thin Film Thermocouples: These are compatible with alumina ceramics. The relatively low anticipated upper temperature limit (1400°-1500° C) is balanced by the mature technology associated with application of these sensors.

2.11.2 Long Wavelength Radiation Pyrometer

The thrust of effort in this area will be to evaluate the effectiveness of long, narrow band wavelength detectors (8 μm) in reducing reflected radiation errors from ceramic materials which have low emittance at short wavelengths (1 μm). Such an evaluation will include setting up an experiment with known reflection component geometric effects and testing alumina and/or zirconia target materials in a combustion gas environment.

It is anticipated that this will be accomplished using a commercially available instrument which will not have the short time response required for a rotating turbine blade measurement. We will then compare requirements with capabilities of existing detector types and viewing optics to determine if a system with microsecond time response is feasible.

The basic reason for using the long wavelength approach as outlined in another section of this report is to reduce the correction for reflected radiation to 10%-15% of the total energy at the detector (from 85%-90% at 1 μm). This makes the task of correcting for reflected energy much less critical with respect to target surface temperature accuracy. Negative factors related to long wavelength pyrometers include lower energy sensitivity, slower time response, and more limited optical view path materials selection. Comparing the impact of the negative factors with the advantages of higher target surface emittance will be part of the evaluation effort devoted to this concept.

2.11.3 Ceramic or Intermetallic Thin Film Thermocouples

This concept was selected because of its applicability to silicon based substrates (such as silicon nitride and silicon carbide) which are not compatible with platinum at elevated temperatures on the basis of chemical inertness or thermal expansion.

The materials of interest include silicon carbide and silicides of molybdenum, tantalum, and tungsten. All have a similar oxidation protection mechanism which is based on the formation of a surface layer of SiO_2 which reduces additional oxidation and should be effective up to 1600° C.

Although the thermoelectric properties of these materials have been known for many years, relatively few applications have been used and virtually all of these have included large sensing elements made from bulk material and are inappropriate for the anticipated needs of this program. The technology for manufacturing thin film thermocouples of these materials is not well developed and will require some attention in this program, the goals of which are as follows:

- Select thermocouple element materials based on available application techniques and anticipated probability of success.
- Fabricate sensors on silicon carbide coupons with and without top coats for oxidation protection.
- Test coupons in ovens and high velocity combustion gases to determine thermoelectric stability and upper temperature limit.
- Fabricate sensors.
- Calibrate and test in laboratory ovens.

Since the fabrication of ceramic thermocouples in a thin film configuration is not a well developed technology, we anticipate some problems in fabricating adherent films and modifying them to establish thermoelectric properties. We do have the ability to sputter silicon carbide (SiC) and $MoSi_2$ but do not have in-house capability to dope films after application (films of pure SiC do not have thermoelectric properties and must be modified by application of impurities to be used as thermocouple elements). Preliminary testing indicates chemical vapor deposition (CVD) forms of SiC are superior to sputtered films. Doping of CVD SiC may be less practical than applying the CVD in the as doped form. A significant part of coupon and sensor fabrication effort may be subcontracted to firms with specialized equipment and expertise in this area.

2.11.4 Platinum-Rhodium Alloy Thin Film Thermocouple

This concept was selected because we think it can be used for near term applications on alumina (or other relatively high expansion, non-silicon based ceramic substrates) with upper temperature limits between 1300° and 1650° C. The goals of this effort include the following:

- Select an alloy for best life and thermoelectric stability.
- Conduct coupon tests to determine upper temperature limit and calibration stability as a function of thickness in oven tests and a combustion gas stream.
- Evaluate the effectiveness of top coats in extending upper temperature limits.
- Fabricate sensors.
- Calibrate and test in laboratory ovens.

A great deal of work has gone into development of technology related to application of sputtered platinum-rhodium alloy thermocouples. We plan to use that technology base in this program. We have in-house facilities suitable for sputtering and plan to use them as much as possible.

3.0 Strain Measurement

3.1 Concept Description and Analysis - Applied Sensors - Nonoptical

3.1.1 Resistance Strain Gages

Resistance strain gages are currently the primary sensing devices for gas turbine hot section strain measurement. In Reference 3-1, Perry and Lissner describe historical development, theory, and practical applications of gages, including attachment techniques, excitation/readout circuits, and interpretation of data. Because strain gages respond to changes in temperature as well as changes in strain of the surface to which they are attached, quantitative interpretation of gage output requires isolating the strain effects from the temperature effects. Dynamic strain measurement, which involves measuring a time varying signal whose time constant is short compared with the thermal time constant of the substrate on which the gage is mounted, is less temperature dependent than static strain measurements. Lead wire effects, thermal expansion mismatch, and metallurgical transformations are not usually significant for dynamic measurements. Static strain is sensitive to all these effects and is more difficult to measure at elevated temperature.

3.1.1.1 Current Capabilities

Nickel-based alloy wire filament grids, applied to metal substrates with ceramic cements or flame sprayed alumina (FSA), are currently used to 1280 K for dynamic measurements as described by Weise and Foster (Reference 3-2). Static strain measurements using FeCrAl grid elements are discussed by Lemcoe (Reference 3-3) to 1366 K, Stetson (Reference 3-4) to 977 K, and Wu et al. (Reference 3-5) to 1073 K. Static measurements using FeCrAl gage elements have significant accuracy problems and are reported to be cooling rate and strain level dependent (Reference 3-6). Hulse et al. discuss development of a palladium-chrome alloy for static measurement to 1250 K in Reference 3-7. This alloy has a high temperature coefficient of resistance which makes accurate strain measurement dependent on precise temperature measurement.

The evaluation of a number of alternate gage alloys for static strain measurement up to 1273 K is discussed by Brittain, Geslin, and Lei in Reference 3-8. Both metallic and nonmetallic alloys, including B_4C and SiC, have been tested.

Unpublished work at GE and others regarding the use of platinum alloys is ongoing, but does not look promising compared with FeCrAl alloys. The upper temperature limit for dynamic gages applied with ceramic cements or FSA appears to be in the vicinity of 1500 K. Limits are set by fatigue strength and oxidation of the grid and adherence of the bonding agent.

Due to the aerodynamic disturbance caused by surface buildup of wire grids applied with ceramic cements or FSA (typically 0.4 mm), significant effort has been directed toward the development of thin film strain gages with insignificant thickness. Gages made from nickel-chrome films on alumina

insulating films are currently used (at GE) up to 920 K for dynamic strain measurements.

3.1.1.2 Potential Capabilities

Potential for extending upper temperature limits for dynamic resistance gages beyond 1500 K is based on identifying sensing element materials with stable resistance characteristics and adequate fatigue strength at high temperatures. The best candidates for this application are refractory metals (such as W-Re alloys) with an adherent, impervious oxidation protective film, or ceramic elements (such as SiC). The current outlook is less than promising for either approach.

At present, precision static strain measurement capability with reasonable long-term stability is limited to approximately 920 K using PtW alloy gages in an Inconel sheath as described in Reference 3-9. Use of FeCrAl gages for higher temperatures is possible at great sacrifice in accuracy and stability. Potential for extending service temperature above 1073 K decreases exponentially as a function of temperature.

3.1.2 Capacitance Strain Gages

3.1.2.1 Concept History and Current Status

During the past 15 years, attached capacitance strain gages have become widely used to measure static strain up to about 1100 K where long-term stability is a major consideration. Most commercial gages are based on designs from either the Boeing Co. (marketed by Hitec Products, Ayer, Massachusetts) or by the Central Electricity Research Laboratory and the G.V. Planer Co. in the United Kingdom (this gage is marketed by Gael Tech Ltd. of Isle of Skye, U.K.). In the CERL gage, strain is related to the separation between capacitor plates, whereas in the Boeing gage strain is a function of the overlap between a pair of sliding plates. The change in capacitance is measured as a surface deforms, and the surface strain is related to this capacitance change. Descriptions of each of these gages may be found in Reference 3-10. Both gages require attaching a relatively bulky sensor to the test surface. The maximum working temperature of these gages is about 1350 K.

Several problems have made using capacitance strain gages at elevated temperatures a difficult task. Stray capacitance is a major source of spurious readings for capacitance probes. Because capacitance gages detect changes in capacitance of less than 0.5 pf, stray capacitance of less than 0.01 pf may induce significant errors in displacement measurement. The capacitance plates, lead wire, and cables are all subject to stray capacitance which can interfere with the direct capacitance between the plates. Three terminal capacitors, in which one plate is shielded with a conductor, can be used with capacitance bridges to minimize the effects of stray capacitance. Techniques for measuring capacitance from strain gages in the presence of stray and lead capacitance are discussed in Reference 3-11. In addition, the high temperature portion of the lead wire is often a source of electrical noise and therefore should be kept as short as possible.

Both the Boeing-Hitec and CERL-Planer gages use air as the dielectric between the capacitance plates. A now abandoned effort by the Hughes Aircraft Co. to develop high temperature strain gages used solid dielectrics such as mica, silica, and alumina (Reference 3-12). The developer of the Hughes gage believed that solid dielectrics

were more stable than air at temperatures approaching 1400 K and offered better possibilities for attaining even higher temperatures [Gillette, O.L., Batelle Memorial Insitute (Retired), personal communication].

3.1.2.2 Current Developments

Current developments in capacitance strain gage are oriented toward developing miniature, low profile devices capable of withstanding hostile environments. For example, Hitec Products is developing a rugged Boeing type capacitance gage, about 0.25 inch high, which is capable of withstanding turbulent environments up to about 1350 K (Wnuk, S., Hitec Products, Inc., personal communication). Work on thin film versions has been reported by G.V. Planer and United Technologies. Unfortunately, thin film capacitance gages, even if practical, will probably involve a tradeoff with upper temperature limit (the Planar program envisions a useful upper temperature of less than 1000 K (Reference 3-13). They will also probably require shielding and so will be more intrusive than, for example, thin film thermocouples.

Although we have found no attached capacitance gages capable of operating at temperatures exceeding about 1400 K, researchers at Southwest Research Institute (SWRI) have developed a biaxial capacitance extensometer to measure strains on the interior of tubular elements (Reference 3-14). The SWRI gage uses extension rods to connect a capacitance sensor to the specimen surface. The relative displacement of the extension rods is measured outside the hot zone with a standard capacitance-type strain gage. Difficulty in maintaining a stable temperature distribution along the extension rods limits the accuracy of strain measurements. Although the gage reported in Reference 3-14 was only used up to 1200 K, SWRI has used a similar extensometer to measure strains at temperatures up to about 1500 K. They are currently working to extend the upper temperature limit to over 1900 K and expect to demonstrate the ability to measure strain ranging from less than 50 microstrain to over 1% in the near future. It should be noted, however, that the SWRI design is intended for use in a laboratory; it almost certainly does not have application in hostile environments.

3.1.2.3 Potential Capabilities

The capacitance strain gage appears to have significant undeveloped potential. As a laboratory device, it may lend itself to strain measurements over a wide dynamic range at temperatures up to 1900 K, albeit in restricted experimental setups. The capacitance gage may be useful in a combustor environment up to 1400 K. The use of solid dielectrics probably warrants further investigation.

3.2 Concept Description and Analysis - Optical Discontinuity Methods

Several strain measurement techniques have been developed based on tracking the movement of light reflected from or emitted by materials attached to the specimen surface. Although the fact of attaching a marker to the sample is a significant restriction, particularly in an engine environment, these methods are generally simpler, both in terms of the equipment required and in terms of the data interpretation, than are holographic or speckle based methods.

3.2.1 Marion Method (Attached Targets - Optical Follower)

Robert Marion, then of Sandia National Laboratory, developed a method of measuring strain by optically tracking small targets attached to the specimen (Reference 3-15). Marion used an argon ion laser to irradiate ceramic targets whose reflectance differed from the specimen and tracked their position with a digital line scan camera in which the field of view was imaged by a lens onto a photodiode array. The photodiode array was then scanned electronically to produce an analog pulse train in which the amplitude of each pulse was proportional to the light intensity on the corresponding diode. The pulses before or after a dark-to-light transition on the specimen surface were electronically counted to determine the position of a target.

The system built by Marion and his coworkers was used for a project that has been abandoned, and the equipment is no longer intact. The system demonstrated a very large dynamic range; it was capable of measuring strains from less than 50 microstrain to several percent, from room temperature to over 2800 K. Although a complete analysis of the strain measurement capabilities seems not to have been performed, the method demonstrated the capability of measuring strains with an accuracy of about ±4 microstrain with a gage length of as small as 2.5 mm.

The system as developed by Marion used thin film tantalum carbide (TaC) targets as well as nodules of graphite cement. The thin film targets did not provide sufficient contrast for routine use, although film targets were not thoroughly investigated. Target survivability and contrast with the substrate can be expected to be a major constraint on the Marion method. Neverthless, we believe that film targets can be developed that should adhere to a wide variety of ceramic substrates. The techniques of plasma spray and physical vapor deposition that have been used successfully in attaching thermal barrier coatings should be useful in applying targets for strain measurement by Marion's technique. Targets of thermographic phosphors could also be used if contrast were a limiting factor.

We believe that Marion's method of measuring strain has considerable potential as a laboratory tool. It can be used to measure static strain or dynamic strain with a frequency response limited only by scan rate of the photodiode array. The conceptual simplicity of the method and the relative ease of data interpretation make it a good candidate for routine use.

3.2.2 The Sharpe Method (Reflection Interference from Target Indentations)

The Sharpe method uses a laser based interferometer to measure in-plane displacements and strains at elevated temperatures over very short gage lengths (100 μm) (References 3-16 and 3-17). The method involves pressing two small diamond-shaped indentations into the specimen and illuminating them with a laser. The indentations act as sources of reflected monochromatic light from a coherent source and so form Young's fringes. This fringe pattern is monitored to measure the relative motion between the indentations. Sharpe claims the method can be used to measure strains with an accuracy of ±3% ± 150 microstrain, so that a measured strain of 1.5% would have an uncertainty of ± 600 microstrain.

As with any interferometric method, rigid body motions and rotations may cause serious errors in strain measurements using this method. For example, rigid body motion normal to the surface introduces spurious fringes that appear identical to strain induced fringes. Stability and proper alignment of test rigs is therefore important to achieve the quoted accuracy of the Sharpe method. Furthermore, although the matter appears not to have been seriously studied, we would expect this technique to be sensitive to convective currents which introduce phase changes in the fringe pattern. Nevertheless, Sharpe has reported using the method successfully up to temperatures of 1000 K. The upper temperature limit at which the method can be used is not yet established.

The Sharpe method is a useful laboratory measurement device capable of measuring strain in real time. Significant improvements as suggested by Sharpe (Reference 3-18) may be attainable with more development of the method. It is highly unlikely, however, that the method can be used in a combustor environment or if indentations used to generate the reflected interference fringes would be acceptable for many ceramic materials.

3.2.3 Simpson-Welch Method (Applied Pattern Duty Cycle Variation)

Recently, Simpson and Welch (Reference 3-19) introduced a method of measuring radial strain of a rotating disk. The Simpson-Welch method involves photoetching a pattern of light and dark regions on the disk and monitoring changes in the pattern of light and dark regions with a stationary optical probe. For best results, the probe would include a laser coupled with appropriate optics to focus an intense small diameter spot on the pattern.

As the disk rotates, the output of the optical probe fluctuates high/low, depending on whether or not the probe is positioned over the light or dark area of the disk. Deformation caused by centrifugal forces results in a change in the width of the pulses, or the duty cycle, from the optical probe. Simpson and Welch selected a spiral shaped pattern so that the duty cycle sensed by the probe was a linear function of the radial position of the pattern relative to the probe. In this way, the change in the observed duty cycle provided a direct measure of the total radial expansion of the disk up to the radius of the point being measured. Simpson and Welch established that their method was capable of measuring strains as low as 1000 microstrain; optimizing their system should allow good measurements at less than 500 microstrain. The method should be capable of measuring percent level strains without difficulty.

A complete error analysis for the effect of rigid body motion on surface strain measurements by the Simpson-Welch method has not been performed. Translation of the entire disk along the axis of rotation should have no effect on a system using a collimated light source. Bending of the disk would affect the detector output, since the projected image of the pattern would be distorted with the outer edges of the pattern appearing closer to the pattern center. Surface tilt would produce a selective foreshortening of the pattern in the direction of the tilt. A correction for this error could be made if the degree of surface tilt were known.

Testing of the Simpson-Welch method has only been performed on room-temperature disks at low pressure. The method should,

however, be useful at pressures higher than ambient because it is less sensitive to turbulence and fluctuations in refractive index in the sight path than are methods based on optical interference. Applying the method to high temperature environments would require another method of applying the pattern to the test part. Simpson and Welch applied a photographic emulsion to the test surface that would not hold up to high temperatures. One intriguing approach would be to substitute a pattern of thermographic phosphors; fluorescent radiation from laser excited phosphors would then substitute for reflected radiation. Thin films of materials with different reflectance than the substrate material could also be used (see the Marion technique above).

It should also be possible to extend the Simpson-Welch method to the measurement of strain in a prespecified direction on a stationary surface by using a scanning excitation system. To our knowledge, there have been no experimental investigations using this approach.

In conclusion, the Simpson-Welch method of measuring strain could be employed for high temperature strain measurement and large strain levels under a rather restricted set of conditions: measurement of radial strain of rotating disks. This could be valuable for laboratory evaluation of materials. Extending the approach to more general applications would require extensive modifications, to the extent that it may not be a practical general strain measurement techhnique.

3.3 Concept Description and Analysis - Surface Pattern Distortion Methods

3.3.1 Moire Methods

3.3.1.1 Introduction

Moire fringe patterns are formed when two gratings with slightly different pitch or orientation are superimposed. To obtain displacements or strains from moire fringes, it is necessary to know the relationship between two gratings (a specimen grating attached to the test surface and a fixed reference grating), the recording system, and the object under study. Moire methods can be divided into three general categories:

- Intrinsic, or in-plane moire, methods can be used to determine the displacement field in a given plane. It is a powerful general technique for investigating a wide variety of problems in solid mechanics. In-plane moire methods have been used in laboratory studies of fracture mechanics (Reference 3-20), thermal stress studies (Reference 3-21), dynamic problems (Reference 3-22), vibration studies (Reference 3-23), and strain analysis (Reference 3-24).

- Intrinsic moire methods use a specimen grating attached directly to the specimen surface and a reference grating remote from the surface. The specimen and reference gratings normally are superimposed by imaging one onto the other using a lens. The specimen grating follows the deformations of the surface underneath, while the reference grating is rigid and so has an invariant pitch and spatial orientation. Although numerous techniques have been developed for attaching the specimen grating to the

surface, specimen grating survivability has been described as the main impediment to the use of intrinsic moire methods in hostile environments (Reference 3-25).

Moire techniques traditionally used noncoherent sources of illumination and were limited to gratings of 40 lines/mm, although higher frequency gratings can be used to increase sensitivity. Diffraction effects make fine gratings (over 100 lines per mm) difficult to use, although much higher frequency gratings have been used in low temperature applications (References 3-26 and 3-27). Coherent illumination is used to generate more fringes from high density gratings. Moire methods using coherent radiation suffer from poor fringe visibility when the specimen surface radiates at the wavelength of the illumination.

- Shadow or projection moire methods can be used to measure out-of-plane deformation and shape of an object (Reference 3-28). Shadow moire methods do not use physical gratings attached to the specimen surface; instead the specimen grating is formed as the shadow of the reference grating is cast on the specimen surface. The specimen grating is distorted by out-of-plane movement of the surface and so forms moire fringes with the reference grating. Reference 3-29 discusses various methods of casting the shadow and viewing the moire fringes. Because the specimen grating is formed optically, shadow moire methods are not considered good candidates for use in hostile environments.
- Reflection moire is applied to specular surfaces in which a virtual image of the reference grating serves as the specimen grating. Reflection moire methods have been used primarily to determine slope and curvature, not for strain measurement.

Moire methods generally have the advantage of being full field methods of strain determination. With moire, it is possible to obtain three displacement components simultaneously and so to determine the complete strain tensor of the specimen surface (Reference 3-25). Using fringe multiplication techniques, the sensitivity of moire can approach that of classical interferometry with a resolution of less than 10 microstrain.

3.3.1.2 Theory

Moire fringes are the interference pattern created when two gratings with slightly different pitch or orientation are superimposed. The relationship between the fringe pattern and the displacement field has been reviewed by Theocaris (Reference 3-30) and Durelli and Parks (Reference 3-31).

To measure in-plane deformation, a physical grating is usually applied to the specimen surface. When stressed, this specimen grating deforms and optically interferes with the undeformed reference grating, causing "moire fringes" to appear. Each fringe corresponds to the locus of points of equal displacement in a direction normal to that of the reference ruling. Assuming there is no rigid body displacement or rotation between the two gratings, the displacement u in a direction normal to the grid lines of the associated grating is given by:

$$u = N p \qquad (5)$$

where N is the fringe order and p is the pitch of the deformed grating. If strain information is desired, the displacement must be differentiated either numerically or graphically to calculate strain. For sufficiently small displacements, the strain fields are given by:

$$\varepsilon_y = \partial u / \partial x$$

$$\varepsilon_x = \partial u / \partial y \qquad (6)$$

$$\varepsilon_{xy} = 1/2(\partial u / \partial y + \partial u / \partial x)$$

where ε_y and ε_x are the components of strain in the x and y directions, ε_{xy} is the shearing strain, and u,v are the displacements in the x and y directions, respectively. Various methods of differentiating moire fringe patterns are discussed in Reference 3-32. At best, the process of differentiation is tedious; at worst, it is a source of significant error. It should be noted that moire is not limited to analysis of small deformations. For finite displacements, the strain-displacement relation includes higher order displacement derivatives than are present in equation (6) above, and the calculations are correspondingly more complex.

3.3.1.3 Discussion

The need to apply a grating to the specimen surface severely limits the use of moire methods in high temperature environments. In many field situations, practical considerations preclude applying a grid to the test surface. Even in laboratory situations, grating survivability is a major impediment to the use of moire methods in high temperature studies (Reference 3-25). Cloud (References 3-21 and 3-25) used a ceramic paint as an adhesive for a nickel mesh grating of 40 lines per millimeter to produce a grid capable of surviving up to 1650 K on metal superalloys. He believes that continued development of gratings should improve their durability (Cloud, G., Michigan State University, personal communication).

Unfortunately, rigid body rotations between specimen and master gratings may produce fringes independent of strain. It is important to avoid or account for this movement when using moire techniques to measure strain. Even in the absence of rigid body motions, moire has troubling limitations as a method of measuring strain. In the case of uniaxial stress, the distance between successive moire fringes becomes the "effective gage length" and the pitch of the grating determines the resolution of the measurement. Since small deformations produce few fringes with wide spaces between them, large errors can result from differentiating these displacement fringes to determine strain. Moire has, therefore, been used primarily to measure relatively large deformation strains.

Considerable effort has been made to increase the sensitivity of moire techniques. One solution is to use a specimen grating with a higher pitch, even though increasing pitch generally reduces the fringe contrast. Bowles et al. formed a replica specimen grating of approximately 600 lines per mm (Reference 3-33), although these gratings are for low temperature use only. It is unlikely that replica gratings suitable for high temperature moire can be increased by more than a factor of two or three from the traditional 40 lines per millimeter.

The sensitivity of moire analysis can be increased by more than an order of magnitude by techniques known as fringe multiplication. Fringe multiplication occurs when the reference grating pitch is an integral multiple of the specimen grating pitch, so that the number of moire fringes is determined by the

higher pitch. Twenty years ago, Post formulated three techniques of fringe multiplication (References 3-34 and 3-35). These methods used a relatively coarse specimen grating coupled with a fine reference grating to effectively multiply the number of fringes by as much as a factor of 20. Unfortunately, the techniques used by Post require methods of applying and recording the gratings that are not well suited for high temperature applications.

Several years ago, Post introduced a technique he named "moire interferometry" that uses gratings formed by the interference of two coherent beams (References 3-26 and 3-27). Post refers to gratings generated by optical interference as "virtual" gratings and has produced them with 2400 lines/mm or more. By applying a replica of a photographic image of the interference of coherent beams to a specimen surface, very high frequency (2000 lines/mm) real specimen gratings can be achieved. Because thermal currents severely reduce the fringe visibility of virtual reference gratings, and because of temperature limitations of the specimen gratings, this concept is not well suited to high temperature, ambient pressure environments. It may, however, be possible to generate good quality virtual gratings in a high-temperature vacuum, although moire interferometry has not been attempted under such conditions.

3.3.2 Optical Filtering Methods

Several researchers have proposed optical filtering techniques in conjunction with moire to accomplish fringe multiplication and reduce noise (References 3-36 through 3-38). Optical filtering also can be applied to the diffraction pattern from a specimen grating in the absence of a reference grating. These methods may be considered extensions of moire, even though they do not use a reference grating.

In 1971, Boone made one of the first attempts to use spatial filtering of the diffraction pattern generated by a grating applied to a specimen (Reference 3-39) to measure strain. The image that was reconstructed from the filtered pattern was composed of light and dark areas in which the boundary between these areas represented the locus of points of equal strain. Boone also showed how the magnitude of the strain could be calculated by translating a suitable mask used as a filter. He cited several advantages of his technique as compared to classical moire. First, the absence of a reference grating eliminated problems associated with grating mismatch. Second, the method gave information about the strain field in the form of equal lines of strain and, therefore, avoided the error-prone process of differentiating displacement data. Third, for a given grating pitch, the sensitivity of the method exceeded that of classical moire. In addition, the sign of the deformation was determined. Boone applied his technique to measuring percent level strain of low temperature steel and appears not to have considered its use at elevated temperature. His technique was not suited to real time measurement as it relied on a photographic process to record the image of the grating.

Recently, Burger and his coworkers at Texas A&M University have developed a method of measuring strain, dubbed the Spectral Density Indication (SDI) method, that is based on evaluating the Fourier transform of a coarse grid (or any quasi-regular feature) on a specimen surface (Reference 3-40). In the SDI method, the spatial frequency of the grid is measured at both unstressed and stressed conditions and changes in the

frequency spectrum of the grid are then related to strain. The transform of the grid is made on-line from a digitized image recorded by a charge coupled device camera so that the method is capable of calculating full-field strain in real time. Although the SDI method measures displacement of the grid pattern, the calculations used to determine strain are less prone to error than is the process of differentiating fringes.

The SDI method reportedly is significantly more sensitive than moire methods for a given specimen grating pitch: Burger et al. used a grid of 8 lines/mm to achieve a resolution of 200 microstrain (Reference 3-40). The use of coarse grids is a major advantage since such grids can be made more durable than the fine grids used in moire interferometry. The inventors suggest that SDI can be used for accurate strain measurements from about 10 microstrain to several percent (Reference 3-41). Because the SDI method has not been tested at elevated temperatures, it is not possible to fully assess the usefulness of SDI for measuring strain of high temperature ceramics. The team at Texas A&M plans to investigate high temperature applications in the near future.

3.3.3 Conclusions

Moire methods of measuring strain have exerted a strong appeal for over a quarter century. The inherent advantages of moire include an essentially noncontacting capability and a wide dynamic range. Moire techniques are an established means of measuring percent level strains at ambient temperature. They are particularly useful where qualitative measures of strain are desired. In recent years, Post and others have extended in-plane moire to the high sensitivity domain in laboratory studies. Despite predictions that moire would find its way onto the factory floor, widespread use of moire outside the laboratory remains elusive. Difficulties associated with maintaining the relative spatial orientation of specimen and reference grids and in differentiating moire fringes to calculate strain are challenging hurdles for which no simple, generally applicable solution is available.

Although researchers in the field remain optimistic that moire can be applied to high temperature strain measurements, there has been little progress to date in measuring strains at temperatures exceeding 1300 K. This lack of progress thus far is partly a reflection of the lack of concerted effort to apply moire to such difficult environments. Techniques analogous to moire, but in which the reference grating is eliminated, may provide a more promising avenue for high temperature strain measurement. One such technique is the Spectral Density Indication method, which we believe should be evaluated for high temperature applications.

3.4 Concept Description and Analysis - Holographic Methods

3.4.1 Holographic Interferometry

3.4.1.1 Concept Description and History

Holography is a two-stage imaging process for recording and wavefront reconstruction. The illumination is usually by a monochromatic laser light source. The photographic record of the interference pattern of the reference beam modulated by the object beam of the object surface is called a hologram. The process of recording and reconstruction of the resulting images can be analytically described.

In holography, the illumination from the laser is divided into two beams, one to illuminate the object and the other for use as a reference beam. The scattered object wave is optically superimposed with the reference beam and recorded on the photographic plate. The recorded image can be reconstructed by illuminating the processed and exactly repositioned hologram with a reference beam identical to the original reference beam.

Holograms can be classified according to the way of forming the object and reference waves or according to the type of recording procedure (Reference 3-42). Based on the position of the object, a hologram can be classified as a Fresnel, Fraunhofer, or Image Plane hologram. A Fresnel hologram is one in which the hologram is recorded in the near field diffraction region. A Fraunhofer hologram is recorded when the object is located at the focus of the imaging lens. An image plane hologram results when the object is in the plane of the hologram or is focused onto it (Reference 3-43). The resulting phase and distribution of the hologram are identical with that of the object.

Superposition of two holograms of an object in different strain states or the hologram of the object in initial strain state with the scattered object wave in a second state in real time, results in an interference pattern. This technique is known as Holographic Interferometry (HI). The resulting interference pattern is the mapping of the displacements of the object surface and is due to the changes in phase of points on the object surface as the surface is displaced. There is, therefore, a one-to-one correspondence between the same object point under the different strain states. Interference from noncoincident points does not occur, as the diffracted waves from these points exhibit random phase differences.

One of the most significant developments in holography has been the application of HI to the analysis of surface deformation. Developed in the 1960's, HI attracted considerable interest because, unlike classical interferometry, it could be used to analyze optically rough surfaces. Holographic interferometry has been extensively reviewed in several publications (References 3-41, 3-44, 3-45, and 3-46).

Holographic interferometry has been used for two decades to measure small static and dynamic strains (Reference 3-47 and 3-48). For static strain measurement, the interference pattern is recorded at particular instants of time, while for dynamic strain, recording is averaged out over a period of time.

Based on the method of recording, HI can be categorized as either a double exposure or a real time method. In the double exposure method, different strain states of the object surface are illuminated by a pulsed laser and are recorded on the same plate so that upon reconstruction the interference pattern can be studied. In real time HI, a hologram of the initial state of the surface is compared with the stressed state in real time. The two techniques are similar in terms of experimental setup, although the double exposure method freezes the interference pattern and therefore results in a better image. Double exposure HI can be used to measure relatively large periodic displacements [on the order of 1000 times the wavelength of the light source (Reference 3-44)]. However, the real time technique has other advantages, such as relative ease of compensation for rigid body movements and its ability to lend itself to

television imaging and electronic data processing.

Powell and Stetson conducted one of the earliest studies of vibrating objects using holographic interferometry (Reference 3-49). They proposed recording a multiple-exposed hologram with a single reference beam. The object beam consisted of a set of scattered object waves corresponding to the successive positions of the vibrating object. On reconstruction, the hologram will simultaneously reconstruct the superposition of all the recorded object waves, each properly weighted by the fractional duration or time average of the total exposure time of the object field. Because the object is allowed to vibrate during exposure, this method is an example of Time-Averaged Holography. The resulting image displays the contours of the vibrational mode shapes and amplitudes. The Powell-Stetson technique has several significant shortcomings that limit its application. Because the brightness of the fringes decreases with increased amplitude, it is difficult to analyze surfaces whose amplitude of vibrations exceeds several times the wavelength of the scattered radiation. Furthermore, it is limited to studying nodal vibrations only. Last, because displacements are averaged over a vibration cycle, it is not possible to obtain information on the relative phases of vibrations of different points on the surface.

Improvements and applications of the Powell-Stetson method have been reported by several workers (Reference 3-42). In the study of vibrations, these methods allow determination of the vibrational modes and amplitudes over a frequency spectrum.

3.4.1.2 Limitations

Sensitivity to rigid body motions have generally restricted the use of holographic methods to experimental setups in which the test object is interferometrically stable. It is necessary to ensure that translation or rotation does not occur between the exposures of the hologram. Heflinger, et al. (Reference 3-50) showed that the requirement for rigid body stability could be relaxed somewhat in HI with an optical configuration termed coincident illumination and viewing (CIV) in which the paths of illumination and viewing are coincident. This configuration is reportedly capable of obtaining fringes in the presence of rigid body motions a few times the wavelength of the reflected light.

Although HI is in principle a very sensitive technique for the measurement of surface displacement and strain analysis, in practice, making quantitative measurements with it can be very demanding. In addition to the requirements for specimen stability, HI is susceptible to interference from changes in the optical path length between exposures. Although holography has been successfully performed on surfaces significantly hotter than 1250 K (Reference 3-51), HI is not well suited for high temperature measurements in air where thermal gradients can introduce spurious fringes that can in turn introduce large errors in displacement measurement. It probably can be used effectively when the hot specimen is in a vacuum, although very little use has been made of HI in measuring material properties at high temperature. In addition, HI is much more demanding of the user than is real time "TV holography," which is discussed below (Electronic Speckle Pattern Interferometry). Although the use of high resolution photographic plates enables HI to have greater resolution to HI than live recording methods, this factor will rarely dic-

tate the use of double pulsed or real time HI when other real time methods are available. In our opinion, speckle techniques (which are discussed below) are better candidates for routine displacement and strain measurement than is HI.

3.4.2 Electronic Speckle Pattern Interferometry

3.4.2.1 Concept Description and History

Electronic Speckle Pattern Interferometry (ESPI) is a technique that allows speckle pattern correlation fringes to be observed in real time. It was developed independently about 15 years ago by three groups. The first paper was published by Butters and Leendertz at Loughborough University in England (Reference 3-52); this group is credited with most of the early development in ESPI. Macovski et al. from the U.S. described their work with TV holography shortly after Butters' pioneering paper (Reference 3-53), while an early patent on the ESPI design was filed by Schwomma in Austria (Reference 3-54). The principles of ESPI have been amply discussed in a monograph by Jones and Wykes (Reference 3-55) and will not be detailed here. ESPI fringe patterns have been studied theoretically and have been shown to be similar to those obtained by holographic interferometry (Reference 3-56).

ESPI can be considered as an image plane holographic system with an in-line reference wave in which the recording and reconstruction steps are performed by video recording and electronic processing. The in-line configuration is necessary to allow the television camera to record the pattern resulting from the interference of the object and reference waves. Instead of recording a hologram, the initial state is recorded in a video storage device and compared in real time to a deformed state. The two images are electronically subtracted to produce the fringe pattern. The ESPI system uses a closed circuit television in which the target of the vidicon tube of the TV camera replaces the photographic plate used in holography. In contrast to traditional holographic systems, ESPI involves imaging the test surface onto the detector plane. Figure 10 depicts a simple ESPI system. The light from a laser is divided into two beams by a beam splitter. One beam is expanded to illuminate the test surface while a lens images this surface on a television camera via mirror M1. The reference wavefront is mixed with the image wavefront to produce an interferogram whose intensity is converted into a corresponding video signal by the photoelectric action of the camera. The resulting video signal is then high pass filtered and full wave rectified in a process that is analagous to wavefront reconstruction in holography (Reference 3-57). The processed video signal is then converted to a reconstructed speckled image of the test surface on the television monitor.

It is necessary in ESPI that the optical system be interferometrically stable during image scanning. This imposes a stringent stability requirement when continuous wave lasers are used as light sources. Jones and Wykes (Reference 3-58) analyzed speckle interferometry theoretically and determined that speckle correlation would not be maintained if rigid body displacements exceeded about 100 microns or out-of-plane rotations exceeded 0.001 radian between exposures. The exact values are a function of the focal length of the lens and the particular optical configuration employed. However, use of a pulsed laser in which the illumination is

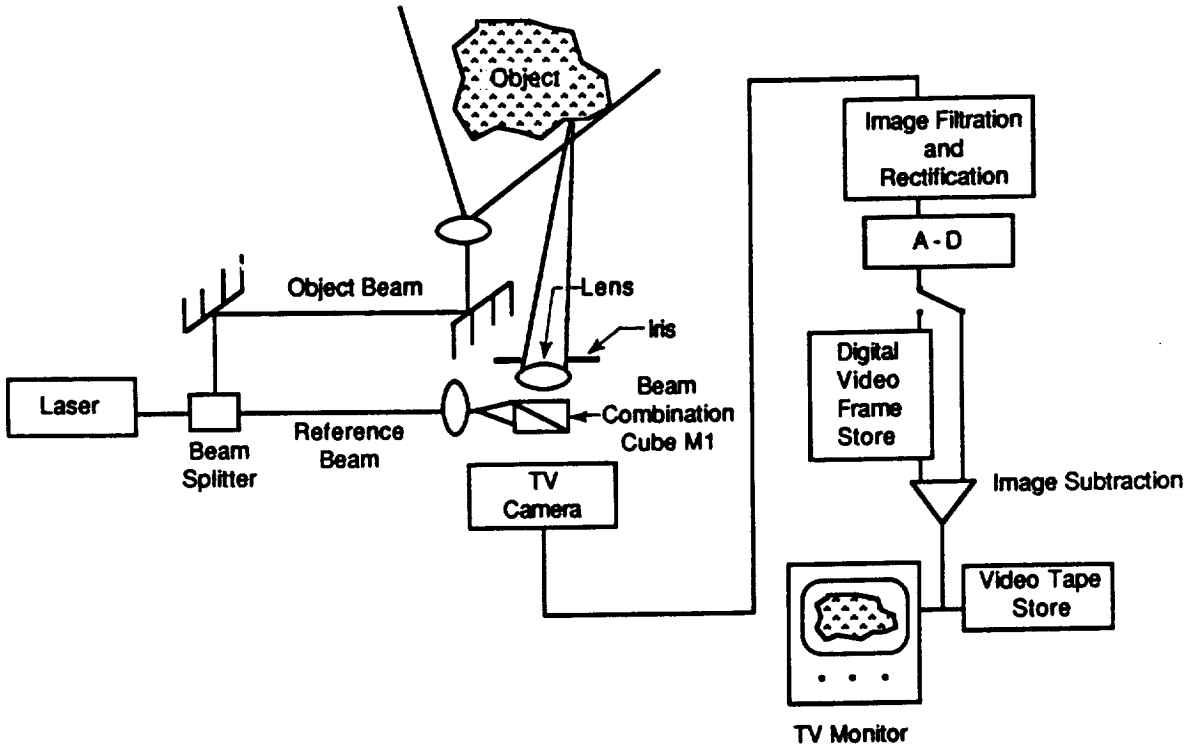

Figure 10. *ESPI Optical Schematic.*

delivered in a very short time enables interference fringes to be observed on relatively unstable structures. For example, Cookson et al. (Reference 3-59) used a Q-switched ruby laser to obtain ESPI fringes from an object moving at 2 m/s. Alternatively, a high speed, low light camera such as a Charge Injection Device (CID) camera can be used to obtain exposures over very short time intervals. In any case, the movement between any two exposures must be sufficiently small that decorrelation of speckle fringes does not result.

Although ESPI methods lend themselves most readily to analysis of periodic vibrations, they can be used to measure both in-plane and out-of-plane displacements and strains. The configuration illustrated in Figure 15 was intended to detect out-of-plane movements. For in-plane measurements, the object is illuminated symmetrically by two plane waves so that no reference wave is used. In-plane measurements of displacements in a pre-specified x direction are, in principle, insensitive to interferences from displacements in the orthogonal y and z directions as long as the following conditions are met: (1) the wave fronts are plane, (2) the surface is flat, and (3) the angles of incidence of the two beams are equal and opposite (Reference 3-60).

Denby and Leendertz (Reference 3-61) applied ESPI techniques to in-plane strain measurements at room temperature and

found them most useful in determining strain distributions. In comparing strain measurements made with strain gages with those made using ESPI, they found that the two methods agreed within about 5% at about 150 microstrain. Although Denby and Leendertz only examined conditions in which the direction of the principal stresses were known, they proposed an ESPI method using two sets of illuminating beams in which all the principal strains could be determined.

One technique that could extend the capabilities of ESPI involves the use of shearing interferometry (References 3-62 and 3-63). Shearing interferometry is a speckle interferometric method that is sensitive to derivatives of surface displacements instead of the displacements themselves that ESPI and other speckle interferometric techniques typically measure. A major advantage of shearing methods is that it relaxes significantly the requirements for vibration isolation because rigid body translations do not change the displacement gradient (Reference 3-63). Its disadvantages include the requirement for higher levels of illumination and the fact that fringe interpretation is not as straightforward. By coupling shearing interferometry with ESPI recording and data processing methods, it may be possible to evaluate strains in the presence of random vibrations, although we know of no published data to confirm this.

Another way in which ESPI methods could be enhanced for some applications would be to replace the analog image processing used by the television camera with digital image processing. Digital image processing, in which the intensity of the image is converted into digital form based on the grey level of the illumination, has several advantages over analog processing. Automation of fringe analysis can be obtained using digital imaging technique (References 3-64 and 3-65). In digital techniques, the speckle size does not govern the image resolution, so better fringe visibility and accuracy can be expected. With the image already in digital form, further processing such as addition, subtraction, and averaging of images can be performed with relative ease. Use of low light level, fast time response cameras should allow a large reduction in the exposure time and a concomitant reduction in the time interval between exposures.

3.4.2.2 Applicability to High Temperature Applications

There has been very little effort made to use ESPI for high temperature strain measurements. This is probably due in part to the difficulty of recording good speckle patterns through air which is disturbed by thermal turbulence. When air turbulence is sufficiently severe, complete decorrelation of the speckle patterns can result. ESPI strain measurements would be much simpler if the test piece were in a vacuum environment. It has been established, however, that ESPI techniques can be used to observe and measure deformation and crack growth of very hot objects in air. For example, Lokberg et al. (Reference 3-66) observed fringes from deformation of Kanthal specimens heated by resistance heating to about 1800 K and suggested that, with better filtering of background radiation, ESPI techniques should be useful at temperatures exceeding 2200 K. Nevertheless, strain determination in the presence of convective currents can be expected to be a difficult challenge for ESPI or any purely optical technique.

In addition to the problem posed by thermal gradients in the sight path, speckle interferometry at temperatures above 1300 K

faces difficult challenges. Oxidation, contamination, and other changes in the surface microstructure during the measurement will result in decreasing fringe contrast. Changes in the surface structure greater than about 1/8 wavelength of the illuminating light can be expected to cause difficulties for ESPI measurements. Additional difficulties may be encountered from multiple internal reflections from translucent materials such as ceramics which depolarize the reflected radiation and reduce the visibility of ESPI fringes. Good quality ESPI fringes on ceramics have been obtained at room temperature, however (Babb, J., Ealing Electro-Optics, personal communication).

Further experimental investigations are needed to evaluate the usefulness of ESPI techniques as a measurement tool at high temperatures. High temperature tests of a commercial ESPI system are in the planning stage (Maddux, E., WFAPL, personal communication). Initial high temperature testing will concentrate on the more tractable problem of vibration analysis; high temperature tensile and compressive strain will probably not be investigated until 1989 or 1990. Nevertheless, if the problems associated with high temperature ESPI measurements can be successfully addressed, it could be an extremely powerful technique. The potential of a contactless method for which an entire strain field of a large surface can be analyzed in real time warrants close attention to developments in the field of high temperature ESPI measurements. Developing ESPI methods to measure strain at high temperatures can be expected to be a difficult task.

3.5 Concept Description and Analysis - Laser Speckle Methods

3.5.1 Concept Description

Laser speckles are the result of multiple interference of reflected light when an optically rough surface is illuminated by a coherent laser beam. Based on the imaging system employed, a speckle pattern is classified as an objective or subjective speckle (Reference 3-67). An objective speckle pattern is formed in the region in front of the coherently illuminated object or in the region behind a coherently illuminated diffuser. On the other hand, if light from the specimen surface is imaged by an optical system, the resulting speckle pattern is known as subjective speckle. The spatial frequency of an objective speckle pattern is determined by the roughness of the surface, whereas that of subjective speckles is controlled by the imaging system.

Speckle dimension is related to the average distance between two bright speckles and is usually called average diameter of the speckle. It is described by the wavelength, λ, and the angle subtended by the scattering area on the screen (Reference 3-68). This can be written for objective speckle as:

$$\tau(o) = 1.22\,(\lambda)\,L/D \qquad (7)$$

and for subjective speckle pattern

$$\tau(s) = 1.22\,(1+M)\,(\lambda)\,F \qquad (8)$$

where $\tau(o)$ and $\tau(s)$ are the average diameter of the resulting speckle, L the distance between the surface and observation plane, D the size of the object, M is the magnification, and F the f number of the imaging system. The resulting speckle pattern acts as a

naturally printed grid on the surface. When two such patterns are superimposed, the resulting intensity distribution depends only on the relative phases of the individual patterns. By measuring the correlation of the speckle patterns in two states, a change of phase is detected which can be related to surface displacements.

Leendertz (Reference 3-69) was one of the first to use the speckle phenomenon to measure displacements. He used a double illumination method to measure in-plane displacements in real time. This was later extended to the "frozen fringe" technique by Archbold et al. (Reference 3-70). Duffy (Reference 3-71) showed that nonlinear recording properties of the recording film along with optical filtering could be used to obtain correlation fringes. The technique developed by Duffy and by Archbold et al., known as speckle photography, has found a number of applications. For example, Barker and Fourney (Reference 3-72) used speckle photography to study displacements at the interior points of a transparent object. Hung and Hovanesian (Reference 3-73) have applied the technique to a generalized three dimensional field and have also proposed speckle shearing interferometry techniques to obtain slope contours directly.

Speckle metrology can be divided into two broad categories: (1) those involving photographic recording, and (2) those using other methods. Photographic recording techniques can be subdivided according to methods used to extract the desired information from the photographs as described in the following section.

3.5.2 Speckle Photography

Speckle photography and speckle interferometry are both powerful optical techniques for measuring surface displacements. These methods make use of interference fringes produced by the scatter of coherent radiation from an optically rough surface in both initial and displaced positions. Stetson (Reference 3-74) proposed categorizing speckle metrology based on the correlation between the images formed by speckle patterns on the initial and displaced surfaces. If there exists a region in the speckle pattern of the image of the initial position that is always well correlated with that of the displaced surface, Stetson proposed naming the process speckle photography. If the fringes derived from fluctuations in the correlation of the speckle patterns between the two images, Stetson named the process speckle interferometry. Interferometric methods require distinguishing between parts of the field where the speckle is correlated and those parts where it is not; the methods require that individual speckles in the image plane are displaced by no more than their own diameter. Speckle interferometry is, therefore, limited to the measurement of small lateral displacements unless the speckle size is made large by reducing the lens aperture. In speckle photography, correlation methods are used to measure the displacement of a localized area of a speckle pattern where the speckle shift is greater than the speckle size (Reference 3-75). Operationally, speckle photography differs from speckle interferometry by the absence of a reference beam at the recording stage.

In speckle photography, a surface is illuminated with a divergent beam of light and is photographed. After the object has been deformed, the film is exposed again, resulting in a double exposed negative from which correlation fringes can be extracted by optical processing to determine displacement of the surface (References 3-76 and 3-

77). The speckle photograph, or specklegram, consists of speckles from an undeformed exposure and the same speckles from the deformed exposure. In the absence of interfering phenomena, the distance between each speckle pair is directly proportional to the in-plane displacement of the target surface. Analysis of the photograph is performed by directing a laser beam at normal incidence through the specklegram to generate the Fourier transform of the photograph. This transform is in the form of a diffraction halo modulated by a pattern of equispaced parallel fringes similar to Young's fringes. These fringes are aligned perpendicular to the displacement and have a fringe spacing that is inversely proportional to the magnitude of the displacement.

Provided that the image movement between exposures is greater than one speckle diameter, and that the speckle patterns remain correlated with each other, the speckle pattern on the photographic film will scatter a beam of light into a diffraction halo. The interference generated by the two sets of speckles creates parallel equispaced fringes in the halo, the number of which is proportional to the in-plane displacement of the point. The direction of the fringes is perpendicular to the direction of the displacement vector. Therefore, after measuring the spacing and direction of the fringe patterns at closely spaced points on a photograph, the complete 2D deformation field can be analyzed. The speckle diameter on the test surface can be shown to be approximately $M(\lambda)F$, where M is the magnification, F is the f number of the lens, and (λ) is the wavelength of the scattered radiation. Lateral movements greater than $M(\lambda)F$ are, in principle, measurable by speckle photography. Therefore, with an f/4 lens used at unit magnification, the surface movement must be greater than about 3μm; with a 10X magnification, movements greater than about 30 μm are measurable.

Accurate fringe counting is a major challenge in speckle photography for which several techniques have been proposed. The first, proposed by Burch and Tokarsky, involves examining the photograph point by point to determine the corresponding surface displacement. A second method, proposed independently by Butters and Leendertz (Reference 3-78) and Archbold et al. (Reference 3-70) uses a spatial filtering technique. Duffy (Reference 3-71) used a double circular aperture to interpret fringes as a moire pattern. The goal of several researchers in the field has been to develop an automatic computer-based method of analyzing fringe patterns. For example, Kaufmann et al. (Reference 3-79) proposed a semiautomated hybrid readout system wherein a photodiode array scanned a fringe pattern which was later processed in a computer using digital filtering. Sciammarella (Reference 3-80) described a low-cost automatic fringe analysis in which the scanned profile is processed on-line by computers using digital filtering programs. Ansari and Ciurpita (Reference 3-81) developed a fully automated microcomputer-based system for analysis of speckle photographs.

Measurement of surface displacement using speckle photography is subject to several significant sources of error which have been discussed in detail in Archbold and Ennos (Reference 3-70), and Archbold, Ennos, and Virdee (Reference 3-82). It is important that the focus in the image plane not vary over the field of view. For flat surfaces, this may occur when the surface is imaged by a large aperture lens that introduces aberrations causing

the image to be curved. Parts of the speckle patterns are then defocused and are, therefore, sensitive to surface tilt as well as to in-plane displacement. Archbold, Ennos, and Virdee (Reference 3-82) showed that this effect could be minimized by using a long focal length lens so that only a narrow field of view is employed.

Compared to interferometric techniques, speckle photography is less sensitive to motion of the surface in the direction of the line of sight. Archbold and Ennos calculated that the depth of focus ΔZ within which speckles would remain correlated in the object plane was given by

$$\Delta Z = 2M^2F^2(\lambda) \qquad (9)$$

where M is magnification, F is the f number of the camera objective lens, and λ is the wavelength of the illuminating light. Archbold and Ennos found, somewhat to their surprise, that the experimentally determined correlation was maintained for at least four times the ΔZ. For and f/4 lens with a 7x magnification, they found a depth of focus of about 8 mm, instead of the predicted 2mm. Nevertheless, restrictions on rigid body motion in the line of sight direction severely limit the applications of double exposure speckle photography outside the laboratory environment. Even under optimal conditions in which a flat object is evaluated, uncertainties in strain measurement of 100 microstrain are likely to occur; errors are likely to be larger when the specimen is not flat or when surface tilt or rigid body motions occur. For example, Archbold found that a movement of 50 μm in the line of sight direction gave rise to an apparent strain of 300 microstrain (Reference 3-83). Surface tilt also gives rise to apparent strain that, at least for small angles, is proportional to the tilt angle. Typically, a one milliradian tilt would induce an apparent strain of up to 300 microstrain.

In speckle photography the displacement of the object must be such that the displacement of the speckle pattern in the recording plane is greater than the speckle size in that plane (Reference 3-84). For in-plane measurement, the smallest displacement that can give rise to fringes is given by

$$\begin{aligned} &Dmin > Qs/M \qquad \text{or} \\ &Dmin > 0.5(\lambda)(F) \qquad (10) \end{aligned}$$

where Qs is the speckle size and M is the magnification of the viewing system and Dmin is the smallest measurable displacement. For a lens with a numerical aperture of 2, the minimum speckle diameter is about 0.5 micron. It has been shown, however, that when the resolution-element diameter is small, object tilt and out-of-plane displacement give rise to apparent in-plane displacements so that errors occur except when the motion is purely in-plane (Reference 3-84).

The practical application of double exposure speckle photography is restricted to measuring displacements over a range of little more than a factor of 10, a significant limitation for strain measurements. Smith and Stetson (Reference 3-85) reported an interferometric readout system for specklegrams that addressed the problems of limited dynamic range and sensitivity to rigid body movements. This technique, called heterodyne speckle photogrammetry, uses separate photographic plates to record exposures of the specimen before and after deformation. Stetson claimed that this technique could improve the accuracy of fringe measurement by between one and two orders of magnitude. The specklegrams were

then analyzed in a heterodyne interferometer to provide a precise measurement of differential displacement. Stetson (Reference 3-86) successfully used this system to measure biaxial strain distributions in a laboratory furnace up to about 1150 K. Stetson reported agreement within 10% between measured strain and strain calculated on the basis of material properties. Accurate determination of mechanical strain required measuring the surface temperature of the specimen and compensating for thermal gradients in the atmosphere surrounding the test piece, however.

Stetson (References 3-87 and 3-88) also attempted to use speckle photogrammetry to measure static strain in a combustor test rig. Results were less satisfactory than in oven based tests. He concluded that turbulence in the optical sight path could cause decorrelation in of the speckle patterns. Turbulence was particularly troublesome at pressures exceeding 3 atmospheres at 1000 K. At higher temperatures, turbulence would probably reach unacceptable levels at lower pressures. The effect of turbulence in the optical path could be significantly reduced by simultaneously taking multiple photographs from different angular positions and subtracting out effects due to distortion in the sight path.

Speckle photogrammetry also is susceptable to errors caused by out-of-plane movement and surface tilt of the specimen surface. Although a thorough analysis of these factors on strain measurements by speckle photogrammetry has not been performed, Stetson found that rigid body movements severely restricted strain measurements made in a combustor gas stream.

3.5.3 Dual Beam Doppler Interferometer (Optra, Inc.)

Laser Doppler Anemometry (LDA) has long been used to measure the velocity of particles in a gas. The principles of LDA are well known and are amply discussed in the literature on the subject. The measurement principle of LDA is based on detecting the Doppler frequency shift of light scattered from a moving object. Often, the Doppler shift is detected by optically heterodyning the scattered light with the incident radiation so that the output from a suitable photodetector is related to the Doppler shift, which is a linear function of the particle velocity. Alternatively, the particle can pass through a moving fringe pattern generated by intersecting frequency shifted beams. The output of the photodetector is then processed electronically in real time to yield the particle velocity irrespective of direction.

To determine both velocity and direction of a particle, a particle passes through a sensing area consisting of the intersection of two frequency shifted beams. The intersecting beams form a moving fringe pattern so that when a stationary particle is inside the sensing area, it scatters light that is frequency modulated by the difference frequency Δf between the intersecting beams. The light scattered by a moving particle may be modulated by a frequency greater than or less than Δf, depending on whether the motion of the particle is in the same direction as, or opposite to, that of the fringe motion. Particle velocity, in this case, is proportional to the magnitude of the difference between the modulation frequency of light scattered by the moving particle and the frequency of light scattered by a stationary particle. Particle displacement can be determined by integrating the velocity over time.

Optra, Inc. of Peabody, MA, has recently introduced an optical displacement and strain measuring system that can be understood as an implementation of LDA principles (Reference 3-89). If a sensing area created by the intersection of frequency shifted laser beams is formed on a diffusely reflecting surface, it irradiates small spots which are part of the natural surface geometry. The displacement of these spots can be determined by using LDA techniques to determine the average of the motion of the spots. For strain measurement, two pairs of intersecting beams form two sensing areas on the target surface; the distance between the sensing areas determines the gage length. Strain is determined by measuring the relative displacement of the sensing areas (Reference 3-90).

Although a thorough assessment of the Optra system's response to rigid body movements has not been performed, both theoretical analysis and limited experimental evidence suggests that the technique is relatively insensitive to out-of-plane rigid body motions so long as the sensing areas remain focused on the target surface. For a current prototype system, the depth of focus is fixed at 5.1 mm, suggesting that rigid body movements of 2.5 mm are tolerable. According to the manufacturer, rigid body translations along the line joining the two sensing volumes (the "x" axis) can be tolerated as long they do not exceed about five times the displacement due to strain. In-plane movement perpendicular to the "x" axis should not cause errors more than one fringe (typical fringe spacing is 8 μm).

The Optra system has not yet been evaluated in terms of its response to changes in the index of refraction between a heated sample and the receiving optics, although this can be expected to contribute to measurement errors. Measurements of thermal expansion coefficients have been made in air up to about 1900 K, with little observable effect from interference from thermal gradients surrounding the specimen, according to the manufacturer. Evaluation of a prototype system used as an extensometer in an elevated temperature vacuum environment at Oak Ridge National Laboratory indicated that the systems agreed well with theory which indicated a resolution capability of 3.5 microstrain (Liu, K., Oak Ridge National Laboratory, personal communication).

3.6 Concept Descriptions and Analyses - Miscellaneous Optical Displacement Measuring Techniques

3.6.1 Blade Tip Deflection Sensors

Blade tip deflection measurements have been an effective tool in detecting vibratory motion of shroudless turbine rotor blades and in inferring blade stress. Tip deflection measurements can provide stress amplitude and spectral information comparable to that obtained from dynamic strain gages if measurements are made at a sufficiently high sampling rate. According to the well-known Nyquist criteria, this requires that the sampling frequency be at least twice that of the highest frequency vibration in the system. In practice, this may require over two dozen probes mounted circumferentially around the engine casing, a prohibitive task for most developmental work.

McCarty and Thompson (Reference 3-91) developed a blade tip deflection system using optical fiber light probes and demonstrated that they could extract the amplitude and frequency of blade vibrations that were non-

integral multiples of engine speed. They validated their blade tip deflection data by comparing the results obtained with the tip deflection system with strain gage data. GE has an ongoing effort to reduce the number of probes needed to obtain the tip amplitude and frequency information and also to reduce the time needed to sample the data. A parallel effort is in progress to speed up the data processing to the point where the stress-related amplitudes could be determined in less than one second. This would provide the stress safety monitoring capability that is needed on developmental engine testing.

As is the case for strain gage measurements, prior knowledge of blade characteristics is required to correlate tip deflections and maximum blade stress. Blade tip deflection versus stress must be obtained from laboratory tests of representative blades. Finite element analysis then permits calculation of blade stresses from the tip deflection data. It has shown that finite element methods can be used to model entire blade/disk assemblies. It should be possible to perform the finite element analysis before engine testing so that quasi-real-time stress measurements from tip deflection measurements are possible. Tip deflection methods used to date have lent themselves only to steady state analysis.

We believe that there is significant unrealized potential in blade tip deflection measurements. It should be possible to apply the methods used so far on compressor and fan blades to turbine blades. Furthermore, recent work at GE has shown that both integral and nonintegral vibration amplitude and frequency data can be acquired in as little as one revolution of the blade. This would permit tip deflection methods to determine transient blade stresses. Although blade tip deflection methods are restricted in terms of the engine parts to which they can be applied, they address what is probably the single most important stress measurement in turbine engine development.

3.6.2 Laser Doppler Methods

This measurement concept is based on use of an optical heterodyne technique for detecting the Doppler frequency shift between backscattered laser light and the laser excitation beam. The frequency shift is proportional to velocity of the target surface in the direction of the excitation beam. Integration of the velocity signal can be used to obtain displacement. Information which describes frequency and displacement can be used to calculate strain if a suitable model of the component has been defined.

Although limited in scope to nonrotating components where vibration displacement amplitude and frequency can be related to strain, this concept has some significant advantages:

- Nonintrusive, noncontacting sensing where vibratory displacement normal to the surface is obtained by integrating the measured velocity along the excitation axis.
- Existing technology is available and has been used for low temperature applications. Feasibility for high temperature measurements is promising.

An example of where such a technique may be usable would be measurement of vibratory strain in an exhaust nozzle liner panel where finite element modeling methods had been developed to relate displacement to strain.

Characteristics of a commercial system which has been used for vibration measurements on low temperature applications are as follows (Reference 3-92):

- Measuring Distance (Instrument to Target): 1.2 to 20 m
- Target Spot Size: < 0.1 mm/m
- Response Time: 1 μs
- Wavelength: 633 nm
- Frequency Range: DC - 740 kHz
- Amplitude Range: 10^{-8} to 1 M

Problems associated with detection of backscattered light from high temperature ceramic materials include the following.

- Optical windows may interfere with backscattered light.
- Background interference from emitted target radiation may cause adverse effects.

Pleydell (Reference 3-93) describes an alternate technique based on a Laser Doppler (Michelson) Interferometer wherein coherent detection is used to extract the Doppler shift in reflected light from an unprepared target surface with motion along the beam axis. This system is based on focusing the reference beam on the detector surface so that its size is smaller than the speckle size in the reflected pattern from the target. This optimizes coherent detection by allowing it to occur only in an area of the detector common to both the reflected reference beams.

3.7 Concept Description and Analysis - X-ray Diffraction Methods

3.7.1 Concept Description

Stress analysis by x-ray diffraction (XRD) is based on measuring changes in the lattice spacings of crystalline planes. These changes are referred to as lattice strains. XRD stress determination requires correlating changes in lattice strain with uniaxial or biaxial stresses. This correlation requires measuring the x-ray elastic constants (defined as $(1 + \nu)/E$ and ν/E, where ν and E are Poisson's ratio and Young's Modulus, respectively) in a direction normal to the lattice planes (Reference 3-94). Because only elastic strains result in changes in the lattice spacing, XRD measures only elastic strains. When the elastic limit is exceeded, further strain results in a disruption of the crystal lattice and XRD techniques do not apply.

X-ray diffraction methods have been used primarily to measure residual strains, both because of the lack of alternative nondestructive methods capable of measuring residuals and because of the difficulties in applying x-ray methods. In principle, however, there is no reason why strains from applied stresses cannot be evaluated. Because of the recognized importance of residual stress measurement in both manufacturing and design, this discussion will focus on residual stress/strain determination. Much of the discussion also applies to applied stress, however.

Metallic and polycrystalline ceramic materials consist of innumerable randomly oriented crystalline grains. When such materials are stressed, the interatomic distance of the crystal lattice changes proportionally with the applied stress (within the

elastic limits of the material). The relationship between the wavelength λ of the x-ray beam, the angle of diffraction 2θ, and the lattice spacing d is given by the Bragg equation:

$$n\lambda = 2\,d \sin\{\theta\} \qquad (11)$$

where n is the diffraction order (see Figure 11(a). This equation states that for a given wavelength and diffraction order, the diffraction angle 2θ is a simple function of the lattice spacing. Any change in the lattice spacing d results in a corresponding change in the diffraction angle.

The essentials of XRD applied to stress and strain analysis can be illustrated by considering tensile stress measurements. Placing a specimen in tension results in a Poisson's ratio contraction, which in turn reduces the lattice spacing and so increases the diffraction angle 2θ. If the specimen is rotated through a known angle ψ as shown in Figure 11(b), the tensile stress present in the surface will result in an increase of the lattice spacing oriented at an angle ψ with respect to the surface, and a corresponding decrease in 2θ. By measuring the change in the angular position of the diffraction peak for at least two values of ψ, the stress in the plane of the incident and diffracted x-ray beams can be calculated. To measure strains in different directions, the specimen is rotated about its surface normal to make the direction of interest coincide with the diffraction plane.

The fundamental equation describing the relationship between lattice spacing and biaxial surface stress is given by

$$d\phi\psi - d0 = \left(\frac{1+\nu}{E}\right)(\sigma_1 \cos^2\phi + \sigma_2 \sin^2\phi) \sin^2\psi - \frac{\nu}{E}\,d0\,(\sigma_1 + \sigma_2) \qquad (12)$$

where σ_1 and σ_2 are the principal surface stresses in the plane of the surface (Reference 3-95), d0 is the unstressed lattice spacing, and $d\phi\psi$ is the spacing between the lattice planes measured in the direction defined by ϕ and ψ (see Figure 11c). Equation 11 provides the basis for the most widely used techniques of XRD stress/strain measurement. If the lattice spacing is a linear function of $\sin^2\{\psi\}$ and if the x-ray elastic constants are known, then the stress can be determined if the lattice spacing is measured for any two angles $\{\psi\}$. This method, called the two-angle technique, has been thoroughly investigated by the SAE (Reference 3-96) and is the primary method of applying XRD to stress analysis in the United States. An extension of the two-angle technique, called the $\sin^2\{\psi\}$ method, is similar to the two-angle technique except that the lattice spacing is determined for numerous angles $\{\psi\}$. The primary advantage of the $\sin^2\{\psi\}$ technique is to establish the linearity of the lattice spacing as a function of $\sin^2\{\psi\}$, thereby demonstrating that the technique is a feasible way to measure strain.

Equation 12 shows that XRD stress analysis requires that the x-ray elastic constants, defined in terms of Poisson's ratio and Young's modulus, be known. It is important that the elastic constants used are not bulk values, but refer to the values for the specific crystallographic direction normal to the planes used for stress measurement. Bulk values of Young's modulus and Poisson's ratio are an average over all possible directions in the crystal lattice and may differ significantly from the values for a specific direction. The elastic constants are determined by measuring the change in the separation of the crystallographic planes used for strain measurement as a function of applied stress. Prevey's method (Reference

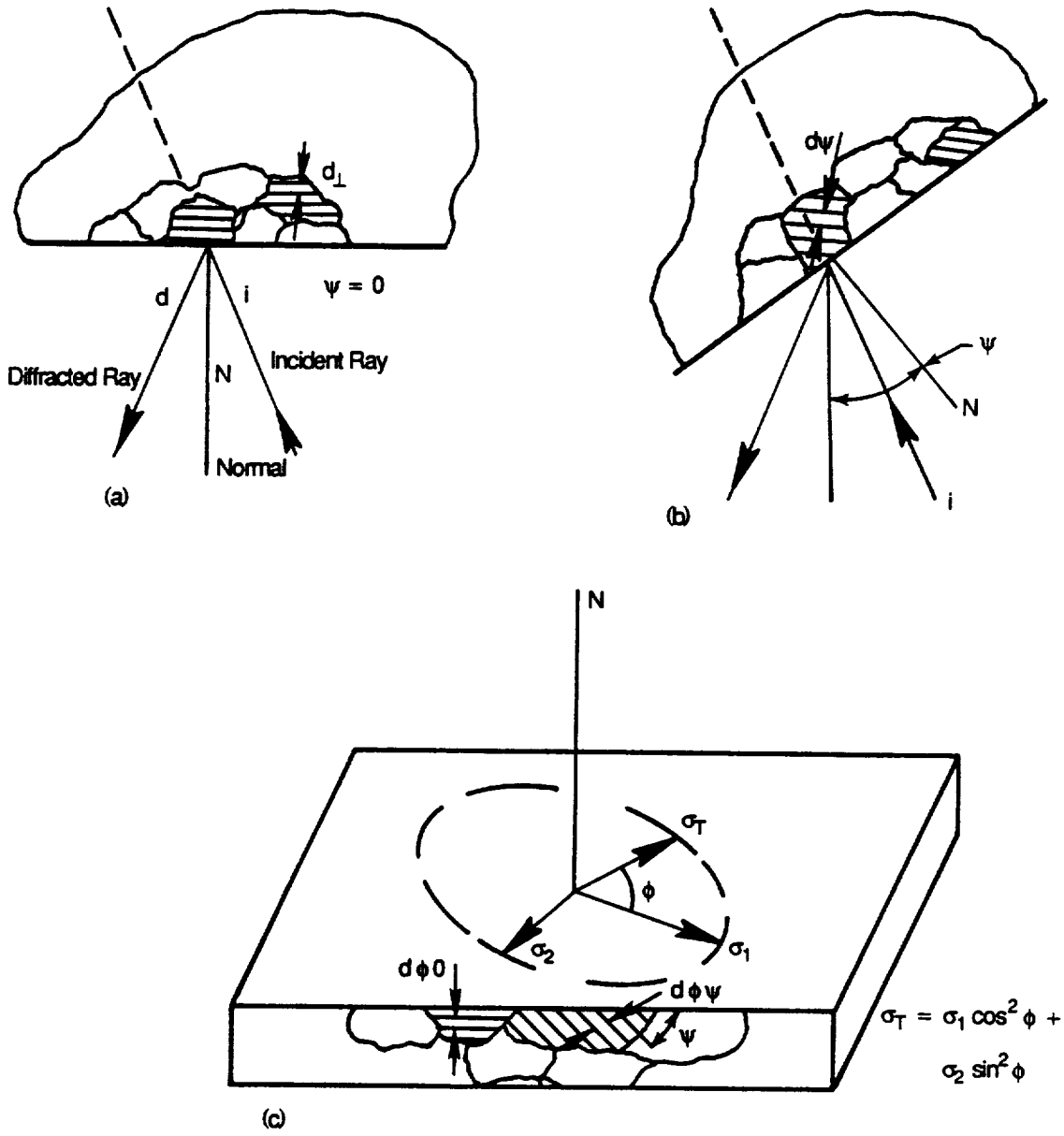

Figure 11. *Coordinates and Angles of X-ray Measurements on a Plane Surface.*

3-94) involves placing a sample of the material of interest upon a diffractometer mounted in a load fixture. Known stresses are applied to the sample and the lattice spacing is measured as a function of the applied stress. The slope of a plot of the change in lattice spacing as a function of applied stress is constant for a given material and diffraction peak, and is proportional to the elastic properties of the material in the appropriate crystallographic direction.

Certain materials, including polycrystalline ceramics, may exhibit a nonlinear relationship between lattice strain and $\sin^2\{\psi\}$. It has been found, for example, that the presence of stress gradients and stress components perpendicular to the specimen surface makes application of the $\sin^2\{\psi\}$ method difficult (Reference 3-97). Experts disagree over whether or not reliable data can be obtained using the $\sin^2\{\psi\}$ method in the presence of stress gradients and orthogonal stress components. Peiter and Lode (Reference 3-98) proposed an extension of the $\sin^2\{\psi\}$ method, the x-ray integration method (RIM), that permits accurate determination of the entire strain field of polycrystalline materials in the presence of orthogonal stresses and stress gradients. Marion and Cohen also developed a technique to measure lattice strains in materials exhibiting a nonlinear dependence of lattice strain on $\sin^2\{\psi\}$ (Reference 3-99). The Marion-Cohen method has not yet been widely adopted, although Prevey has shown that it leads to essentially identical results as the two angle and $\sin^2\{\psi\}$ methods for a variety of materials (Reference 3-94). Unfortunately, the methods designed to eliminate the requirement of a linear dependence of lattice spacing on $\sin^2\{\psi\}$ also require precise knowledge of the unstressed lattice spacing. Because the value of unstressed lattice spacing is generally unknown, these methods probably will have limited application.

3.7.2 Current Status

There has been very little effort to date in applying x-ray diffraction methods to high temperature strain measurement, although facilities are available for such studies. Commercial equipment is available from manufacturers such as Rigaku Denki (U.S. Headquarters in Danvers, MA) and Technology for Energy Corporation (TEC) of Knoxville, TN, that permits residual stress analysis up to about 1800 K in air. The former, which uses a rather conventional diffractometer that scans a range of angles with a single detector to obtain a diffraction peak, may require over 1 hour to determine each peak. TEC supplies a relatively new detector developed by James and Cohen (Reference 3-100) called the position-sensitive proportional counter (PSPC). With this detector, data are obtained simultaneously over a range of diffraction angles 2θ so that a diffraction peak is obtained without moving the detector. The only required motion is moving either the specimen or the diffractometer to obtain diffraction peaks at several values of ψ. The time required to obtain diffraction peaks is typically less than a tenth that required by conventional diffractometers.

The High Temperature Materials Laboratory (HTML) at Oak Ridge National Laboratory has recently brought on line a facility to perform high temperature x-ray diffraction studies on ceramics. This new facility, which uses a PSPC detector, should facilitate determination of essential material properties. Although not specifically intended for measurement of stress and strain, it may be possible to evaluate elastic

constants at high temperature and to investigate XRD methods in high temperature stress analysis.Although there is no fundamental reason why lattice strains cannot be measured in polycrystalline ceramics, XRD measurements will probably be more complicated on ceramics than with metals. For example, specimens with large grain sizes or preferred grain orientations are probably not well suited for x-ray diffraction because such materials provide few irradiated grains. Furthermore, single phase materials are generally the best candidates for x-ray analysis, whereas most structural ceramics contain polycrystalline or amorphous phases. In these materials, lattice strains are primarily determined by a small fraction of one phase only, so that care must be taken in drawing conclusions about the entire specimen. The extent to which the presence of multiple phases limits x-ray analysis has not been established.

Finally, diffraction peak broadening caused by variations in crystallite size will probably be a more important factor in ceramic materials than with metals. Although peak broadening caused by strain in the crystal lattice can be separated from broadening caused by reduction in the crystallite size, the method is a rigorous one involving Fourier analysis of the diffraction peak profile and collection of sufficient data to precisely define the shape of the entire diffraction peak. The method is highly dependent upon the precision with which the tails of the diffraction peak can be separated from the background intensity. Even if accurate strain measurements can be made on ceramics, the relatively high Young's modulus of ceramics means that strain measurements on ceramics can be expected to be less sensitive than with metals.

3.7.3 Future Prospects

X-ray measurements at high temperatures pose challenges beyond those encountered at room temperature. Ovens limit both the access of the x-ray beam to the sample and the angles at which diffracted radiation can be analyzed. For extensive high temperature strain analysis, it would be desirable and perhaps necessary to design a heating system that allows better access than do existing ovens. Laser heating has been suggested as one way in which specimens could be heated while preserving access to the specimen for x-ray sources and detectors. More fundamental problems may make x-ray diffraction analysis at high temperatures difficult. For example, thermal diffuse scattering of the diffracted x-rays can be expected to result in a loss of signal intensity, although the extent to which this may limit strain measurements can only be determined by experimentation. In general, strain measurement by x-ray diffraction needs to establish itself at room temperature before high temperature measurements are attempted.

Before x-ray diffraction can be considered for high temperature strain analysis, certain fundamental material studies must be made. The x-ray elastic constant must be measured for each material of interest over the range of relevant thermomechanical conditions. Using bulk or theoretical values of this constant has been shown to produce large errors in residual stress measurements, even at room temperature (References 3-94 and 3-101). The facilities at Oak Ridge might be a logical place to pursue the required studies.

Despite more than two decades of research and development, x-ray diffraction methods cannot be regarded as an established technique for measuring strain, even at room temperature. Studies to date have focused on

residual stress/strain measurement for which traditional x-ray diffraction methods are best suited by virtue of the long time required to resolve peaks. We believe, however, that x-ray diffraction is probably suitable for strain measurements at room temperature. Its applicability to high temperature strain measurements cannot be evaluated until further research is done. There is room for optimism that high temperature strain measurements can be made under laboratory conditions by highly trained personnel. A 3- or 4-year development program that employed experts in the field of x-ray diffraction could probably determine how effective a tool XRD would be in measuring strain of high temperature ceramics.

3.8 Concept Description and Analysis - Photoelastic Methods

3.8.1 Introduction

Certain transparent materials exhibit a phenomenon known as double refraction, or birefringence, in which incident light is resolved into two components having planes of vibration parallel to the directions of the principal stresses. The component waves generally have distinct velocities (that is, the material has distinct indices of refraction for each wavefront) so that the relative phase between the component wavefronts changes as they traverse the material. By allowing the component waves to optically interfere after traversing the bifringent material, the relative phase of the components can be measured by standard fringe counting techniques. Photoelastic stress measurements are based on measuring the relative retardation of the optical components derived from polarized light that has traversed a birefringent layer called a photoelastic coating (Reference 3-103). In photoelastic materials, the birefringence (that is, the difference in the indices of refraction) is a function of the strain at each point of the material. Stress and strain measurements using photoelastic coatings have been introduced commercially by Measurements Group, Inc. of Raleigh, NC. Although restricted to low temperatures by virtue of temperature limits of the polymeric coatings used, commercial photoelastic methods are capable of measuring strains over the range from about 100 microstrain to several percent.

3.8.2 Theory

When a beam of polarized light propagates through a stressed birefringent coating of thickness t, the light divides into two polarized beams that propagate at different velocities. It may be shown that the relative retardation δ between the two beams is given by

$$\delta = t(N_x - N_y) \tag{13}$$

where N_x and N_y are the indices of refraction in the x and y directions. The birefringence $(N_x - N_y)$ is proportional to the difference of the principal strains E_x and E_y, or

$$(N_x - N_y) = k(E_x - E_y) \tag{14}$$

where k is the strain optic material constant, a physical property of the material analagous to the gage factor of resistance strain gages. Combining the above equations yields the basic equation for the measurement of strain using birefringent sensors:

$$E_x - E_y = \delta/kt \tag{15}$$

In many applications, light passes through the birefringent material, reflects off of a diffusely reflecting substrate surface, and passes

through the birefringent material a second time. An instrument known as a photoelastic polariscope is then used to measure the retardation. It may be shown that the image obtained by a circular polariscope is unaffected by the direction of the principal strains and that the intensity I of the light emerging from the polariscope is given by:

$$I = A \sin^2[\pi(\delta/\lambda)] \quad (16)$$

where λ is the wavelength of the light and A is a proportionality constant. The light intensity, therefore, becomes zero when

$$\delta = N\lambda \quad (17)$$

where N, the isochromatic fringe order, is an integer.

Once δ is known, the difference in the principal strains is obtained by:

$$E_x - E_y = \delta/(kt) = N\lambda/(Kt) = Nf \quad (18)$$

where f is a proportionality constant. In theory, therefore, the principal strain difference can be obtained by counting isochromatic fringes.

3.8.3 Discussion

In practice, it is often difficult to measure the retardation accurately. Recently, a method called Spectral Contents Analysis (SCA) has been proposed to overcome many of the limitations associated with conventional techniques (Reference 3-104). In the SCA method, the reflected light is analyzed with a spectophotometer so that the intensity of numerous spectral bands is measured. The retardation is then calculated from the spectral intensity measurement. Strainoptic Technologies, Inc. of North Wales, PA, is currently exploring the feasibility of using SCA for high temperature strain measurement as part of an SBIR project with NASA Ames. They have used fused quartz as a sensor material up to 1300 K and will investigate several candidate materials for higher temperatures, some of which are proprietary. While in principle it would be possible to operate the SCA system in reflection mode by irradiating the surface normally and detecting light reflected by the test surface, in practice this may be difficult. Sensitivity would probably be low for any reasonable coating thickness unless a coating with a high strain optical coefficient is found. The outstanding problem with high temperature photoelastic measurements involves the selection of the birefringent coating. The material must retain its birefringent properties and adhere to the substate at operating conditions. If the strain-optic coefficient is temperature dependent, then temperature compensation is required. Until a satisfactory coating has been identified, successful application of photoelastic methods to high temperature strain analysis is problematic. If such a coating is found, photoelastic methods appear quite promising as a laboratory tool for high temperature strain analysis.

3.9 Concepts Recommended for Future Development

3.9.1 Discussion

No single measurement technique is ideally suited to all the diverse applications of high temperature strain measurement. These applications range from the the relatively straightforward case of tensile testing in a materials laboratory to the intractable case of measuring static strain on a rotating blade in an operating gas turbine engine. There is

currently considerable interest in the former measurement techniques suitable for determining the stress-strain response of materials at high temperature. Our recommendations are oriented toward techniques that have wide application and not toward those intended for specialized enviroments.

Despite the importance of materials testing in the laboratory, one of the most important applications in turbine engine development is stress/strain determination of hot rotating parts. Two of the strain measurement techniques reviewed in this report, the Simpson-Welch method (Section 3.2.3) and blade tip deflection methods (Section 3.6.1), could be considered for this difficult application. Based on proprietary data, we believe tip deflection methods are a very promising method of determining stress in rotating turbine blades. However, because tip deflection analysis has little application aside from turbine engine development, we do not recommend it within the context of the present study.

Point contact gages such as resistance and capacitance strain gages have been standard strain measurement tools for over 20 years. We believe there is room for growth in the resistance strain gage and that it may be the preferred measurement tool in a variety of applications for short term static strain measurement up to about 1200 K and for dynamic measurements up to 1450 K. However, given the problems associated with gage attachment, temperature compensation, deterioration of insulation resistance, and material degradation, we have little confidence that the resistance strain gage can extend beyond these limits. Therefore, although we believe the resistance strain gage warrants continued development, it does not appear promising given a target temperature over 1600 K.

Like the resistance strain gage, capacitance strain gages require contact with the test surface. The gage may be mounted directly on the surface or used as an extensometer with the capacitance element remote from the surface. In the former design, most lead wire-related problems that limit resistance gages also probably affect capacitance gages. Incremental improvements in the capacitance gage may allow this concept to be used up to 1400 K. We are not optimistic that direct mounted capacitance gages can successfully address higher temperatures, although it may be possible with gages using dielectrics other than air. As part of a remote extensometer, the capacitance gage may be usable to significantly higher temperatures in a controlled laboratory environment. Nevertheless, we believe that the extensometer approach will have limited application even if current efforts to reach 1900 K are successful.

Ideally, strain measuring devices should not contact the test urface, and indeed much effort has been devoted to this end. One promising method of contactless strain measurement is speckle interferometry. A real time implementation of speckle interferometry, known as either ESPI (Electronic Speckle Pattern Interferometry) or as TV holography, has recently been introduced. Existing commercial units are not primarily intended for strain measurement however. Although ESPI has been used to measure full-field static and dynamic strains, it suffers from a problem inherent to all interferometric techniques: thermal gradients in the atmosphere surrounding a specimen surface appear as spurious strains. In addition, strain measurement in the

presence of random vibrations is a major challenge. Despite the enormous progress made in developing the ESPI technology, these fundamental problems restrict its usefulness. Experts in the field consider strain measurement in hostile environments to be a difficult challenge for ESPI, but they are hopeful that the challenge can be met. We regard ESPI applied to hostile environments as a speculative technology and, therefore, we reluctantly cannot endorse ESPI as one of the most promising technologies for high temperature strain measurement.

Moire methods also have been regarded as a promising contactless method of measuring full field displacement and strain. Moire methods provide a mapping of the surface displacements from which it is possible to calculate extensional and shearing strains. Unlike ESPI, moire does not use the natural features of the specimen surface to diffract light, but instead requires attaching or engraving a specimen grating to the test surface. It is, therefore, not totally contactless, and indeed, specimen grating survivability is a major constraint on the use of moire methods in hostile environments. Conventional moire uses coarse specimen grids (about 40 lines/mm) and is, therefore, limited to measuring percent level strains. High sensitivity moire techniques have dramatically increased the sensitivity of moire methods so that under favorable conditions moire can measure as low as tens of microstrain.

Moire techniques have been applied in numerous ways in displacement and strain measurement. Several hybrid techniques couple moire methods with other technologies. One example is holographic moire (HI), in which moire procedures are applied to holographic interferometry. Holographic moire can provide sensitive real-time measurement of strain. As suggested by its name, HI requires isolation from mechanical vibrations and is sensitive to thermal gradients in the atmosphere surrounding the specimen. Another hybrid technique is moire interferometry, which combines the advantages of moire with those of two or four beam interferometry. Moire interferometry has been used with very high frequency gratings (up to 4000 lines/mm) to achieve high sensitivity strain measurement over a very wide dynamic range. To our knowledge, moire interferometry has not been applied to high temperature measurements, and thermal gradients in the atmosphere surrounding a specimen can be expected to be a difficult challenge.

Moire methods have progressed considerably over the past 15 years to where they can reasonably be applied to practical measurements. Unfortunately, the requirement for attached gratings, the need to maintain alignment between specimen and reference gratings, and, particularly for high sensitivity moire, the effects of thermal gradients between the gratings make moire methods less than ideal candidates for high temperature strain measurement.

3.9.2 Spectral Density Indication

An interesting concept for full-field strain measurement has recently evolved out of moire methods. Called Spectral Density Indication (SDI) by its inventor, it may use either a coarse grid etched onto the specimen surface or the natural surface features of a rough surface. In SDI, the spatial frequency of a digitized image of the grating in a stressed state is compared with that in an initial unstressed state. Eliminating the reference grating and the need to maintain the relative orientation of reference and

sample gratings provides SDI with a major advantage over moire methods. Furthermore, etched gratings can be expected to be more stable in hostile environments than are attached gratings. SDI has a very wide dynamic range: strain from less than 100 microstrain to several percent can be made from a single optical set up. The effect of thermal gradients in the atmosphere surrounding the specimen has not yet been evaluated, but can be expected to be significantly less than is associated with interferometry or moire methods. Although the SDI technique is relatively new and its limitations have not been well defined, we believe it is a very promising technique for strain measurement in hostile environments. Therefore, we recommend SDI for further development so that its applicability to strain measurement in hostile environments can be fully assessed.

3.9.3 Optical Tracking - Attached Targets

The strain measurement technique developed by Robert Marion at Sandia Laboratories over a decade ago was successfully employed on a specific project to measure uniaxial strain of material specimens heated to 3000 K. Marion's system used an optical tracker to measure the elongation between targets attached to the specimen surface. Although used primarily for dynamic uniaxial measurements, it also can be applied to static measurements. The requirement of attaching a target to the specimen surface can be a significant constraint; specifically, the cement nodule targets used by Marion would be a drawback in many strain measurement applications. Development of thin film targets would minimize the problems associated with large targets. The relative simplicity of the Marion method makes it an attractive candidate for general laboratory use and possibly for industrial use. We believe that the Marion technique holds the potential for becoming a useful method of uniaxial strain measurement of high temperature ceramics given relatively modest funding.

3.9.4 Dual Beam Doppler Interferometer

Optra, Inc. has developed a commercial noncontacting extensometer that is suitable for real time displacement and strain measurement for high temperature material testing. The Optra extensometer is capable of very high resolution measurements (less than 10 microstrain) under favorable test conditions. The upper temperature limit at which strain can be measured reliably has not been determined. Background radiation seems to become a significant problem above 1500 K, although the manufacturer believes that substantially higher temperatures can be tolerated if optical bandpass filters are used. Thermal gradients in the sight path also may introduce measurement errors, although the manufacturer believes these should not pose a major problem for steady state measurements. The OPTRA extensometer requires that rigid body movements be carefully controlled, preferably to within 10 times the movement due to strain. This stringent requirement may be relaxed significantly by optically tracking the rigid body movements. Such an enhancement could allow this instrument to be used outside of the controlled laboratory environment.

The Optra extensometer is no panacea for high temperature strain measurement. Rigid body movement and surface tilt may cause a loss of phase correlation and thereby contribute significantly to total measurement error (Optra refers to such errors as "dead-reckoning errors"). In its current state, the

Optra systen affords no way to eliminate or determine the magnitude of dead reckoning errors, although Optra believes that integrating optical tracking into the system may help solve this problem. Additionally, the extent to which multiple reflections from subsurface scattering centers may constrain measurements on ceramic materials has not yet been determined. However, the Optra system is sufficiently advanced that we believe that it has application in high temperature strain measurement. Enhancements to the existing design may allow the Optra extensometer to play a major role in material testing of ceramics in hostile environments. We therefore recommend the Optra extensometer as a candidate for further development.

4.0 Heat Flux

4.1 Background Information

Heat flux sensors described in the technical literature can generally be categorized as steady state or transient measurement devices. In basic terms, a steady-state device consists of a means for generating a differential temperature across a thermal barrier such that temperature difference is proportional to heat flux. Transient devices are capable of generating an output proportional to a change in heat flux.

Practical applications for heat flux sensors related to development of advanced gas turbine engines are generally related to verification of computer models used to generate input for thermal analyses of hot section components. A typical environment for both rotating and stationary components is a combustion gas flowpath. Steady-state heat flux sensors are suitable for most applications involving cooled structural components based on current materials limitations. Advances in materials temperature cability may lead to use of noncooled (nonmetallic) components for which transient heat flux sensors will be needed.

The requirements for steady-state and transient heat flux transducers for application in a gas turbine hot section component include the following.

- Must be capable of surviving in the test environment
- Must generate a signal proportional to heat flux or change in heat flux with minimum interference with heat flow
- Must not cause significant aerodynamic interference
- Must be installed in, or be a part of, the component being tested
- Response changes caused by variations in absolute temperature level must be repeatable and calibratable
- Must have spatial resolution consistent with requirements.

Although the literature survey did not include any references to heat flux sensors suitable for use on ceramic materials at temperatures above 1350 K, it did turn up a significant quantity of useful information about heat flux sensors for use on superalloy materials operating at temperatures up to 1250 K. Such sensors are of interest because they are directly applicable to hot section components using thermal barrier coatings over superalloy materials.

The concepts which have been most thoroughly investigated include the following:

1. Embedded Thermocouple (normal gradient sensor)
2. Gardon Gage (lateral gradient sensor)
3. Slug Calorimeter
4. Surface Mounted Sensor
5. Indirect Measurement.

General characteristics of various types of heat flux sensors are compared in Table 8.

4.2 Concept Description and Adaptability to Ceramic Materials

4.2.1 Embedded Thermocouple

The concept is usable for both steady state and transient measurements where the conditional assumption of one dimensional heat flow is valid (Reference 4-1). Steady-state heat flux through the wall is a function of temperature drop across a known wall thickness according to the following relationship.

$$Q = k/x\,(T_1 - T_2) \qquad (19)$$

Where:

Q = Heat Flux
k = Thermal Conductivity
x = Wall Thickness Between T_1 and T_2
T_1 = Wall Temperature, Hot Side
T_2 = Wall Temperature, Cold Side

Under conditions of transient heat flux, it is necessary to measure both the differential temperature across the wall and the absolute temperature of either wall. The equation which relates heat flux to temperature and time is as follows.

$$Q(t) = k/x\,[T_1(t + x^2/3d) - T_2\,(t - x^2/6d)] \qquad (20)$$

Where:

t = time
d = diffusity of wall

The embedded thermocouple concept (Figure 12) is directly applicable to metal parts which can be slotted to accept the sensors. Good results up to 1250 K have been reported (Reference 4-2). The concept is adaptable to fabrication as a separate entity that can be calibrated and subsequently welded into the component where it will be used. An alternate fabrication method consists of manufacturing the sensor directly into the component. This may complicate the calibration procedures but will avoid compromising the component or its coating by joining the preassembled sensor.

A serious limitation is related to the need to have access to the cold side for sensor installation and/or lead routing. This would limit usefulness because many hot section components of interest (such as airfoils with internal cooling passages) do not have cold side access required for sensor installation.

The problem of finding a suitable thermocouple alloy may be serious, depending on upper temperature capability requirement. As shown in Figure 12, the metal wall is one element of the differential thermocouple. Choices for the other thermocouple element become more limited as temperature levels increase.

Adaptability to ceramic materials is severely limited. It is unlikely that grooves will be permitted for placement of the thermocouples, as this would lead to structural compromise. For nonconducting ceramics, the concept of a differential thermocouple becomes a significant design task.

4.2.2 Gardon Gage

This concept, as illustrated in Figure 13, can be used for both steady-state and transient measurements and depends on the radial

Table 8. *Heat Flux Sensor Concept Characteristics.*

Description	Adaptable To			Upper Temperature Limit, K	Probability of Success, %	Minimum Sensing Area, mm	Minimum Wall Thickness, mm	Rework to Part	Cold Side Access Required	±5% Accuracy for $Q = \frac{5\ MW}{M^2}$	Additional Comments
	Metal Substrate	Thermal Barrier Coating Over Metal	Nonconducting Ceramic								
Differential Temperature Across Wall (Embedded Thermocouple)	Yes	Yes	No	1250 (Type K) 1650 (Type S)	80 40	1.5	1.0	Grooves for Leads	Yes	Yes-Based on Calibration	• Steady State or Transient (see Figure 11)
Differential Temperature In Plane of Wall (Gardon Gage)	Yes	Marginal	No	1250 (Type K) 1650 (Type S)	80 40	1.5	1.5	Hole From Cold Side to Form Foil	Yes	Yes-Based on Calibration	• Steady State or Transient (see Figure 12)
Slug Calorimeter	Yes	Yes	Yes	1650	50	15.0	1.0	For Reduced Sensing Area	Yes	Yes-Based on Calibration	• Transient Only (see Figure 13)
Differential Temperature Across Thermal Barrier (Surface Mounted Thin Film Sensor	Yes	Yes	Yes	1650 (Type S)	40	1.0	1.0	Hot Side Shallow Groove (100 μm Depth)	No	Yes-Based on Calibration	• Steady State (see Figure 15)
Surface Mounted Thin Film Sensor	Yes	Maybe	Yes	1650	50	15.0	1.0	No	No	Yes-Based on Calibration	• Transient Only
Indirect Measurement - Use a Single Temperature Sensor at a Specific Location to Verify Finite Element Model	Yes	Yes	Yes	1650	50	1.0	Depends on Model and Sensor Type	Depends on Model and Location Selected	No	Yes	• Requires a Well Developed Model to be Effective
Dual Wavelength Radiation Pyrometer	No	Yes	Only With Coating	No Limit	50	1.0	No Minimum	No	No	Questionable	• Line of Sight Required • Steady State

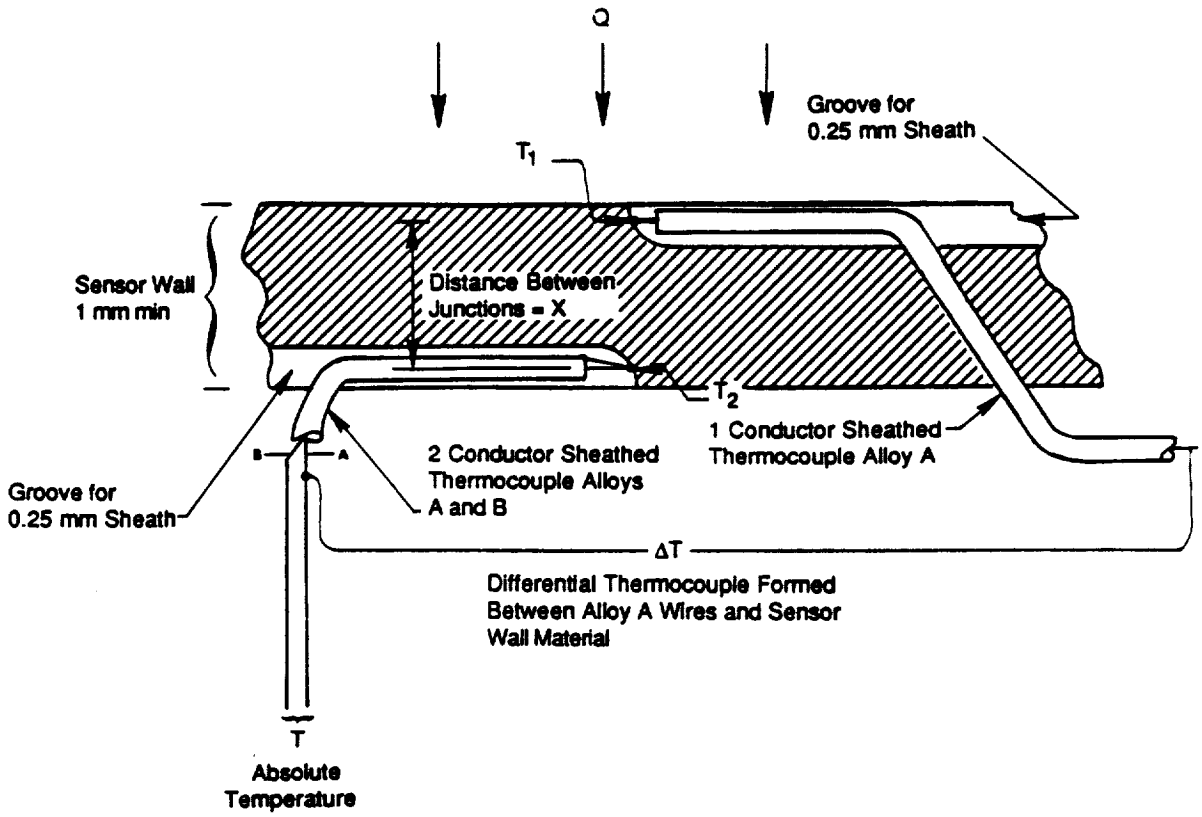

Figure 12. *Embedded Thermocouple Heat Flux Sensor Concept Schematic.*

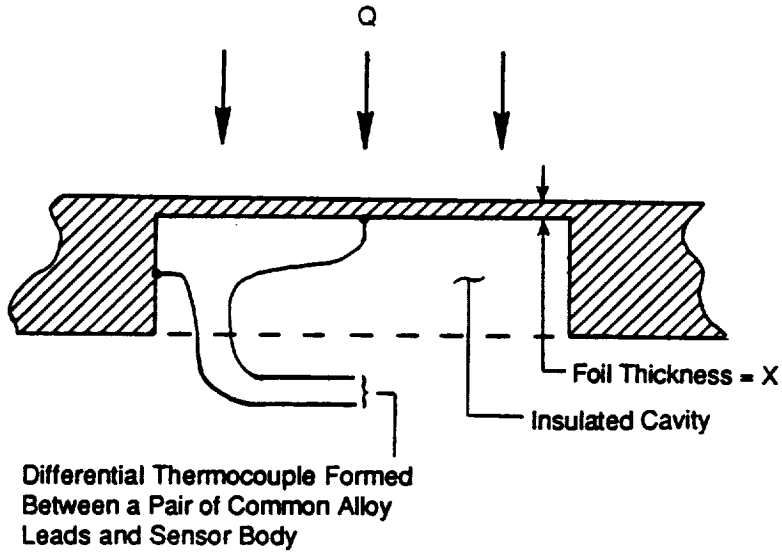

Figure 13. *Gardon Gage Concept Schematic.*

flow of heat from the center of the sensor (thin foil disk) to the sidewall heat sink. For steady-state conditions, the basic relationship between heat flux and differential temperature is as follows (Reference 4-1):

$$Q = 4kx/r^2 \ (T_1 - T_2) \qquad (21)$$

Where:

Q = Heat Flux
k = Thermal Conductivity
x = Foil Thickness
r = Foil Radius
T_1 = Temperature at Center of Disk
T_2 = Temperature at Radius of Disk

For transient heat flux measurements with frequency components less than $4d/r^2$ rad/sec, the relationship becomes (Reference 4-1):

$$Q = \rho c[3/4(dT_1/dt) + 1/4(dT_2/dt) + 4d/r^2 \ (T_1 - T_2) \qquad (22)$$

Where:

ρ = Disk Density
c = Disk Specific Heat
d = Disk Diffusivity

These units are commercially available for use up to 1300 K and have been evaluated in References 4-2 and 4-3. Units have been fabricated as part of a component by machining a flat-bottom hole into the wall from the cold side leaving a thin foil disk which is instrumented with a differential thermocouple from the cold side.

The need for cold side access represents a serious limitation for practical applications. A thermal barrier coating over the sensor would reduce the sensitivity by increasing the effective thickness of the foil disk. Adaptability to ceramic parts is difficult because of geometry considerations and limited differential thermocouple design problems.

4.2.3 Slug Calorimeter

This concept is based on measurement of time rate of change of absolute temperature of a mass with thermal inertia exposed to a change in heat flux. Figure 14 illustrates the concept and additional information is included in References 4-1 and 4-4.

The sensor can be added to or made as part of the wall of the component. If heat flux gradients exist along the component wall and local fluxes are required, a means of thermally isolating sections of the wall around the sensor is needed.

Cold wall access is necessary, with inherent restrictions concerning limited usefulness associated with many components and difficulty in adapting to ceramic components. Because of interference with the measurement of temperature, the technique is not practical where a coolant fluid is present.

4.2.4 Surface-Mounted Sensor

This concept consists of two temperature sensors isolated from each other by a thermal barrier as illustrated in Figure 15. When such a device is mounted on a surface through which heat is flowing, a difference in temperature across the thermal barrier proportional to heat flux is generated in accordance with the equation for embedded thermocouple heat flux sensors operating in the steady-state mode. Although most applications of this technique reported in the literature are not suitable for high temperature (References 4-5 and 4-6), there is reason

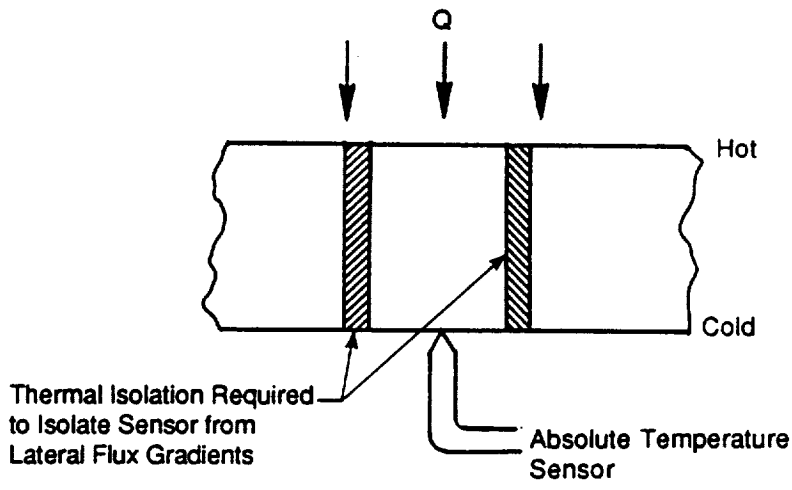

Figure 14. *Slug Calorimeter Concept Schematic.*

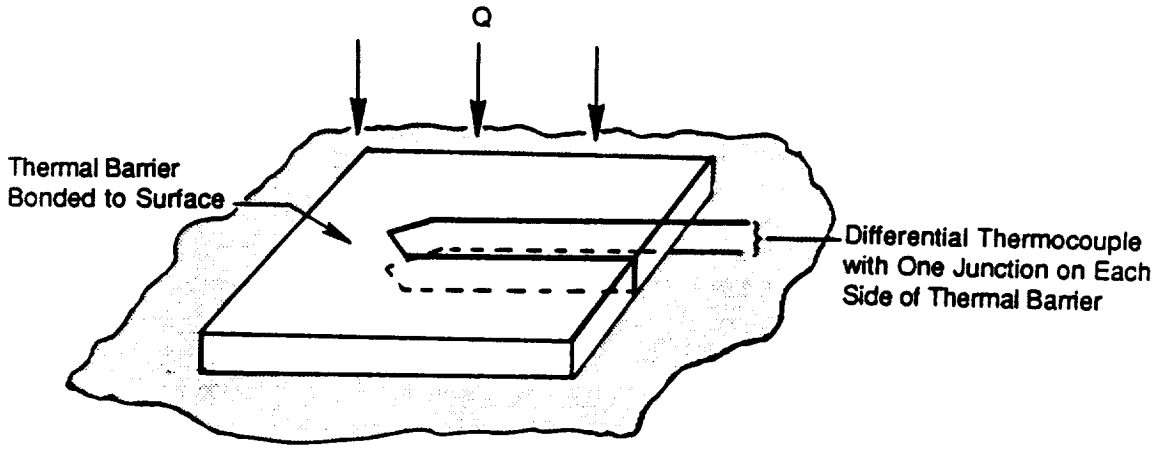

Figure 15. *Surface Mounted Heat Flux Sensor Using Plastic or Kapton for Thermal Barrier.*

for optimism concerning the use of thin film sensors in a configuration which could extend the upper temperature limit to the point where it could be of interest for the current program.

A major advantage of this sensor is that it does not require access to the cold side. It does require attachment to the hot side surface and may be thick enough to cause boundary layer interference unless recessed in the component surface or used under thermal barrier coatings. Development of thin film technology is required for successful application of this concept for temperature levels beyond 1250 K.

4.2.5 Indirect Measurement

This concept is based not on a direct measurement of heat flux but on its inference from temperature measurements and data matching techniques. This has been the method most often used in gas turbine applications in the absence of acceptable direct heat flux measurement techniques. Advances in finite element modeling and inverse conduction codes have significantly improved this procedure. Measurement of absolute temperatures at specific locations is required (Reference 4-4). The concept is appropriate for both steady-state and transient heat flux modes. This technology is directly applicable for thermal barrier coated parts. The adaptation of the concept for use with ceramic composites operating at high temperatures depends on the development of techniques for measurement of surface or internal temperature at specific locations in such materials.

4.2.6 Radiation Type Heat Flux Sensor

No reference was found in the literature regarding this concept. The idea is based on the fact that some ceramic materials may be transparent at certain wavelengths and opaque at others. Considering the case of a thermal barrier coated blade (100-500 μm of coating on a metal substrate), it should be possible to measure either the metal substrate surface or the coating surface temperature by selecting two radiation pyrometer detector wavelengths. If the thermal conductivity and thickness of the coating is known, it will be possible to calculate heat flux. This also necessitates a knowledge of surface emittances at both wavelengths. Temperature change across the coating needs to be relatively high to allow determination of differential temperature from two absolute values.

4.3 Heat Flux Sensors Recommended for Further Development

4.3.1 Surface-Mounted (Differential) Sensor

Adaptation of the classical concept of differential temperature across a thermal barrier is shown in Figure 16. This sensor does not require access to the cold side at the point of measurement. It does require development of thin film technology beyond current capabilities. Use of SiC as the sensing element would limit upper temperature to 1850 K in air due to softening of SiO_2 which forms on the surface of SiC. Insulation resistance may restrict upper temperature limit to much lower levels, depending on the resistivity of the substrate. Application and doping of the SiC films will require extensive process development.

Interference with boundary layer due to the sensor application thickness may require mounting below the normal substrate sur-

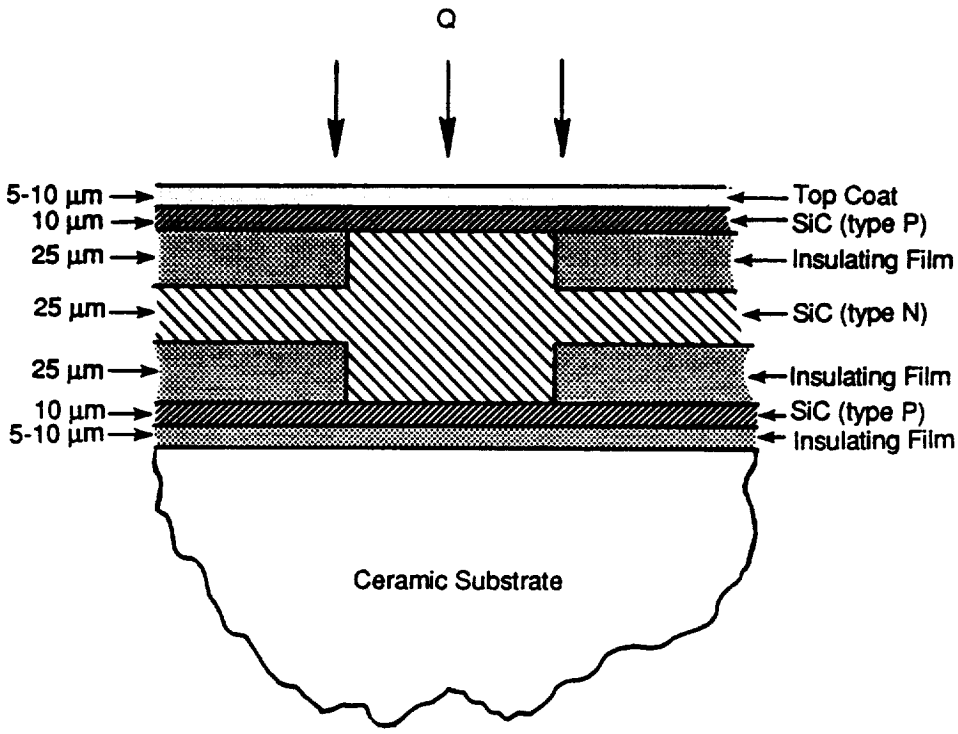

Estimated Transducer Sensitivity $= 3\ \mu V/KW/m^2$

Based on:

$$\Delta T = Q\frac{\Delta x}{k}$$

ΔT = temperature difference, K

Q = heat flux, $5\times10^{6} W/M^2$

Δx = transducer thickness, 75×10^{-6} M

k = thermal conductivity, 2.4×10^{-2} KW/MK

$$\Delta T \text{ across } (SiC)_N = 5000\times\frac{75\times10^{-6}}{2.4\times10^{-2}} = 15.625 \text{ K}$$

$$\text{Volts output} = 15.625 \text{ K} \times 960\frac{\mu V}{K} = 15{,}000\ \mu V$$

$$\text{Transducer sensitivity} = \frac{15{,}000\ \mu V}{5{,}000\ KW/M^2} = 3\frac{\mu V}{KW/M^2}$$

Note: $960\frac{\mu V}{K}$ Thermoelectric potential based on measurements between $(SiC)_N$ and $(SiC)_P$ at 1100 K (by GE)

Figure 16. *Surface Mounted Heat Flux Sensor for High Temperature Applications.*

face. Sensor interference with heat flux will depend on thickness and property differences between sensor and substrate.

4.3.2 Thin Film Surface Mounted (Absolute) Sensor

This concept is based on application of a thin film temperature sensor on the surface of a component exposed to transient heat flux normal to the surface. If the thin film sensor has insignificant temperature drop across its thickness and if the component wall can be considered infinitely thick, then a transient heat flux can be determined by measuring the time rate of change of the surface mounted thermocouple in accordance with the following (Reference 4-1):

$$Q(t) = \frac{1}{2}\sqrt{\pi}\,\rho c k\left[\frac{T(t)}{\sqrt{t}} + \frac{1}{\pi\sqrt{t}}\int_0^t \frac{\sqrt{\lambda}T(t) - \sqrt{t}T(\lambda)}{(t-\lambda)^{3/2}}\right]d\lambda \qquad (23)$$

Q = Heat Flux

t = Time

ρ = Density of Wall

c = Specific Heat

k = Thermal Conductivity

λ = Dummy Time Variable for Integration

Although there are specific limits on sensor and wall thicknesses and transient heat flux frequency components, this type of sensor appears to have potential for use on ceramic components. Access from one side only is necessary and no rework is required.

4.3.3 Indirect Measurement

Although this is not a specific technique for direct measurement of heat flux, it does allow validation of thermal analysis modeling techniques and should be considered for that purpose. This method is applicable to thermal barrier coated components using embedded thermocouples in the metal substrate and on ceramic composite components using surface mounted thermocouples or radiation pyrometer readings of surface temperature.

5.0 References

1-1. Lockheed Aeronautical Systems Company - California, "Instrumentation Development for the National Aerospace Plane - Final Report," Contract No. F33657-86-2125, February 1988.

1-2. Moffat Thermosciences Inc., "Surface Temperature Measurements at High Temperatures - The State Of The Art, 1986".

2-1. Samsonov, G.V.and Kislyi, P.S., "High Temperature Non-Metallic Thermocouples and Sheaths," Consultants Bureau, New York, 1967.

2-2. Kaplan, R.B., Fry, V., Harding, J.T., "Oxidation Protection of Rhenium Thrusters for 2480 K Cyclic Operation by Means of CVD Coatings," NAS3-24868, July 1986.

2-3. Phillips, W.L., "Oxidation of Platinum Metals in Air," Trans. ASM, Vol. 57, 1964.

2-4. Schlichting, J., "Oxygen Transport Through Silica Surface Layers on Silicon-Containing Ceramic Materials," High Temperatures-High Pressures, Vol. 14, 1982.

2-5. Manufacturing Data Sheet, "KANTHAL SUPER" Electric Furnace Heating Elements.

2-6. "Platinum", Bulletin A-445, Pub. International Nickel Company.

2-7. von Muench, W., et al., "Preparation of Pure and Doped SiC by Pyrolysis of Silane Compounds", J. Electrochemical Soc., Vol.125, No. 2, February 1978.

2-8. Seaward, K.L., et al., "The Synthesis of SiC_x Films by Dual-Source Sputter Deposition," J. Vac. Sci. Technol., A4 (1), Jan/Feb 1986.

2-9. Hamilton, D.R., "Sublimation Grown Silicon Carbide," J. Electrochemical Soc., 105, 735, 1958.

2-10. Addamiano, et al., "Implantation Effects of Nitrogen, Boron, and Aluminum in Hexagonal Silicon Carbide," J. Electrochemical Soc., October 1972.

2-11. Kiyotaka, Wasa, et al., "Highly Reliable Temperature Sensor Using RF-Sputtered SiC Thin Film," Rev. of Sci. Instrum. 50 (9), September 1979.

2-12. Fitzer, E., and Schwab, J., Journal Metallk 9, 1955.

2-13. Minamoto, M.T., "Thermocouple Furnace for Device Fabrication," *Proceedings of the Conference on Silicon Carbide,* Pergamon Press, April 1959.

2-14. Franks, E., "High Temperature Thermocouples Using Non-Metallic Members," *Temperature, Its Measurement and Control in Science and Industry,* Vol. 3, Reinhold Pub. Corp., 1962.

2-15. Lauenko, V.A., et al. "High Temperature Oxidation of Silicon Based Materials," Oxidation of Metals, Vol. 27, Nos. 1/2, 1987.

2-16. Schiroky, G.H., "Corrosion Pitting of SiC by Molten Salts," J. Electrochemical Society, Vol. 133, No. 12, December 1986.

2-17. Brook R., et al., New Scientist, 101, 13, 1984.

2-18. Keyes, R.W., IEEE Proc., 60, 225, 1972.

2-19. Parson, J.D., Solid State Technology, 28, November 1985.

2-20. von Muench, W., IEDM, Washington, DC, 1977.

2-21. Murarka, S.P., *Silicides for VLSI Applications*, Academic Press, NY, 1983.

2-22. Tauc, J., *Photo and Thermoelectric Effects in Semiconductors,* Pergamon Press, NY, 1962.

2-23. Bauer, A.A., and Bates, J.L., "An Evaluation of Electrical Insulators for Fusion Reactors," Battelle Memorial Institute Report BMI 1930.

2-24. Galasso, F., Kuntz, U., Croft, W.J., "Pyrolytic Si_3N_4," J. Amer. Ceramic Soc., Vol. 55, 1972.

2-25. Weast, R.C., *Handbook of Chemistry and Physics*, 48th Edition, The Chemical Rubber Co., Cleveland, OH, 1968.

2-26. Samsanov, G.S., *The Oxide Handbook,* Plenum Press, NY, 1973.

2-27. "Refractory Ceramics for Aerospace," Compiled by Battelle Memorial Inst., Columbus, OH, 1964.

2-28. 1975 Materials Selector, Vol. 80, No. 4, 1974, Materials Eng., Reinhold.

2-29. Union Carbide, "Boralloy"-Manufacturing Data Sheet, 1975.

2-30. Ceramic Data Book, 63rd Edition, 1984.

2-31. Hodgman, C.D., et al., "Handbook of Chemistry and Physics," Chemical Rubber Co., Cleveland, OH, April 1962.

2-32. Johnson, W.W. Jr., High Temperature Thermometry, March 1966, N69-70676.

2-33. Pittenpaul, E., et al., Inst. Phys. Conf., Ser. No. 53, 21, 1980.

2-34. Costello, J.A., and Tressler, R.E., "Oxidation Kinetics of Silicon Carbide Crystals and Ceramics," J. Amer. Ceramic Society, Vol. 69, No. 9, September 1986.

2-35. Kostkowski, H.J., and Lee, R.D., "Theory and Methods of Optical Pyrometry," NBS Monograph 41, 1962.

2-36. Dewitt, D.P., and Kunz, H., "Theory and Technique for Surface Temperature Determinations by Measuring the Radiance Temperatures and the Absorptance Ratio for Two Wavelengths," *Temperature, Its Measurement and Control in Science and Industry,* Instrument Society of America, 1972.

2-37. Svet, D.A., "Independent Determination of Emissivity from Natural Thermal Radiation Spectra," Soviet Phys. Dok., Vol. 20, No. 3, 1975.

2-38. Quinn, T.J., and Compton, J.P., Rep. Prog. Phys., Vol. 38, 1975.

2-39. Babelot, J.F., Magill, J., Ohse, R.W., "Microsecond and Sub-Microsecond Multi-Wavelength Pyrometry for Pulsed Heating Technique Diagnostics," *Temperature - Its Measurement and Control in Science and Industry,* American Institute of Physics, 1982.

2-40. Hunter, G.B., Allemand, C.D., and Eagar, T.W., "Multiwavelength Pyrometry - An Improved Method," Optical Engineering, Vol. 24, No. 6, Nov./Dec. 1985.

2-41. Coates, P.B., "Multiwavelength Pyrometry," Metrologia 17, p. 103, 1981.

2-42. Nordine, P.C., "The Accuracy of Multicolor Optical Pyrometry," High Temperature Science, Vol. 21, 1986.

2-43. Atkinson, W.H., and Strange, R.R., "Pyrometer Temperature Measurements in the Presence of Reflected Radiation," ASME 76-HT-74, 1976.

2-44. Murray, T.P., "Polaradiometer - A New Instrument For Temperature Measurement," The Review of Scientific Instruments, Vol. 38, No. 6, 1967.

2-45. Touloukian, Y.S., DeWitt, D.P., - *Thermophysical Properties of Matter,* Vols. 8 and 9, Plenum Press, 1970.

2-46. "Pyro-Laser" Descriptive Brochure, the Pyrometer Instrument Company, Northvale, NJ, February 1987.

2-47. Crovini, L., "Resistance Thermometry," High Temperatures - High Pressures, Vol. 11, 1979.

2-48. Quinn, T.J., and Compton, J.P., Rep. Prog. Phys., Vol. 38, 1975.

2-49. Evans, J.P., and Burns, G.W., "A Study of Stability of High Temperature Platinum Resistance Thermometers," *Temperature, Its Measurement and Control in Science and Industry,* Instrument Society of America, Vol. 3, 1972.

2-50. McAllan, J.V., "Practical High Temperature Resistance Thermometry," *Temperature, Its Measurement and Control in Science and Industry,* Instrument Society of America, Vol. 5, 1982.

2-51. Anderson, A.R., and Stickney, T.M., "The Use of Ceramic Resistance Thermometers at Temperature Standards Above 2300 R," *Temperature, Its Measurement and Control in Science and Industry,* Reinhold, Vol. 3, 1962.

2-52. Fry, E.M., "Thermographic Phosphor Surface Temperature Measurement Technique: Application to Integrated Circuits," *Temperature, Its Measurement and Control in Science and Industry,* Instrument Society of America, Vol. 4., 1972.

2-53. Zizak, G., Omenetto, N., and Winefordner, J.D., "Laser-Excited Atom Fluorescence Techniques for Temperature Measurements in Flames - A Summary," Opt. Eng., Vol. 23, No. 6, 1984.

2-54. Wickersheim, K.A., Heinemann, S.O., Tran, H.N., and Sun, M.H., "Second Generation Fluoroptic Thermometer," ISA paper No. 85-0072, Instrument Society of America, Research Triangle Park, NC, 1985.

2-55. Cates, M.R., et al., "Remote Thermometry of Moving Surfaces of Laser-Induced Fluorescence of Surface-Bonded Phosphor," ICALEO Proc. Vol. 39, 1983.

2-56. Cates, M.R., et al., "Applications of Pulsed-Laser Techniques and Thermographic Phosphors Dynamic Thermometry of Rotating Surfaces," ICALEO Proceedings, Vol. 4, 1984.

2-57. Noel, B., et al., "A Proposed Method for Remote Thermometry in Turbine Engines," AIAA Publication No. AIAA-85-1468, 1985.

2-58. Cates, M.R., et al., "Laser-Induced Fluorescence of Europium-Doped Yttrium Oxide Remote High-Temperature Thermometry," Martin Marietta Energy Systems Report No. K/TS-11, 1985.

2-59. Leskovar, B., et al., "Photon Counting System for Subnanosecond Fluorescence Lifetime Measurements," Rev. Sci. Inst., Vol. 47, No. 9, 1976.

2-60. Babelaar, D., "Time Response of Various Types of Photomultipliers and its Wavelength Dependence in Time Correlated Single Photon Counting With an Ultimate Resolution of 47 ps FWHM," Rev. Sci. Inst., Vol. 57, No. 6, p. 1116, 1986.

2-61. Wickersheim, K.A., and Lefever, R.A., "Luminescent Behavior of the Rare Earths in Yttrium Oxide and Related Hosts," J. Electrochem. Soc., Vol. 3, 1964.

2-62. Borella, H.M., et al., "Development of Bonding Techniques for High-Temperature Applications of Thermographic Phosphors" EG&G Report No. 10282-2085, 1985.

2-63. Garrison, J.B., and Lawson, A.W., "Absolute Noise Thermometer for High Temperatures and High Pressures," Rev. Sci. Inst. 20, p. 785, 1949.

2-64. Crovini, L., and Actis, A., "Temperature Measurement," Billing, B.F., and Quinn, T.J., Eds., Institute of Physics Conference, Vol. 26, London, 1975.

2-65. Brixy, H., et al., "Ceramics as Materials for Measurement Resistors in Noise Thermometry," High Temperature - High Pressure, Vol.15, 1983.

2-66. Mallinckrodt, D., Hausser, H., and Brixy, H., "Ceramic Resistors for Noise Thermometer," High Temperature - High Pressure, Vol.17, 1985.

2-67. Decreton, M.C., "High Temperature Noise Thermometry for Industrial Applications," *Temperature, Its Measurement and Control in Science and Industry,* American Institute of Physics, J.F. Schooley, ed., 1982.

2-68. Brophy, J.J., Epstein, M., and Webb, S.L., "Correlator Amplifier for Very Low Signal Levels," Rev. Sci. Inst., Vol. 36, p. 1803, 1965.

2-69. Brixy, H., et al., "Application of Noise Thermometry in Industry Under Plant Conditions," *Temperature, Its Measurement and Control in Science and Industry,* American Institute of Physics, 1982.

2-70. Klempt, G., "Errors in Johnson Noise Thermometry," *Temperature, Its Measurement and Control in Science and Industry,* American Institute of Physics, 1982.

2-71. Borkowski, C.J., and Blalock, T.V., "A New Method of Johnson Noise Thermometry," Rev. Sci. Inst., Vol. 45, 1974.

2-72. Blalock, T.V., Horton, J.L., and Shepard, R.L., "Johnson Noise Power Thermometer and its Application in Process Temperature Measurement," *Temperature, Its Measurement and Control in Science and Industry,* American Institute of Physics, 1982.

2-73. Tasman, H.J., and Richter, J., "Unconventional Methods for Measuring High Temperatures," High Temperature - High Pressure, Vol. 11, p. 87, 1979.

2-74. Culshaw, B., et al., Electronic Letters 13, 1977.

2-75. Eickhoff, W., "Temperature Sensing by Mode-Mode Interference in Birefringent Optical Fibers," Optics Letters, Vol. 6, No. 4, p. 204, April 1981.

2-76. Corke, M., Kersey, A.D., and Jackson, D.A., "Temperature Sensing With Single Mode Optical Fibers," J. Phys. E: Sci Instrum., Vol. 17, No. 11, p. 988, 1984.

2-77. Redner, A.S., Voloshin, A.S., "Final Report, Spectral Contents Readout of Birefringent Sensors," NASA 2-12351, Strain Optic Technologies Inc., 1986.

2-78. Dunphy, J.R., Meltz, G., "Development of a Fiber Optic Sensor for Turbine Disk Diagnostics," AIAA/SAE/ASME/ASEE 21st Joint Propulsion Conference, July 1985.

2-79. Jackson, D.A., "Monomode Optical Fibers for Precision Measurement," J. Phys. E, Vol. 18, No. 12, p. 981, 1985.

2-80. Dils, R.R., "High Temperature Optical Thermometer," J. Appl. Physics, Vol. 54, No. 3, March 1983.

2-81. Tasman, H.A., and Richter, J., "Unconventional Methods for Measuring High Temperatures," High Temperatures - High Pressures, Vol. 11, 1979, p. 87.

2-82. Lynnworth, L.C., and Carnevale, E.H., "Ultrasonic Thermometry Using Pulse Techniques," *Temperature, Its Measurement and Control in Science and Industry,* Instrument Society of America, 1972.

2-83. Benjaminson, A., and Rowland, F., "The Development of a Quartz Resonator as a Digital Temperature Sensor With a Precision of 1×10^{-4}," *Temperature, Its Measurement and Control in Science and Industry,* Part 1, p. 701, Instrument Society of America, 1972.

2-84. Bell, J.F.W., "Ultrasonic Thermometry Using Resonance Techniques," *Temperature, Its Measurement and Control in Science and Industry,* p. 709, Instrument Society of America, 1972.

2-85. Bell, J.F.W., et al., International Colloquium of High Temperature In-Pile Thermometry, Vol. 2, pp. 649-680, 1975.

2-86. Bell, J.F.W., "The Velocity of Sound in Metals," Phil. Mag. 2 (8), p. 1113, 1957.

2-87. Tasman, H.A., et al., "Ultrasonic Thin Wire Thermometry for Unclean Applications," *Ultrasonic Temperature, Its Measurement and Control in Science and Industry,* Part 2, p. 1191, American Institute of Physics, 1982.

2-88. Tasman, H.A., et al., "The TRESON Experiments - Measurement of Temperature Profiles in Nuclear Fuels by Means of Ultrasonic Thermometers," High Temperature - High Pressures, Vol. 9, No. 4, p. 387, 1977.

2-89. Miller, G.N., et al., Ultrasonic Symposium Proceedings, IEEE Cat. No. 80 CH 1602-2, 1980.

2-90. Lynnworth, L.C., "Use of Ultrasonics for High Temperature Measurements," Materials Evaluation 27 (3), 1969.

2-91. Fam, S.S., Lynnworth, L.C., and Carnevale, E.H., "Ultrasonic Thermometry," Instrumentation and Control Systems, p. 107, October 1969.

2-92. Tasman, H.A. et al., "Ultrasonic Thin-Wire Thermometry for Nuclear Applications," *Temperature, Its Measurement and Control in Science and Industry*, Part 2, American Institute of Physics, 1982.

2-93. Shepard, R.L., et al., "Thermoelectric, Resistance, and Ultrasonic Centerline Thermometry for a $(U_2Pu)O_2$ Fuel Pin," Trans. Am. Nuc. Soc., Vol. 15, p. 766, 1972.

2-94. Bildstein, H., and Eck, R., "Eigenschoften Hochverformter Wolfram-Legierungen für die Vakuumtechnologie," High Temperature - High Pressures, Vol. 10, No. 2, p. 215, 1978.

2-95. Arave, A.E., and Meservey, R.H., "High Temperature Ultrasonic Thermometer for Meauring Reactor Fuel Temperature," Idaho Nuclear Corp. Report IN-1413, TID-4500, 1970.

2-96. Lapp, M., and Penney, C.M., "Laser Raman Gas Diagnostics," Plenum Press, New York, NY, 1974. *Temperature, Its Measurement and Control in Science and Industry*, American Institute of Physics, 1982.

2-97. Compaan, A.O., and Trodahl, H.J., "Resonance Raman Scattering in Si at Elevated Temperatures," Phys. Rev. B, Vol. 29, No. 2, p. 793, 1984.

2-98. Compaan, A.O., "Raman Studies of Surface Temperature of Laser-Heated Semiconductors," DTIC Report No. AD-A151377, 1985.

2-99. Goodman, P., "Maximum Surface Temperature Measurement by Means of Kryptonates" *Temperature, Its Measurement and Control in Science and Industry,* Instrument Society of America, 1972.

2-100. Albertson, W.R., "Temperature Paints" General Electric, R 61 FPD 143, 1961.

2-101. Kasanof, D.R., Kimmel, E., "Recent Developments in Fusible Temperature Indicators," *Temperature, Its Measurement and Control in Science and Industry,* Vol. 3, Reinhold, 1962.

3-1. Perry, C.C., Lissner, H.R., *The Strain Gage Primer,* McGraw Hill, 1955.

3-2. Weise, R.A., Foster, J.H., "High Temperature Strain Gage System For Application to Turbine Engine Components," AFWAL-TR-80-2126, January 1981.

3-3. Lemcoe, M.M., "Characterization of BCL Strain Gages for Use to 1366 K (2000° F)," Final Report - NASA CR 132739, August 1975.

3-4. Stetson, K.A., "Demonstration Test of Burner Liner Strain Measurement System," Final Report - NAS3-23690, R84-926376-15, CR-174743, June 1984.

3-5. Wu, T.T. and Ma, L.C., "Comparison Characteristics of Temperature - Compensated Resistance Strain Gages for Use to 700° C and 800° C," 4th Annual Hostile Environments and High Temperature Measurements Conference, March 1987.

3-6. Anderson, B.R., "Development of a 1300° F Self Temperature Compensated Static Strain Gage," GE Technical Information Series Report No. R83AEB634, December 1983.

3-7. Hulse, C.O., Bailey, R.S., Grant, H.P., and Przybuszewski, J.S., "High Temperature Static Strain Gage Development Contract," NASA R87-916527-1, CR-180811, July 1987.

3-8. Brittain, J.O., Geslin, D., and Lei, J.F., "Elevated Temperature Strain Gages," NASA Conference Publication 2444 (Host 1986).

3-9. Battiste, R.L., "High Temperature Strain Measurements In Nuclear Reactor Research and Development," presented at High Temperature Measurements for Experimental Mechanics Conference, March 1985.

3-10. Smith, J.E., "Assessment of Current High-Temperature Gages," ORNL TM-7025, 1979.

3-11. Lelzter, S.G., "The Lock-in Amplifier as Capacitance/Conductance Meter," Princeton Applied Research Application, Note AN-110-2M-2/72-DW.

3-12. Gillette, O.L., "Research and Development of a High Temperature Capacitance Strain Gage for Operation at 2000° F," Technical Report AFFDL-TR-71-103, 1971.

3-13. Hammond, V.J., "High Temperature Capacitance Strain Transducers," from Strain Measurement at High Temperatures, R.C. Hurst, Ed., Elsevier Applied Science Publishers, New York, 1986.

3-14. Yeakley, L.M., and Lindholm, U.S., "Development of Capacitance Strain Transducers for High-Temperature and Biaxial Application," Exp. Mech., August 1974.

3-15. Marion, R.H., "A New Method of High-Temperature Strain Measurement," Exp. Mech., April 1978.

3-16. Sharpe, W.N., "Application of the Interferometric Strain/Displacement Gage," Opt. Eng., Vol. 21, No. 3, 1982.

3-17. Sharpe, W.N., "In-Plane Interferometric Strain/Displacement Measurement at High Temperatures," University of Strathclyde, 1981.

3-18. Sharpe, W.N., Opt. Eng., 1982

3-19. Simpson, M.L., and Welch, D.E., "Optoelectronic Strain Measurement System for Rotating Technique," Exp. Mech., March 1987.

3-20. Sciammarella, C.A., and Roo, M.P.K., "Failure Analysis of Stainless Steel at Elevated Temperatures," Experimental Mechanics, 19 (11), 1979.

3-21. Cloud, G., et al., "Moiré Gratings for High Temperatures and Long Times," Exp. Mech. 19 (10),1979.

3-22. Chiang, F.P., J. Appl. Mech. Trans., SME 39 Series E (3), 1972.

3-23. Liang, C.Y., et al., "Time Averaged Moiré Method for In Plane Vibrational Analysis," J. Sound Vibration, 62 (2), 1979.

3-24. Weissman, E.M., and Post, D., "Full Field Displacement and Strain Rosettes by Moiré Interferometry," Exp. Mech., Vol. 2, No. 9, 1982.

3-25. Cloud, G., "High Temperature Moiré," SEM Fourth Annual Hostile Environments and High Temperature Measurements Conference, March 1987.

3-26. Post, D., "Moiré Interferometry for Deformation and Strain Studies," Opt. Eng., Vol. 24, No. 4, 1985.

3-27. Post, D., "Developments in Moiré Interferometry," Opt. Eng. Vol. 21, No.3, 1982.

3-28. Meadows, D.M., Johnson, W.O., and Allen, J.B., "Generation of Surface Contours by Moiré Patterns," Appl. Optics 9 (4), 1970.

3-29. Chiang, F.P., "Moiré Methods of Strain Analysis," Manual on Experimental Stress Analysis, SESA, Third Ed., 1979.

3-30. Theocaris, P.S., *Moiré Fringes in Strain Analysis*, Pergamon, London, 1969.

3-31. Durelli, A.J., and Parks, V.J., *Moiré Analysis of Strain*, Prentice-Hall, Inc., Englewood Cliffs, NJ, 1970.

3-32. Sciammarella, C.A., "The Moiré Method - a Review," Exp. Mech., Nov. 1982.

3-33. Bowles, D.E. et al., "Moiré Interferometry for Thermal Expansion of Composites," Exp. Mech., Dec. 1981.

3-34. Post, D., "Sharpening and Multiplication of Moiré Fringes," Exp. Mech., April 1967.

3-35. Post, D., "New Optical Methods of Moiré Fringe Multiplication," Exp. Mech., Vol. 8, No. 2, Feb. 1968.

3-36. Chiang, F.P., "Techniques of Optical Spatial Filtering Applied to the Processing of Moiré-fringe Patterns," Exp. Mech., Vol. 9, No. 4, 1969.

3-37 Sciammarella, C.A., "Moiré Fringe Multiplication by Means of Filtering and Wavefront Reconstruction Process," Exp. Mech., Vol. 9, No. 11, 1969.

3-38. Post, D and Baracat, W.A., "High Sensitivity Moiré Interferometry - A Simplified Approach," Exp. Mech. Vol.21, No.3 p.100, 1981

3-39. Boone, P.M., "A Method for Directly Determining Surface Strain Fields Using Diffraction Gratings," Exp. Mech., November 1982.

3-40. Burger, C.P., Smith, J.A., and Bremand, F., "Spectral Density Indication: A New Optical Method for Full Field Strain Analysis," VPI Center for Adhesion Science: 5th Annual Review, May 1987.

3-41. Bremand, F., Smith, J.A., and Burger, C.P., "An Optical Method for the Nondestructive Evaluation of Damage in Composites," from Design and Analysis of Composite Material Vessels, Pressure Vessels and Piping Conference, San Diego, CA, June 1987.

3-42. Vest, C.M., *Holographic Interferometry,* John Wiley and Sons, NY, 1979.

3-43. Brandt, G.B., "Image Plane Holography," App. Opt. 8:1421, 1969.

3-44. Jones, R., and Wykes, C., *Holographic and Speckle Interferometry,* Cambridge University Press, 1983.

3-45. Robertson, E.R., and Harvey, J.M. (eds), *The Engineering Uses of Holography,* Cambridge University Press, 1970.

3-46. Ostrovsky, Y.I., Butusov, M.M., and Ostrovskaya, G.V., *Interferometry by Holography,* Springer-Verlag, NY, 1980.

3-47. Haines, K.A., and Hildebrand, B.P., "Surface-Deformation Measurement Using the Wavefront Reconstruction Technique," App. Oct., Vol. 5, 1966.

3-48. Ennos, A.E., "Measurement of In-Plane Surface Strain by Hologram Interferometry," J. Phys. E. Sci. Instrum., Vol. 1, 1968.

3-49. Powell, R.L., and Stetson, K.A., "Interferometeric Vibration Analysis by Wavefront Reconstruction," J. Opt. Soc. Am. 55, 1965.

3-50. Heflinger, L.O., Spetzler, H., and Wuerker, R.F., "Thermal Expansion Coefficient Measurement of Diffusely Reflecting Sample by Holographic Interferometry," Rev. Sci. Instrum., Vol. 44, 1973.

3-51. Meyer, M.D., and Spetzler, H., "Material Properties and Strain Determination Using Holographic Interferometry," Sandia National Laboratory Report SLL-73-5325, 1973.

3-52. Butters, J.N., and Leendertz, J.A., Optics and Laser Tech., Vol. 3, 1971.

3-53. Macovski, A., Ramsey, S.D., and Schoefer, L.F., "Time-Lapse Interferometry and Contouring Using Television Systems," App. Optics, Vol. 10, No. 12, p. 2722, 1971.

3-54. Schwomma, O., Austrian pat. no. 2988340, 1972.

3-55. Jones, R., and Wykes, C., *Holographic and Speckle Interferometry,* Cambridge University Press, London, 1983.

3-56. Slettemoen, G.A., "General Analysis of Fringe Contrast in Electronic Speckle Pattern Interferometry," Optica Acta, Vol. 26, No. 3, p. 313, 1979.

3-57. Lokberg, O.J., "Electronic Speckle Pattern Interferometry," Phys. Technol., Vol. 11, No. 16, 1980.

3-58. Jones, R., and Wykes, C., "Decorrelation Effects in Speckle-Pattern Interferometry," Opta Acta, Vol. 24, No. 5.

3-59. Cookson, T.J., Butters, J.N., and Pollard, H.C., "Pulsed Lasers in Electronic Pattern Interferometry," Opt. and Laser Tech., June 1978.

3-60. Wykes, C., "Use of Electronic Speckle Pattern Interferometry (ESPI) in the Measurement of Static and Dynamic Surface Displacements," Opt. Eng., Vol. 21, No. 3, 1982.

3-61. Denby, D., Leendertz, J.A., "Plane Surface Strain Examination by Speckle-Pattern Interferometry Using Electronic Processing," J. of Strain Analysis, Vol. 9, No. 1, 1974.

3-62. Erf, R.K. (Ed.), *Speckle Metrology,* Academic Press: NY, 1978.

3-63. Hung, Y.Y., "Shearography: A New Optical Method for Strain Measurement and Nondestructive Testing," Opt. Eng., Vol. 21, No. 3, 1982.

3-64. Nakadate, S., Yatagai, T., and Saito, H., "Electronic Speckle Pattern Interferometry Using Digital Image Processing Techniques," App. Optics, Vol. 19, 1980.

3-65. Peters, W.H., Ransom, W.F., "Digital Imaging Techniques in Experimental Stress Analysis," Opt Eng, Vol. 21, No. 3, 1982.

3-66. Lokberg, O.J., Malmo, J.T., and Slettemoen, G.A., "Interferometric Measurements of High Temperature Objects by Electonic Speckle Pattern Interferometry," App. Opt., Vol. 24, No. 19, 1985.

3-67. Tyrer, J.R., "Critical Review of Recent Developments in Electronic Speckle Pattern Interferometry," SPIE, Vol. 64, *Holographic Nondestructive Testing* (1986)."

3-68. Ennos, A.E., "Speckle Interferometry," Progress in Optics, Vol. 16, North Holland Pub. Co., Amsterdam, 1978.

3-69. Leendertz, J.A., "Interferometric Displacement Measurement on Scattering Surface Utilizing Speckle Effect," J. Phys. E. Sci. Instrum., 1970.

3-70. Archbold, E., Burch, J.M., and Ennos, A.E., "Recording of In-Plane Surface Displacement by Double Exposure," Optica Acta 17:883, 1970.

3-71. Duffy, D.E., "Measurement of Surface Displacement Normal to the Line of Sight," Experimental Mechanics, Vol. 14, 1974.

3-72. Barker, D.B., and Fourney, M.E., "Displacement Measurements in the Interior of 3-D Bodies Using Scattered-Light Speckle Patterns," Experimental Mechanics, Vol. 16, 1976.

3-73. Hung, Y.Y., and Hovanesian, J.D., "Full Field Surface Strain and Displacement Analysis of Three-Dimensional Objects by Speckle Interferometry," Experimental Mechanics, Vol. 12, 1972.

3-74. Stetson, K.A., "A Review of Speckle Photography and Interferometry," Opt. Eng., Vol. 14, No. 5, 1975.

3-75. Ennos, A.E., "Speckle Interferometry," Chapter 6, of *Topics in Applied Physics, Vol. 9 - Laser Speckle and Related Phenomena*, Dainty, J.C. Ed., Springer-Verlag, New York, 1975.

3-76. Cloud, G., "Practical Speckle Interferometry for Measuring In-Plane Deformation," Appl. Optics, Vol. 14, 1975.

3-77. Park, V.J., "The Range of Speckle Metrology," Experimental Mechanics, Vol. 20, 1980.

3-78. Butters, J.N., and Leendertz, J.A., J. Phys. E., Vol. 4, 1971.

3-79. Kaufmann, G.H., Ennos, A.E., Gale, B., and Pugh, D.J., "An Electro-Optical Read-Out System for Analysis of Speckle Photographs," J. Phys. E Sci. Instrum., Vol. 13, 1980.

3-80. Sciammarella, C.A., and Ahmadshahi, M., "An Optoelectronic System for Fringe-Pattern Analysis," Experimental Techniques, 1986.

3-81. Ansari, F., and Ciurpita, G., "Automated Fringe Measurement in Speckle Photography," App. Opt., Vol. 26, No. 9, 1987.

3-82. Archbold, E., Ennos, A.E., and Virdee, M.S., "Speckle Photography for Strain Measurement - A Critical Assessment," SPIE, Vol. 136, 1977.

3-83. Ibid.

3-84. *Jones, R., and Wykes, C., Holographic and Speckle Interferometry,* Cambridge University Press, 1983.

3-85. Smith, G.B., and Stetson, K.A., "Heterodyne Readout of Speckle-legram Halo Interference Fringes," App. Opt. 19:18, 1980.

3-86. Stetson, K.A., "The Use of Heterodyne Speckle Photogrammetry to Measure High-Temperature Strain Distributions," Proc. SPIE 370, 1983.

3-87. Stetson, K.A., "Demonstration Test of Burner Liner Strain Measuring System," NASA Report No. R84-926376-15 CR-174743, 1984.

3-88. Stetson, K.A., "Demonstration of Laser Speckle System on Burner Liner Cyclic Rig," NASA Report No. CR-179509, 1986.

3-89. Hercher, M., "Final Report: Non-Contact High Temperature Strain Gage," NAS3-24848.

3-90. Hercher, M., Wyntjes, G., and De-Weerd, H., "A Non-Contact Laser Extensometer," Proc. SPIE, Vol. 746, 1987.

3-91. McCarty, P.E., and Thompson, J.W., "Development of a Noninterference Technique for Measurement of Turbine Engine Compressor Blade Stress," AEDC-TR-78, 1980.

3-92. "Laser Doppler Vibrometer System" Brochure, No. 1206E, Dantec (DISA) Electronics, November 1981.

3-93. Pleydell, M.B., "Noncontacting Laser Based Displacement Measurements From Solid Objects," Optics and Laser Technology, Vol. 19, No. 3, June 1987.

3-94. Prevey, P.S., "A Method of Determining the Elastic Properties of Alloys in Selected Crystallographic Directions for X-ray Diffraction Residual Stress Measurement," Vol. 20, *Advances in X-ray Analysis,* Plenum Press, New York, NY, p. 345-354, 1977.

3-95. Macherauch, E., "X-ray Stress Analysis," Exp. Mech., March 1966.

3-96. SAE J874a, "Residual Stress Measurement by X-ray Diffraction," 1971.

3-97. Peiter, A. and Lode, W., "X-ray Strain Field Atlas," Strain, February 1985.

3-98. Peiter, A. and Lode, W., "Strain Field Analysis With The X-ray Integration Method," Strain, May 1983.

3-99. Marion, R.H. and Cohen, J.B., "Anomalies in Measurement of Residual Stress by X-ray Diffraction," Advances in X-ray Analysis, Vol. 18, p. 466, 1975.

3-100. James, M.R. and Cohen, J.B., "The Measurement of Residual Stresses by X-ray Diffraction Techniques," *Treatise on Materials Science and Technology*, Vol. 19, ed. by Herman, Academic Press, New York, 1980.

3-101. MacDonald, B.A., "Application of the X-ray Two Exposure Stress Measuring Techniques to Carburised Steel," Vol. 13, *Advances in X-ray Analysis,* Plenum Press, New York, NY, p. 485-487, 1970.

3-102. Post, D., "Photoelasticity," p. 176, Exp. Mech., Vol. 19, No. 5, 1979

3-103. Redner, A.S., "Photoelastic Measurements by Means of Computer-Assisted Spectral Contents Analysis," Experimental Mechanics 25(2), 1985.

4-1. Baines, D.J., "A Comparative Theoretical Evaluation of Five Commonly Used Types of Heat Flux Sensors," January 1970.

4-2. Atkinson, W.H., Strange, R.R., "Development of Advanced High Temperature Heat Flux Sensors," NASA CR-165618, Sept. 1982.

4-3. Clayton, W.A., "High Temperature Circular Foil Heat Flux Gage," Proceedings of 26th International Instrumentation Symposium, Seattle, WA, 1980.

4-4. "Temperature Measurement Problems...Environmental Errors at High Temperatures," Moffat Thermosciences Inc., June 1986.

4-5. Epstein, A.H., Guenette, G.R., Norton, R.J.G, Yuzhang, C., "High Frequency Response Heat Flux Gage," Review of Scientific Instruments, April 1986.

4-6. Godefroy, J.C., "Thin Film Transducers for Temperature and Heat Flux Measurements," Rech. Aerosp., 1981-2.

Appendix - Excerpts from NAS3-25140 Statement of Work

Sensors for Ceramic Components in Advanced Propulsion Systems

Task 1 - Survey of Sensor Concepts

The Contractor shall conduct a survey of sensors that have the potential for measuring surface temperature, strain, and heat flux on ceramic components in advanced propulsion systems. The Contractor shall compile a list of potential sensor concepts using as a minimum the following approaches: (1) a literature search; (2) consultation with recognized authorities; (3) adaptation of existing concepts to this application; (4) development of advanced concepts. Exhibit A shall be used to define the materials of interest and the parameter range of application.

Task 2 - Analysis of Sensor Concepts

The Contractor shall perform an analysis of all sensor concepts identified in Task 1. As a minimum, the following factors shall be addressed in the analysis:

1. Usable temperature range
2. Accuracy
3. Compatibility with propulsion systems' environment
4. Compatibility of materials in contact (i.e., sensor/substrate compatibility)
5. Life expectancy
6. Size
7. Cost
8. Data acquisition and reduction requirements
9. Fabricability

Exhibit A - Materials and Parameter Ranges to be Considered for Study on Sensors for Ceramic Components in Advanced Propulsion Systems

Materials	Maximum Temperature
Thermal Barrier Coating, ZrO_2/Y_2O_3	1650K
Monolithic Ceramic Si_3N_4 and SiC	1900K
Ceramic Composite Si_3N_4/SiC	1900K
Carbon/Carbon Composite	2200K

Strain: Strain levels to be measured on these materials extend to the limits imposed by fracture.

Heat Flux: Anticipated heat fluxes in advanced propulsion systems may be as high as $5MW/m^2$.

Exhibit B - Performance Goals Overall

Overall Measurement Error	Maximum Acceptable	Target Goal
Temperature	+ 5% of Abs Temp	+ 2% of Abs Temp
Strain (Static)	+ 15% of F.S. Strain	+ 10% of F.S. Strain
Strain (Dynamic)	+ 10% of F.S. Strain	+ 5% of F.S. Strain
Heat Flux	+ 10% of F.S. Heat Flux	+ 5% of F.S. Heat Flux

Sensor Lifetime Goal: 50% Survival After 50 hr. in Test Environment

NASA
National Aeronautics and Space Administration

Report Documentation Page

1. Report No.	2. Government Accession No.	3. Recipient's Catalog No.
NASA CR180900		

4. Title and Subtitle	5. Report Date
Sensors for Ceramic Components in Advanced Propulsion Systems - Summary of Literature Survey and Concept Analysis - Task 3 Report	July 1988
	6. Performing Organization Code

7. Author(s)	8. Performing Organization Report No.
W.H. Bennethum, L.T. Sherwood	
	10. Work Unit No. 535-07-01

9. Performing Organization Name and Address	11. Contract or Grant No.
General Electric Company Aircraft Engines Cincinnati, OH	NAS3-25140
	13. Type of Report and Period Covered Contractor Report-Interim April--December 1987

12. Sponsoring Agency Name and Address	14. Sponsoring Agency Code
NASA Lewis Research Center 21000 Brookpark Road Cleveland, OH 44135	

15. Supplementary Notes

NASA Lewis Research Center Project Manager, Frank G. Pollack, Instrumentation and Control Technology Office.

16. Abstract

This report summarizes the results of a literature survey and concept analysis related to sensing techniques for measurement of surface temperature, strain, and heat flux for (non-specific) ceramic materials exposed to elevated temperatures (up to 2200 K). Concepts capable of functioning in a gas turbine hot section environment are favored but others are reviewed also. Recommendations for sensor development in each of the three areas are as follows:

1. Surface Temperature
   - Thin film thermocouples Pt-Rh alloys and SiC
   - Long wavelength (8-10 um) radiation pyrometer
2. Strain
   - Spectral density analysis
   - Optical tracking of attached targets
   - Dual beam doppler interferometer
3. Heat Flux
   - Surface mounted differential sensor
   - Surface mounted absolute sensor
   - Indirect technique

17. Key Words (Suggested by Author(s))		18. Distribution Statement
Propulsion Systems Ceramics Sensors	Temperature Strain Heat Flux	Publicly Available Star Category 35

19. Security Classif. (of this report)	20. Security Classif. (of this page)	21. No of pages	22. Price*
Unclassified	Unclassified	106	

NASA FORM 1626 OCT 86

*For sale by the National Technical Information Service, Springfield, Virginia 22161

CONTRACTOR'S DISTRIBUTION LIST

NASA Lewis Research Center
Attn: Library, M. S. 60/3
21000 Brookpark Road
Cleveland, OH 44135

NASA Lewis Research Center
Attn: Report Control Office, MS 60/1
21000 Brookpark Road
Cleveland, OH 44315

NASA Lewis Research Center
Attn: Wayne R. Girard, MS 500/305
21000 Brookpark Road
Cleveland, OH 44135

NASA Lewis Research Center
Attn: Frank G. Pollack, MS 77/1
Cleveland, OH 44135
(50 copies)

NASA Headquarters
Attn: RP/John R. Facey
Washington, DC 20546

NASA Headquarters
Attn: MPS/Paul N. Herr
Washington, DC 20546

NASA Langley Research Center
Attn: R. E. Wright, Jr. (MS-234)
Hampton, VA 23665

NASA Langley Research Center
Attn: S. L. Ocheltree (MS-235A)
Hampton, VA 23665

NASA Marshall Space Flight Center
Attn: William T. Powers, EB-22
Marshall Space Flight Center, AL 35812

NASA Marshall Space Flight Center
Attn: Joseph Zimmerman
Code EB-22
Marshall Space Flight Center, AL 35812

NASA Scientific and Technical
Information Facility
Attn: Accessioning Dept.
P. O. Box 8757
B.W.I. Airport, Md 21240
(25 copies)

Air Force Wright Aeronautical
Laboratory
Attn: William Stange, AFWAL/POTA
Wright Patterson AFB, OH 45433

Air Force Wright Aeronautical
Laboratory
Attn: Less Small, AFWAL/POTC
Wright Patterson AFB, OH 45433

Air Force Wright Aeronautical
Laboratory
Attn: John Reed, AFWAL/POTA
Wright Patterson AFB, OH 45433

Air Force Wright Aeronautical
Laboratory
Attn: Roger R. Craig
AFWAL/POPT
Wright Patterson AFB, OH 45433

Applied Sensors International
Attn: Richard Stillmaker
7834 Palace Drive
Cincinnati, OH 45242

Arnold Engineering Development Center
Attn: Carlos Tirres
AEDC/DOT
Arnold Air Force Station, TN 37389

Arnold Engineering Development Center
Attn: Marshall Kingery
AEDC/DOT
Arnold Air Force Station, TN 37389

AVCO Lycoming Textron
Lycoming Division
Attn: Mr. K. Collinge
Diagnostic Technology Manager
550 South Main Street
Stratford, CT 06497

AVCO Lycoming Textron
Lycoming Division
Attn: E. Twarog, Manager
Electronics and Instr.
550 South Main Street
Stratford, CT 06497

Aviation Applied Technology Dir.
USAARTA (AVSCOM)
Attn: Joel Terry/SAVRT-TY-ATA
Ft. Eustis, VA 23604-5577

Babcock & Wilcox
R&D Division
Attn: John Berthold
P. O. Box 835
Alliance, OH 44601

Battelle Columbus Laboratories
Attn: Ross G. Luce, Manager
Aerospace Programs Office
Columbus, OH 43201

Boeing Commercial Airplane Co.
Attn: R. D. (Ric) Tatman
P. O. Box 3707, MS 25-09
Seattle, WA 98124-2207

Boeing Commercial Airplane Co.
Attn: Ted Nykreim
MS 79-22
Seattle, WA 98124

Boeing Aerospace Company
Attn: Darrell R. Harting
P.O. Box 3999, MS 87-09
Seattle, WA 98124-2499

Boeing Aerospace Company
Attn: L. C. (Larry) Shrout
P.O. Box 3999, MS 86-11
Seattle, WA 98124-2499

Boeing Aerospace Company
Attn: J. L. (Larry) Howard
P.O. Box 3999, MS 86-12
Seattle, WA 98124-2499

Calspan Field Services, Inc.
AEDC Div.
Attn: C. T. Kidd
Arnold Air Force Station, TN 37389

Carnegie-Mellon University
Attn: Dr. Norman Chigier
Dept. of Mechanical Engineering
Pittsburgh, PA 15213

Case Western Reserve University
Attn: Dr. Alexander Dydbs
Mechanical & Aerospace Engineering
Department
Cleveland, OH 44106

Case Western Reserve University
Attn: Dr. Robert V. Edwards
Chemical Engineering Department
Cleveland, OH 44106

Caterpillar Tractor Company
Attn: Mr. Donald W. Heston
Research Department
Technical Center, Building F
100 Northeast Adams Street
Peoria, IL 61629

Combustion Engineering
Attn: John Fishburn
Dept. 9001-2226
Windsor, CT 06095

Combustion Engineering
Attn: J. Niziolek
Dept. 9005-0301
Windsor, CT 06095

Cranfield Institute of Technology
Attn: Dr. Robin L. Elder
School of Mechanical Engineering
Cranfield, Bedford MK43 OAL
UNITED KINGDOM

Dantec Electronik
Attn: Dr. Lars Lading
Medicinsk og Videnskabeligt
Maleudstyr A/S
Mile Parken 22, DK-2740 Skovlunde
DENMARK

DFVLR
Attn: Dr. Ing R. Schodl
Inst. Für Antriebstechnik
Postfach 90 60 58
5000 Köln 90
FEDERAL REPUBLIC OF GERMANY

Douglas Aircraft Company
Attn: J. R. S. Findlay
Intl, Mail Code 36-41
3855 Lakewood Blvd.
Long Beach, CA 90846

Eaton Corporation
Attn: Earl D. Jacobs, President
Electronic Instrumentation Division
5340 Alla Road
Los Angeles, CA 90066

Eaton Corporation
Attn: Dr. Lamont Eltinge
P. O. Box 766
Southfield, MI 48037

FluiDyne Engr. Corporation
Attn: Mat Matsuura, Group Leader
Controls and Instrumentation
5900 Olson Memorial Highway
Minneapolis, MN 55422

Garrett Turbine Engine Company
Attn: N. Fred Pratt
M/S 47-40/302-2 C
P. O. Box 5217
Phoenix, AZ 85010

Garrett Turbine Engine Company
Attn: Mr. Joe Allan
M/S 47-451/320-2
P. O. Box 5217
Phoenix, AZ 85010

General Electric Company
Attn: Patrick J. Poinsot, Engineer
Stress & Vibration Instrumentation
1000 Western Avenue, M.Z. 129 KD
Lynn, MA 01910

General Electric Company
Attn: Ronald J. Casagrande-MS 43A
Aircraft Equipment Division
50 Fordham Road
Wilmington, MA 01887

General Electric Company
Aircraft Engine Business Group
Attn: Gary Poppel, MSH-45
Evendale, OH 45215

General Electric Company
Aircraft Engine Business Group
Attn: Paul W. Mossey
Mail Stop H-78
Cincinnati, OH 45215

General Electric Company
Aircraft Engine Business Group
Attn: E. L. Pauly
Mail Stop H-78
Evandale, OH 45215

General Motors Corporation
Allison Gas Turbine Division
Attn: Mr. Ed Nitka
Speed Code T-12
P. O. Box 420
Indianapolis,, IN 46206-0420

General Motors Corporation
Allison Gas Turbine Division
Attn: David Willis
P. O. Box 420
Indianapolis,, IN 46206-0420

General Motors Corporation
Allison Gas Turbine Division
Attn: Ralph Fox, MS W16
P. O. Box 420
Indianapolis, IN 46206-0420

General Motors Corporation
Allison Gas Turbine Division
Attn: Dr. Donald R. Zimmerman
P. O. Box 420
Indianapolis, IN 46206-0420

General Motors Corporation
Allison Gas Turbine Division
Attn: Ken Cross
P. O. Box 420
Indianapolis, IN 46206-0420

HITEC Corporation
Attn: Steve Wnuk
PO Box 790
87 Fitchburg Rd
Ayer, MA 01432

Kulite Semiconductor Products, Inc.
Attn: John R. Hayer
1039 Hoyt Avenue
Ridgefield, NJ 07657

Lewis Engineering Company
Attn: C. B. Stegner
238 Water Street
Naugatuck, CT 06770

Massachusetts Inst. of Technology
Attn: Dr. Alan Epstein, Rm. 31-266
Cambridge, MA 02139

Medtherm Corporation
Attn: Larry Jones
P. O. Box 412
Hunstville, AL 35804

National Bureau of Standards
Attn: George Burns
Inst. for Basic Research
Washington, DC 20234

National Bureau of Standards
Attn: Ken Kreider, 221-B312
Washington, DC 20234

Naval Air Propulsion Center
Attn: Gaeian J. Mangano
P. O. Box 7176
Trenton, NJ 08628

Naval Air Propulsion Center
Attn: Russ Vizzini/Code PE32
Trenton, NJ 08628-0176

Naval Air Propulsion Test Center
Attn: Joseph De La Cruz
P. O. Box 1776
Trenton, NJ 08628

Naval Air Systems Command
Attn: Andrew Glista/Code 933E
Washington, DC 20361

Naval Post Graduate School
Attn: Prof. R. P. Shreeve
Department of Aeronutics (Code 67Sf)
Monterey, CA 93943

O.N.E.R.A.
Attn: Alain Boutier
29 Ave. de la Division Le Clerc
92320 Chatillon Sous Bagneus
FRANCE

Pennsylvania State University
Attn: Prof. B. Lakshminarayana
233 Hammond Building
University Park, PA 16802

Physical Sciences Dept.
Attn: M. G. Dunn
Arvin/Calspan Adv. Tech. Ctr.
Buffalo, NY 14225

PRC Kentron
Attn: Dr. M. M. Lemcoe
P. O. Box 273
Facility Support Complex (FSC)
Edwards, CA 93523-5000

Public Service Elect. & Gas Company
Attn: Dr. Melvin L. Zwillenberg
Research & Development Dept.
80 Park Plaza
Newark, NJ 07101

RdF Corporation
Attn: Frank Hines
23 Elm Avenue
Hudson, NH 03051

Rockwell International
Rocketdyne Division
Attn: Mr. Sarkis Barkhoudarian
6633 Canoga Avenue
Canoga Park, CA 91303

Rockwell International
Rocketdyne Division
Attn: Dr. John C. Lee
6633 Canoga Avenue
Canoga Park, CA 91303

Rosemont, Inc.
Attn: Mr. Larry Miller
Mail Stop F-10
P. O. Box 959
Burnsville, MN 55337

Spectron Development Laboratories
Attn: Dr. Chris W. Busch
3535 Hyland Ave.
Suite 102
Costa Mesa, CA 92626

Stanford University
Attn: Dr. R. J. Moffatt
Asst. Prof., Mech. Engr.
Thermosciences Division
Stanford, CA 94305

Stein Engineering Services, Inc.
Attn: Mr. Peter K. Stein
5602 East Monte Rosa
Phoenix, AZ 85018-4646

Sverdrup (AEDC)
Attn: Paul McCarty
M/S 930
Arnold AFB, TN 37389

Teledyne CAE
Attn: Julie J. Senn
1330 Laskey Road
P. O. Box 6971
Toledo, OH 43612-0971

Teledyne CAE
Attn: Joseph Pacholec
1330 Laskey Road
Toledo, OH 43612

Teledyne CAE
Attn: Jim Shortridge
1330 Laskey Road
P. O. Box 6971
Toledo, OH 43612-0971

The Univ. of Tennessee Space Institute
Attn: James W. L. Lewis
Applied Physics Research Group
Tullahoma, TN 37388

Thermogage, Inc.
Attn: Charles E. Brookley
330 Allegany Street
Frostburg, MD 21534

Thermonetics Corporation
Attn: H. J. Poppendiek
1028 Garnet Avenue
San Diego, CA 92109

TSI Instruments
Attn: Dr. Rajan Menon
P. O. Box 64394
St. Paul, MN 55164

United Technologies Corporation
Pratt and Whitney Aircraft
Attn: M. Carl Williams, MS 116-01
Engineering Division, MS 162-29
400 Main Street
East Hartford, CT 06108

United Technologies Corporation
Pratt and Whitney Aircraft
Attn: W. Gilbert Alwang
Engineering Division, MS 162-29
400 Main Street
East Hartford, CT 06108

United Technologies Corp.
Pratt & Whitney Aircraft
Attn: William Watkins, MS 731-36
Main Plant
P. O. Box 109600
West Palm Beach, FL 33410

United Technologies Corporation
Pratt and Whitney Aircraft
Attn: Bill Davies, MS 731-671
P.O. Box 109600
West Palm Beach, FL 33410-9600

United Technologies Optical Systems
Attn: Dr. Jaime Roman
P. O. Box 4181
West Palm Beach, FL 33401

United Technologies Research Center
Attn: Dr. A. Eckbreth
Silver Lane
East Hartford, CT 06108

United Technologies Research Center
Attn: Dr. G. M. Dobbs
Silver Lane
East Hartford, CT 06108

Virginia Polytechnic Institute
and State University
Attn: W. F. O'Brien, Jr.
Mechanical Engineering Dept.
Blacksburg, VA 24061

Williams International
Attn: Chloral L. Shew, MS 4-10
P.O. Box 200
Walled Lake, MI 48088

Williams International
Attn: David Easton
P.O. Box 200
Walled Lake, MI 48088